Photoresponse and Conductance Mechanisms in Nanoscale Superconductor Normal-Metal Point Contacts

by

Paul S. Westbrook

B. S. Physics
University of Michigan, 1990

SUBMITTED TO THE DEPARTMENT OF PHYSICS IN
PARTIAL FULLFILLMENT OF THE REQUIREMENTS
FOR THE DEGREE OF

DOCTOR OF PHILOSOPHY IN PHYSICS
AT THE
MASSACHUSETTS INSTITUTE OF TECHNOLOGY

JUNE 1998

Signature of Author: _____
Department of Physics
June 1, 1998

Certified by: _____
Ali Javan
Francis Wright Davis Professor of Physics
Thesis Supervisor

Accepted by: _____
Thomas J. Greytak
Professor of Physics
Associate Department Head for Education

Photoresponse and Conductance Mechanisms in Nanoscale Superconductor Normal-Metal Point Contacts

by

Paul S. Westbrook

Submitted To The Department Of Physics on May 15, 1998
In Partial Fullfillment Of The Requirements For The
Degree Of Doctor Of Philosophy In Physics

ABSTRACT

This work presents measurements of the dynamic resistance and photoresponse of high impedance (10-1000Ω) point contacts (SNPCs) between bulk superconducting tantalum and an electrochemically etched (10-200nm radius at tip) tungsten whisker immersed in superfluid He at 1.8K. The dynamic resistance of these nanoscale contacts is well described by the ballistic BTK conductance model which includes the effects of Andreev scattering at the Normal-Superconductor interface.

Deviations from the BTK conductance theory are also observed. The contacts show resistance peaks at symmetric bias voltages much larger than the superconducting gap ($|V|>10\Delta$). The voltage at which these peaks occur is found to be linear in the square root of the measured contact resistance, strongly supporting a model in which the resistance peaks result from the destruction of superconductivity by the magnetic field produced by current flow through the ballistic contact. The model is in quantitative agreement with observation and implies that each resistance peak corresponds to the appearance of a single flux quantum at the contact.

Measurements of the photoresponse at 860nm of the Ta-W point contacts are reported. A model which accurately describes these measurements is presented: The incident light induces an increase in the effective electron temperature of the irradiated W tip and a non-equilibrium quasi-particle density in the Ta resulting in a decrease in the superconducting gap. The photoresponse signal is then proportional to the current

increment resulting from these changes and can be computed from the BTK theory applied to an SNPC in the presence of incident light. Three novel effects and applications follow from this model:

1) In several contacts, photoresponse measurements showed that the W metal electron temperature varied with laser power as $T_{eff}^3 - T_{He}^3 = aP_{laser}$, implying heat conduction from the W to the superfluid He via inelastic scattering of electrons off the W surface oxide.

2) The photoresponse is used in a direct observation of the destruction of superconductivity at the contact when a finite bias resistance peak occurs.

3) The quasi-particle recombination time is measured from the roll-off of the photoresponse signal (proportional to the induced quasi-particle density) as laser intensity modulation frequency is increased. The thesis introduces a technique of measuring this roll-off even when the roll-off frequency is beyond the front-end detection bandwidth of the point contact. The measurement yields a value of τ_R=50ns, implying an average phonon trapping enhancement factor of 10.

Thesis Supervisor: Ali Javan
Title: Francis Wright Davis Professor of Physics

Table of Contents

"O my soul, do not aspire to immortal life, but
exhaust the limits of the possible."
Pindar, *Pythian iii*

"To do successful research, you don't need to know
everything. You just need to know of one
thing that isn't known"
A. L. Schawlow

Acknowledgments

Many thanks to Ali Javan whose guidance, encouragement, and support were essential not only to the work of my thesis but to my development in science as well. Our many long discussions during this work were quite memorable and taught me a lot about life as a researcher. I want to thank the members of my thesis committee, Ray Ashoori, George Clark, and Antonio Sanchez, whose critique of this work was invaluable. I also want to thank Michael Otteson for his support and help while I was learning to run a laboratory. Many thanks to Benjamin Lee for his help in the lab as a UROP. Special thanks goes to Nada Boustany who has been very supportive and inspirational throughout the past few years. Finally I want to acknowledge a few people I've known, learned from, and looked up to over the years, including my brothers, Partha Saha, James Chen, Ron Zamir, Paul von Hippel, and Beatrice Fracchiolla.

Lastly, I thank my parents, who have always stood by me and cheered me on. This thesis is dedicated to them.

Chapter 1

Introduction

Point contact junctions formed between a sharpened tip and a bulk sample in which either side can be a normal metal or a superconductor are important systems used to study the basic properties of these materials. When the tip is sufficiently sharp, the contact diameter can be less than the electron mean free path. Such contacts are said to be in the ballistic regime and their conductance is very sensitive to the single scattering event that occurs at the interface as electrons flow through the contact orifice. Moreover, the current flow can be low enough that neither of the two materials is driven out of equilibrium when a bias voltage is applied across the contact, and the scattering at the interface is therefore sensitive to equilibrium properties of the materials. An important advantage of point contacts is that they can be formed with bulk samples and are useful in studying materials that cannot be formed into thin films. Point contacts have been used in recent times to study the properties of many materials, such as ceramic high temperature superconductors[1], heavy Fermion materials[2], and the electron-phonon interaction in metals[3,4].

This use of point contacts to analyze material properties is analogous to the use of normal-metal superconductor tunnel junctions to measure the gap and electron-phonon interaction in superconductors[5]. However, the current voltage characteristic (IVC) of superconductor normal-metal point contacts (SNPCs) is very different from that of

Superconductor Insulator Normal-metal (SIN) tunnel junctions. Although tunnel junctions were well understood by the late 60s, very little work had been done to understand the conductance of SNPCs until the late 70s when Green function techniques[6] were first applied to explain the SNPC IVC. It was not until 1982 that Blonder[7] et. al. (BTK) published a more intuitive approach to computing the conductance of ballistic Normal-Superconductor (NS) contacts. These authors generalized the method of computing the tunneling IVC to include the crucial effect of Andreev reflection. In Andreev scattering[8], electrons incident on a clean NS interface reflect as holes, thus carrying twice the current as electrons transmitted through a tunnel barrier. The presence of this effect in low barrier NS contacts accounts for the difference between their IVCs and those of tunnel junctions. The method of BTK can be used to compute the IVC of contacts of arbitrary barrier height, including those in the cross-over regime of low barrier, which is useful for analyzing the conductance of most SNPCs. Since its introduction, this theory has been used extensively to compute the conductance of various configurations including interfaces between superconductors and metals[9], and more recently, superconductors and semiconductors[10].

Although the basic conductance properties of SNPCs are well understood within the BTK framework, deviations are observed from the IVC predicted by this theory. This variability of the SNPC conductance is the main trade-off against the advantage of their simplicity and versatility. Theoretical and experimental studies of these novel features are interesting both from a fundamental standpoint and from the practical standpoint of making point contacts more useful as a tool for studying new materials. It is important,

for instance, to know whether an observed conductance anomaly results from a fundamental property of the new material being studied or whether the anomaly is to be expected even in point contacts with well understood materials.

Tunnel junctions have also been used extensively to examine of the effect of light on superconductors, a field of study begun in the early 70s with the work of Testardi[11]. In addition, optical studies on tunnel junctions proved to be an important tool in understanding more generally the properties of nonequilibrium superconductors[12]. In contrast to the many optical studies performed on thin film SIN and SIS tunnel junctions, few studies have examined the optical response of the SNPC system despite the large amount of recent work analyzing the conductance properties of SNPCs.

A primary motivation for using tunnel junctions in optical studies was that experiments could be easily interpreted using tunneling theory to compute the response to light. The lack until recently of a similar theoretical framework to explain the conductance properties of SNPCs whose tunneling barrier is low or non-existent accounts in part for the small number of optical studies on this system. With the solid understanding of the SNPC conductance that has been gained in the last 15 years using BTK theory, one can now expect to develop a model of the response of SNPCs to visible light. The photoresponse of an SNPC is of interest because the conductance is very sensitive to the nonequilibrium properties of the sharpened tip and bulk sample. Therefore the photoresponse should reveal the nature of the nonequilibrium state induced by light. This is of special interest for the tip material which can be of nanoscale dimensions and show effects that depend on its size. Another interesting possibility is the

use of light as a probe to study novel conductance features in SNPCs. Finally, high speed processes, such as the quasi-particle relaxation rates in high temperature superconductors, may be observed on SNPCs because of their small size.

Thesis Outline

This thesis reports measurements on Superconductor Normal-metal Point Contacts (SNPCs) formed between a W metal whisker, electrochemically sharpened to *nanoscale* dimensions, and a bulk sample of superconducting Ta. As is evident from the background just discussed, these studies were motivated by two aims: 1) To explain novel features observed in the conductance of SNPCs and 2) to measure the SNPC photoresponse and develop a model to describe these observations. The photoresponse is then used to study several effects and applications of the irradiated SNPC which are addressed for the first time in this work: a) measurements of non-equilibrium electron distribution in the confined, irradiated metal tip as well as the bulk sample, b) an optical probe of the conductance properties of the SNPC, and c) a method of measuring the superconducting quasi-particle recombination rate in real time.

The work of this thesis therefore reports on two sets of phenomena which were measured experimentally and modeled theoretically: Chapter 3 examines the BTK and non-BTK behavior of the dynamic resistance of the Ta-W SNPCs. Chapters 4 and 5 of the thesis describe observations and modeling of the Ta-W SNPC photoresponse and discuss its novel applications in studying conductance mechanisms and nonequilibrium effects in the irradiated SNPC. Since the analysis of chapters 3-5 make use of the BTK

theory of the conductance of nanoscale NS interfaces, the theoretical background of BTK is first reviewed in chapter 2. A summary of each of the thesis chapters follows.

Chapter 2: Theoretical Background.

This chapter gives an outline of the BTK model of ballistic conductance through superconductor normal-metal interfaces with residual oxide barriers. The chapter will first discuss the theory of the resistance of ballistic point contacts between two normal metals, commonly known as the Sharvin resistance. This result is important in understanding how the resistance of an SNPC changes as the force on the contact is increased and will be used to relate the SNPC contact resistance to contact radius. A brief summary of the BTK model used in this thesis follows. This model includes a refinement of the original BTK model to take into account the effect of inelastic scattering of quasi-particles in the residual barrier region separating the superconductor and normal metal.

Chapter 3: Finite Bias Resistance Peaks.

This chapter discusses the BTK and non-BTK behavior observed in this thesis work on Ta-W SNPCs. First, the dynamic resistance of the contacts near zero bias is shown to be well described by the BTK model.

Then the chapter discusses in detail the measurements of a non-BTK feature observed in the dynamic resistance of the Ta-W point contacts: Resistance peaks at symmetric bias voltages significantly larger than the gap ($V>10\Delta$). Such peaks have been seen in other types of NS nano-constrictions. However, in this thesis, the ability to vary

the contact resistance, and hence contact radius of the Ta-W SNPCs leads for the first time to a quantitative model of the mechanism generating the resistance peaks. The voltage at which the peaks occur is found to be linear in the square root of the measured contact resistance, strongly supporting a model in which the resistance peaks result from the destruction of superconductivity by the magnetic field produced by current flow through the ballistic contact. The model is in quantitative agreement with observation and implies that each resistance peak corresponds to the appearance of a single flux quantum around the current flowing through the contact.

Chapter 4: Photoresponse of Ta-W Point Contacts

This chapter presents measurements of the photoresponse at 860nm of the Ta-W point contacts. A model of the photoresponse is presented which takes into account the effect of light on the bulk superconducting Ta and the W metal tip. In this model, the light induces an increase in the effective electron temperature of the irradiated W tip, δT, and breaks Cooper pairs in the Ta, resulting in an increase in quasi-particle density and corresponding decrease in gap, $\delta\Delta$. When light intensity is modulated, these effects are observed as an oscillating photoresponse voltage on the contact. The photoresponse voltage is shown to be proportional to the current increment resulting from $\delta\Delta$ and δT, and can be computed using the BTK current voltage characteristic discussed in Chapter 2. An expression can then be written for the photoresponse voltage in terms of the parameters $\delta\Delta$ and δT.

This two-parameter model is in excellent agreement with observation and shows how the superconducting gap and metal electron temperature change with laser intensity. The gap decreases linearly with power. The dependence of $\delta\Delta$ on laser intensity is derived from the theory of nonequilibrium superconductivity and found to be linear with a slope that agrees with the value measured in the photoresponse experiments.

The observed effective temperature of the W metal electrons follows the relation: $T_{metal}^3 - T_{He\ bath}^3 = aP_{laser}$, implying heat conduction from the W to the superfluid He via inelastic scattering of electrons off the W surface oxide. This heat conduction is greatly enhanced by the nanoscale dimensions of the tip which can be less than both the cutoff wavelength of bulk phonons in the W tip and the inelastic mean free path of the W electrons.

Lastly, this chapter shows how the photoresponse can be used to directly detect the destruction of superconductivity at the contact which is assumed in Chapter 3 in the model of the finite bias resistance peaks.

Chapter 5: Recombination Time Measurement

This chapter demonstrates a real-time method of measuring the quasi-particle recombination time using the SNPC photoresponse. A consequence of the model of Chapter 4 is that the optically induced quasi-particle density in the superconductor can be determined from the SNPC photoresponse. A technique is introduced in this chapter which exploits this aspect of the photoresponse to measure the quasi-particle recombination rate in Ta. In this method, the quasi-particle recombination time is

determined from the roll-off of the photoresponse as the modulation frequency of the laser intensity is increased.

Of special interest in this measurement is the method used to measure the roll-off: Because the quasi-particle recombination time is very short, signals originating on the point contact at the roll-off frequency cannot be reliably measured due to attenuation by unavoidable stray capacitance and impedance mismatch. The measurement technique presented in this chapter takes advantage of the nonlinearity of the SNPC current voltage characteristic to convert the signal due to the optically induced oscillating quasi-particle density to an intermediate frequency lying within the detection bandwidth. The signal at the intermediate frequency can then be used to determine the roll-off frequency and the recombination time.

The advantages and novelty of this roll-off measurement technique are twofold: 1) It utilizes the simplicity and versatility of point contacts, allowing measurements on superconductors that cannot readily be formed into thin films, such as crystalline and certain high temperature superconductors. 2) It can be used to perform real-time measurements of the quasi-particle recombination rate when the recombination rate is beyond the bandwidth of the front end electronic detection system used to measure signals on the point contact.

---

[1] See for example H. Srikanth, M. Rajeswari, and A. K. Raychaudhuri, Pramana-J. Phys. **36**, 207 (1991); J. R. Kirtley, Int. J. Mod. Phys. **(B)**, (1990).
[2] See for example A. Novack, et. al., Phys. Rev. B **36**, 2436 (1987).
[3] I. K. Yanson, Sov. Phys.-JETP **39**, 506 (1979). First report of NN point contacts in shorted planar N-I-N junctions.
[4] A. M. Duif, A. G. M. Jansen, and P. Wyder, J. Phys.: Condens. Matter **1**, 3157 (1989).

[5] See for example W. L. McMillan and J. M. Rowell, *Superconductivity*, edited by R. D. Parks (Marcel Dekker, New York), Vol 1 p. 561; C. B. Duke, *Tunneling in Solids*, (Academic Press) (1969).

[6] S. N. Artemenko, A. F. Volkov, and A. V. Zaitsev, Pis'ma Zh. Eksp. Teor. Fiz. **28**, 637 (1978) [JETP Lett. **28**, 589 (1978)]; Zh. Eksp. Teor. Fiz. **76**, 1816 (1979) [Sov. Phys.-JETP **49**, 924 (1979)]; Sold State Commun. **30**, 771 (1979).

[7] G. E. Blonder, M. Tinkham, and T. M. Klapwijk, Phys. Rev. B **25**, 4515 (1982).

[8] A. F. Andreev, Zh. Eksp. Teor. Fiz. **46**, 1823 (1964) [Sov. Phys.-JETP **19**, 1228 (1964)].

[9] See for example, S. Chaudhuri, and P. F. Bagwell, Phys. Rev. B **51**, 16936 (1995); P. C. Son, H. van Kempen, and P. Wyder, Phys. Rev. B **37**, 5015 (1988); N. K. Allsopp, J. Sanchez Canizares, R. Raimondi, and C. J. Lambert, J. Phys. Condens. Matter **8**, L377 (1996); H. Pothier, S. Gueron, D. Esteve, and M. H. Devoret, Physica B **203**, 226 (1994).

[10]See for example, T. M. Klapwijk, Physica B **197**, 481 (1994); B. J. van Wees, P. de Vries, P. Magnee, and T. M. Klapwijk, Phys. Rev. Lett. **69**, 510 (1992); C. W. J. Beenakker, Phys. Rev. B **46**, 12841 (1992).

[11] L. R. Testardi, Phys. Rev. B **4**, 2189 (1971).

[12] See for example the review of A. Gilabert, Ann. Phys. Fr. **15**, 255 (1990)

Chapter 2

Theoretical Background

Introduction

This chapter will review the theoretical framework of Blonder et. al.[1] (BTK), which describes the conductance through Normal-metal Superconductor (NS) interfaces with arbitrary barrier heights, and is applicable to the nanoscale superconductor normal-metal point contacts (SNPCs) of this thesis. This model includes the effect of Andreev scattering[2] at the NS interface which accounts for the difference between the SNPC conductance and that of the well know superconductor insulator normal-metal tunnel junctions. Knowledge of the conductance of SNPCs is important for much of the work of this thesis. The next chapter will show that the W-Ta point contacts studied in this thesis can be accurately modeled using the BTK model. In the following chapter the BTK current voltage characteristic will be used to model the optically induced current increment in the contact, leading to applications of the point contact photoresponse in the study of nonequilibrium properties of both the irradiated metal tip and the bulk superconductor.

The first section of this chapter will describe the origin of resistance in a nanoscale contact between two *normal* metals. The results of BTK calculations on SNPCs are normalized to this "normal state resistance" of the NNPC that exists in the absence of superconductivity. These calculations are also important because they relate

the contact radius to the contact resistance, a relationship that is important in understanding the finite bias resistance peaks discussed in the next chapter.

This will be followed by a review of the BTK calculation of current flow through an SNPC when a bias is applied across the contact. The calculation includes a modification to the original BTK model to include the effect of inelastic scattering in the barrier region. The BTK formulation is compared to the well known treatment of tunnel junctions between a superconductor and a normal metal to emphasize the peculiarities of the SNPC conductance resulting from Andreev reflection.

2.1 Resistance of Normal-Normal Contacts

When a sharpened metal tip is pressed into a bulk metal sample and a bias voltage is applied between the tip and sample, the resulting current voltage characteristic (IVC) is approximately linear for voltages (V_{bias}~10mV) significantly less than the Fermi energy (E_{Fermi}~10eV). This resistance arises mainly from the nanoscale dimensions of the contact area joining the two materials, and not from the residual oxide barrier in the region of contact between the two materials. The contact resistance is therefore a measure of the radius, a, of the orifice through which current flow occurs. Depending on the size of the orifice compared to the electron mean free path, ℓ_e, two limiting cases exist: The ballistic or Sharvin limit ($\ell_e > a$), and the diffusive or Maxwell limit ($\ell_e < a$). The two cases are summarized in Fig 2.1.

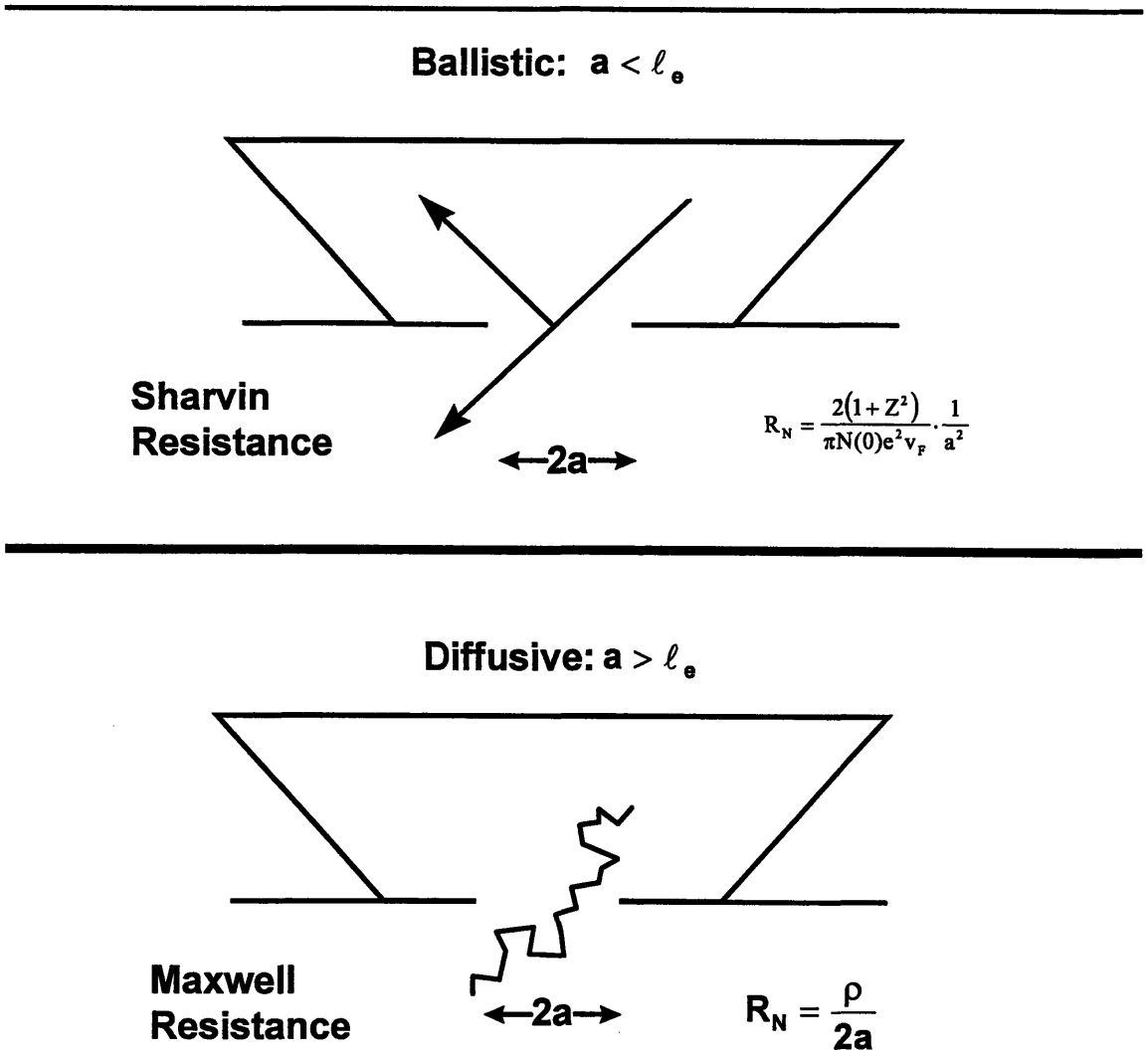

Fig. 2.1 Ballistic vs Diffusive Conductance. Each diagram depicts a point contact between a sharpened tip (the end of which is represented by the trapezoidal shape) and a bulk sample.

2.1.1 Sharvin Resistance

The point contacts of this thesis are in the ballistic regime, which was first treated by Sharvin[3]. When a bias voltage V_{bias} is applied between the two sides, current flow through the contact is essentially proportional to the product of the contact area and the collision rate at the contact of electrons near the Fermi level:

$$I_{Sharvin} = e\left(2N(0)eV_{bias}\right)v_F\left(\frac{\pi}{4}a^2\right) \tag{2.1}$$

N(0) is the single spin density of states at the Fermi energy and v_F is the Fermi velocity. The first term in parentheses is the excess density of electrons striking the contact from the side at larger bias. The factor of $\pi/4$ results from an integral over all the directions of incoming electrons. The resulting resistance is inversely proportional to the square of the contact radius:

$$R_{Sharvin} = \frac{1}{2N(0)e^2 v_F \frac{\pi}{4}a^2}. \tag{2.2}$$

2.1.2 Quantum Point Contact Regime

This form of the Sharvin resistance is useful in the discussions of BTK theory below. It may also be expressed in two other forms which reveal more about the point contact conductance. The Sharvin resistance can be related to the resistivity and mean free path, resulting in a formula which is useful for comparison with the diffusive limit[4]:

$$R_{Sharvin} = \frac{4\rho\ell_e}{3\pi a^2} \tag{2.3}$$

With substitutions from free electron model formulas for the mean free path and resistivity, this formula is the same as the previous one. The product $\rho\ell_e$ depends only on the Fermi momentum and this results in yet another expression for the Sharvin resistance in terms of the fundamental unit of resistance, $\hbar/e^2$:

$$R_{Sharvin} = 4\left(\frac{\hbar}{e^2}\right)\left(\frac{1}{k_F a}\right)^2 \tag{2.4}$$

As is clear from the formula, when the contact resistance becomes of order the quantum resistance, the contact size has become of order k_F^{-1}~lattice spacing, implying that the contact is comprised of a single atom. In this "quantum point contact" regime the conductance is affected by electron confinement in the contact region, and much experimental and theoretical work has been done in this area[4,5]. The resistance of point contacts in this thesis (10-1000Ω) are all well below the quantum resistance (~10kΩ), and effects due to confinement of electrons in the contact may be neglected.

2.1.3 Diffusive Corrections

The limit of $\ell_e < a$ was first treated by Maxwell[6]. In this case the transport is diffusive and the contact behaves like a effective resistor whose size is equal to the length scale over which the voltage drop occurs in the contact. This length scale is simply a, and so, in the Maxwell limit:

$$R_{Maxwell} = \frac{\rho}{2a} \tag{2.5}$$

Wexler[7] used kinetic theory to derive a formula connecting these two regimes. The result is expressed in terms of the Knudsen ratio $K=\ell_e/a$:

$$R = \frac{4\rho\ell_e}{3\pi a^2}\left(1+\frac{3\pi}{8}\Gamma(K)\frac{a}{\ell_e}\right) \tag{2.6}$$

$\Gamma(K)$ varies monotonically from 0.694 in the Sharvin limit to 1 in the Maxwell limit. Therefore, the coefficient of the Maxwell term in the above equation is of order 1 for all values of K.

The effect of a residual barrier on these results can be treated within the BTK framework discussed below. The BTK result for the contact resistance is the same as the Sharvin resistance except for a factor of $1+Z^2$ to take into account reflection off of the barrier. The dimensionless parameter Z is proportional to the barrier strength and is of order 0.5 in most point contacts, including those of this thesis. These results may be combined into a formula for the "normal state resistance" R_N of a contact between two normal metals which includes the effect of a residual barrier as well as diffusive corrections:

$$R_N = \frac{1+Z^2}{2N(0)e^2 v_F \frac{\pi}{4} a^2}\left(1+\frac{3\pi}{8}\Gamma(K)\frac{a}{\ell_e}\right) \tag{2.7}$$

The contacts of this thesis are best described by the ballistic formulas*, and so the diffusive term represented by the second term in parentheses will always be a small (but at times noticeable) correction.

2.2 Superconductor Normal-Metal Point Contact Current Voltage Characteristic

* Use of the diffusive formula to compute the contact radius from a contact resistance of order 10Ω results in a contact radius $a \sim (10^{-8}\Omega m)/(2x10\Omega) = 5x10^{-10}m$ that is inconsistent with the assumption of a diffusive contact since $\ell_e \sim 10^{-8}m$.

When one side of a point contact is superconducting the dynamic resistance will deviate from the normal state value R_N derived in the last section. The resulting bias dependent dynamic resistance is very different from the familiar result for a superconductor-insulator-normal (SIN) tunnel junction.. The essential difference between the conductance of NS contacts with tunneling barriers and those with very small or no barriers results from the effect of Andreev scattering[2]: When the barrier between a superconductor and normal metal is sufficiently low, incident electrons on the metal side can reflect as holes, creating a Cooper pair in the superconductor. Such electrons carry twice the current of normally transmitted electrons. The result, in the limit of a barrierless contact is a factor of two decrease in the dynamic resistance at zero bias. When a residual barrier exists at the NS interface, the zero bias resistance increases, as would be expected in a tunnel junction. In the cross-over regime in between a large tunneling barrier and a clean nanoshort, the dynamic resistance exhibits minima at bias voltages equal to plus and minus the gap Δ. At bias voltages far above $V=\Delta$, the IVC is essentially ohmic, except for a bias-independent excess current that results from the constant number of electrons Andreev reflecting at energies less than $V=\Delta$. The excess current is small at these bias voltages and linear in the superconducting gap Δ: $I_{excess}R_N \sim \Delta$.

Fig. 2.2 shows a schematic picture of a NS contact with a residual barrier and depicts the Andreev and normal reflection that can occur at the interface, below this are plots of the conductance of the contact for various barrier strengths.

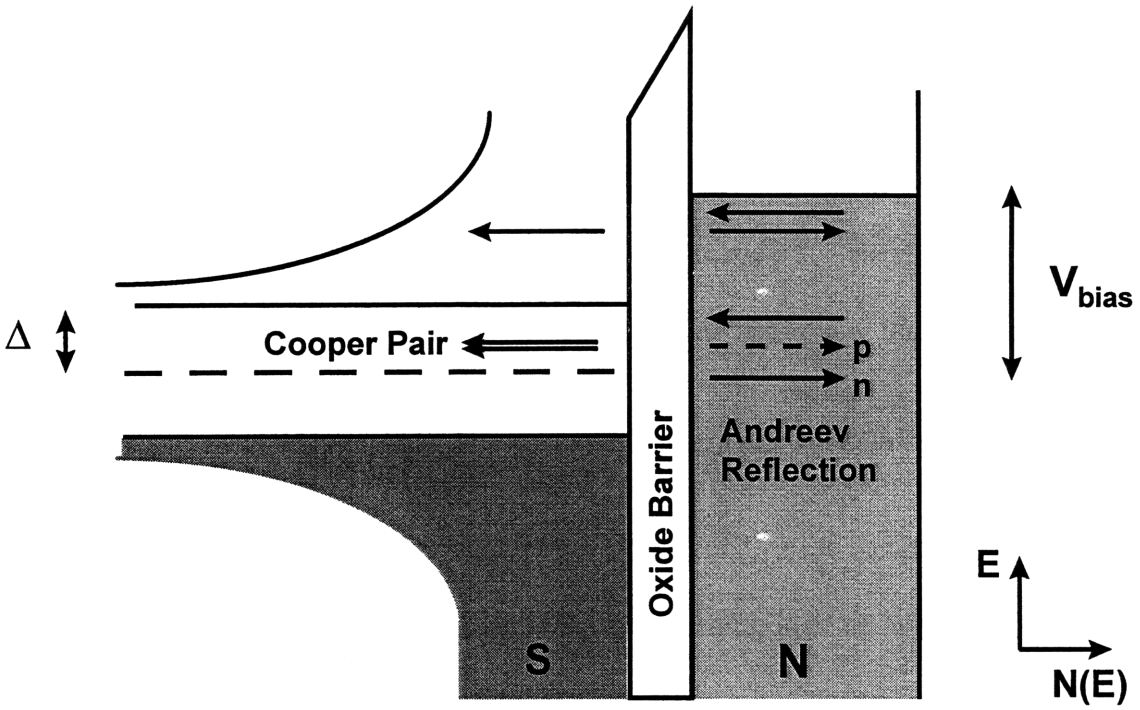

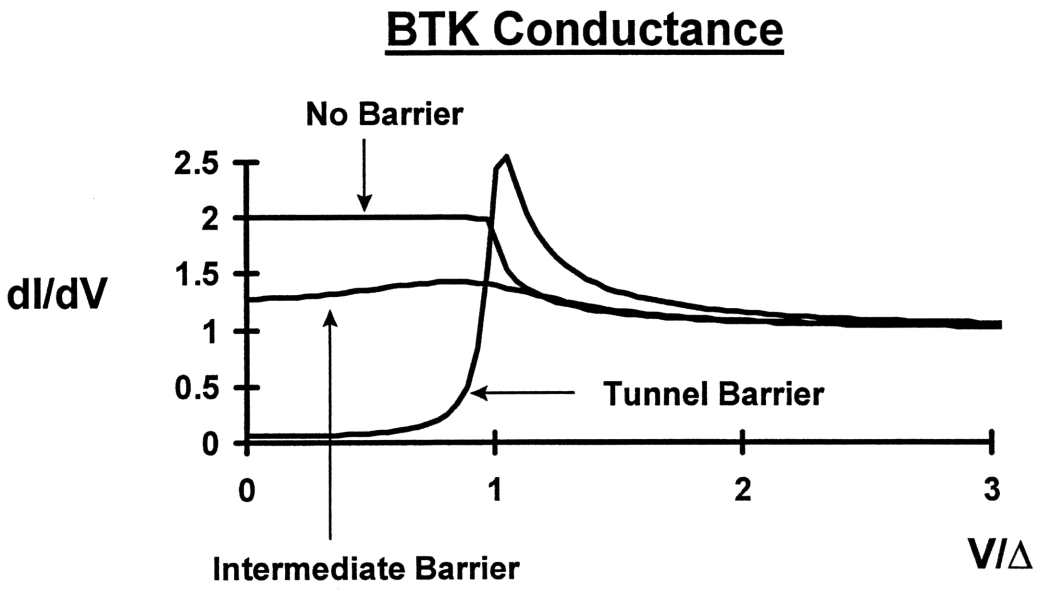

Fig. 2.2 Normal-Superconductor Interface The top diagram depicts the electron reservoirs in a normal metal and superconductor separated by an oxide barrier. N(E) is density of states. Andreev reflection of electrons (n) with E<Δ to holes (p) is shown. For E>Δ only normal reflection occurs. The bottom plots show the BTK conductance for three barrier heights including the familiar tunneling conductance.

The next section will describe the development of the BTK model and some of its refinements and place it in the context of other work on scattering off of NS interfaces. This is followed by a review of the BTK conductance calculation and the version of the model used in this thesis. The last section summarizes the meaning of all of the BTK model parameters and their effect on the dynamic resistance.

2.2.1 Development of BTK Theory

The conductance of low barrier NS contacts was not studied in depth until the late 70s, unlike the conductance of tunnel junctions between superconductors and normal metals which had been well understood since the 60s[8]. The early measurements of Likharev et. al.[9] and Gubankov et. al.[10] on superconductor normal-metal point contacts showed that such low barrier contacts have fundamentally different current voltage characteristics (IVCs) than tunnel junctions. They found that the zero bias dynamic resistance is entirely different in such contacts and that the contacts showed a bias-independent excess current in the ohmic regime at large bias voltages ($V>\Delta$). These studies were followed by the theoretical calculations of Artemenko et. al. [11], and of Zaitsev[12] These authors used Green function methods to compute the IVC of low barrier normal-metal superconductor contacts. This work was followed by the important paper of Blonder et. al.[1] (BTK) which is reviewed in the next section. This work presented a unified view of the conductance properties of SN interfaces with barriers of any strength, ranging from a pure short to a tunnel junction. These authors computed the IVC by finding the reflected and transmitted components at a NS boundary in a manner completely analogous to that used in tunneling theory only replacing the ordinary

Schrodinger equation with the coupled Schrodinger equation of Bogoliubov-deGennes[13], and considering two component wave functions with both hole and electron amplitudes.

As was noted by BTK, such methods had been used before to compute components reflected from NS interfaces. Andreev's original calculation (1964) used these equations to compute the thermal conductivity of a superconductor in a mixed state. In this case the effect of total reflection of electrons as holes at the NS boundary of a vortex greatly decreases the flow of heat since the reflected hole carries energy in the reverse direction. They were also used by Kummel[14] in calculations on charge balance near a vortex core. Calculations of the transmission coefficients of N-S-N and S-N-S structures were performed by Demers and Griffin[15], and the boundary conditions at an NS interface were also examined by Entin-Wohlman[16]. The main contribution of BTK theory, as they themselves stated, was to compute for the first time the bias dependence of current flow through an NS interface, and use the physical intuition gained by their method better to understand the conductance features. The method is more intuitively clear than the earlier Green function treatments, and has become widely used in the analysis of the conductance properties of contacts between superconductors and metals and semiconductors.

The original treatment of BTK accurately described the dynamic resistance of clean SN contacts[17], however the model is not a good description for some contacts which have surface contaminants. This is most significant in the dynamic resistance of point contacts with High T_c superconductors in which it is believed that the effects of surface oxides are unavoidable[18]. This effect was first treated by Srikanth[19] and later put

in more formal terms by Pleceník et. al.[20]. They treated the effect of surface contaminants by including an inelastic scattering term Γ in a manner very similar to the treatment used by Dynes[21] to explain broadening of tunnel junction characteristics. The theoretical treatment used in this thesis includes this modification to the original BTK theory.

2.2.2 BTK Formulation

This subsection is a review of the arguments of BTK along with the modifications due to Srikanth and Pleceník to include the effects of inelastic scattering off of impurities at the interface. Readers wishing to skip this discussion will find a review of the effect of all the model parameters, Δ, T, Z, and Γ, on the IVC of an SNPC in the last section of this chapter.

The idealized NS interface considered by BTK consists of a delta function potential barrier Hδ(x) which represents the effects of residual scattering centers at the NS interface, and a step function pair potential ΔΘ(x) representing the transition from a normal metal to a superconductor. The barrier strength is re-expressed by BTK as a dimensionless barrier strength parameter, Z:

$$Z = \frac{k_F H}{2E_F} = \frac{H}{\hbar v_F}. \tag{2.8}$$

As in the tunneling problem, current flow is computed by assuming an electron is incident on the NS interface and calculating the reflection and transmission coefficients. However, in the limit of very low barrier, the effect of the pairing potential Δ in the

superconductor must be taken into account in the reflection and transmission. The effect of the pair potential is to couple electron and hole states in the superconductor, making the low lying quasi-particle excitations in the superconductor superpositions of electron and hole states. The effect of the pairing interaction on metal electrons incident on the NS interface is to "Andreev scatter" them to reflected hole states in the metal. The appropriate wave functions to use for the reflected and transmitted waves are therefore two component wavefunctions:

$$\psi = \begin{bmatrix} f(x,t) \\ g(x,t) \end{bmatrix}. \tag{2.9}$$

The top component represents the electron-like amplitude and the bottom component represents the hole-like amplitude of excitations in the metal or superconductor. In the superconductor, these two components must satisfy the coupled Schroedinger equations known as the Bogoliubov-deGennes equations[13]:

$$\begin{aligned} i\hbar\frac{\partial f}{\partial t} &= \left[-\frac{\hbar^2\nabla^2}{2m} - \mu + V(x)\right]f + \Delta(x)g \\ i\hbar\frac{\partial g}{\partial t} &= -\left[-\frac{\hbar^2\nabla^2}{2m} - \mu + V(x)\right]g + \Delta(x)f \end{aligned} \tag{2.10}$$

Where V(x) is the lattice potential, μ is the chemical potential ($=E_{Fermi}$), and m is the mass of both holes and electrons. When the superconductor becomes normal, $\Delta=0$, and the Bogoliubov equations decouple into the usual result for a metal. The equations are then solved by assuming that V is constant and that

$$\psi = \begin{bmatrix} \tilde{u}(x) \\ \tilde{v}(x) \end{bmatrix} e^{-iEt/\hbar}$$

Then the wavefunction for a metal electron incident the NS interface and the resulting reflected and transmitted wavefunctions are (following the notation of BTK):

$$\psi_{inc} = \begin{bmatrix} 1 \\ 0 \end{bmatrix} e^{iq^+x}$$

$$\psi_{refl} = a\begin{bmatrix} 0 \\ 1 \end{bmatrix} e^{iq^-x} + b\begin{bmatrix} 1 \\ 0 \end{bmatrix} e^{-iq^+x} \tag{2.11}$$

$$\psi_{trans} = c\begin{bmatrix} u_o \\ v_o \end{bmatrix} e^{ik^+x} + d\begin{bmatrix} v_o \\ u_o \end{bmatrix} e^{-ik^-x}$$

where,

$$\hbar q^{\pm} = \sqrt{2m(\mu \pm E)}$$

$$\hbar k^{\pm} = \sqrt{2m\left(\mu \pm \left(E^2 - \Delta^2\right)^{1/2}\right)} \tag{2.12}$$

$$u_o^2 = 1 - v_o^2 = \frac{1}{2}\left[1 + \frac{\left(E^2 - \Delta^2\right)^{1/2}}{E}\right]$$

Here u_o and v_o are the usual BCS coherence factors proportional to the amplitude of the hole and electron components of an excitation of energy E above the Fermi level in the superconductor.

The metal electron incident on the NS interface represented by ψ_{inc} can then undergo one of four processes: The two terms of ψ_{refl} represent normal reflection of an electron and Andreev reflection of a hole within the metal. The two terms of ψ_{trans} represent transmission into a hole-like or electron-like excitation in the superconductor.

These solutions must satisfy the boundary conditions at x=0:

$$\psi_S(0) = \psi_N(0) \tag{2.13}$$

$$\hbar/2m\left(\dot{\psi}_S(0) - \dot{\psi}_N(0)\right) = H\psi(0)\,.$$

The derivatives are with respect to x. The amplitudes a, b, c, and d can then be related to the reflection and transmission coefficients. In the computation of the current only the normal and Andreev reflection coefficients are needed, because current flow can be determined by considering the electron and hole currents only on the metal side of the contact.

2.2.3 Effect of Inelastic Scattering at the Contact: Γ.

This calculation must be modified if inelastic scattering at the NS interface is to be taken into account. As discussed by Plecenik, the necessary modification to the Bogoliubov-deGennes equations affects the time dependence of f and g. Inelastic scattering results in an additional term:

$$i\hbar\frac{\partial g}{\partial t} = \left[i\hbar\frac{\partial g}{\partial t}\right]_{field} + \left[i\hbar\frac{\partial g}{\partial t}\right]_{inelastic} \tag{2.14}$$

In a linear approximation the rate of change of g (and f) due to inelastic scattering near the contact is taken into account by a single inelastic scattering time $\tau_{inelastic}=\Gamma^{-1}$:

$$\left[i\hbar\frac{\partial g}{\partial t}\right]_{inelastic}=\frac{-i\hbar}{\tau_{inelastic}}g=-i\Gamma g. \tag{2.15}$$

The modified Bogoliubov-deGennes equations are then:

$$\begin{aligned} i\hbar\frac{\partial f}{\partial t}&=\left[-\frac{\hbar^2\nabla^2}{2m}-\mu-i\Gamma+V\right]f+\Delta g \\ i\hbar\frac{\partial g}{\partial t}&=-\left[-\frac{\hbar^2\nabla^2}{2m}-\mu-i\Gamma+V\right]g+\Delta f \end{aligned} \tag{2.16}$$

The solution to these equations is the same as before but with E replaced by E+iΓ, and squared amplitudes replaced by moduli squared of the resulting complex quantities. In this picture the Andreev and normal reflection coefficients A and B, are then (See Pleceník):

$$A(E,\Delta,Z,\Gamma)=\frac{\sqrt{(\alpha^2+\eta^2)(\beta^2+\eta^2)}}{\gamma^2} \tag{2.17}$$

$$B(E,\Delta,Z,\Gamma)=Z^2\frac{\left[(\alpha-\beta)Z-2\eta\right]^2+\left[2\eta Z+(\alpha-\beta)\right]^2}{\gamma^2}$$

with the substitutions

$$\gamma^2=\left[\alpha+Z^2(\alpha-\beta)\right]^2+\left[\eta(2Z^2+1)\right]^2$$

$$u_o^2 = \alpha + i\eta = \frac{1}{2}\left[1 + \frac{\sqrt{(E + i\Gamma)^2 - \Delta^2}}{E + i\Gamma}\right] \tag{2.18}$$

$$v_o^2 = \beta - i\eta = 1 - u_o^2$$

2.2.4 Calculation of Current-Voltage Characteristic

As in a tunnel junction the current through the NS interface is an integral over the current due to electrons at all energies. This integral requires knowledge of the distribution of electrons and quasiparticles in the metal and superconductor. In the limit that current flow does not greatly disturb equilibrium, one may assume that the distributions on both sides of the contact can be approximated by Fermi functions with Fermi levels μ and μ-eV_{bias}. The current is then exactly the same as in a tunnel junction except that the tunneling transmission coefficient, proportional to the superconducting density of states and equal to 1-B in the BTK model, is replaced by 1+A-B to include the effect of Andreev reflection:

$$\begin{aligned} &I(V,\Delta,Z,\Gamma) = \\ &2N(0)ev_F\left(\pi a^2/4\right)\int dE\left[f(E-eV,T) - f(E,T)\right]\cdot\left[1 + A(E,\Delta,Z,\Gamma) - B(E,\Delta,Z,\Gamma)\right] \end{aligned} \tag{2.19}$$

where f(x) is the Fermi function. The factor $\pi a^2/4$ comes from an average over all incident angles for an orifice of radius a separating two semi-infinite regions.

Note that all of the bias dependence in this equation results from the structure in the energy spectrum of the superconductor which is probed by current flow from the metal. Since the excitation spectrum of the metal has no significant energy dependence

the temperature of the superconductor does not affect the bias dependence of I, except through $\Delta(T)$. In Chapter 4 this is important in showing that the photoresponse of an SN contact is not sensitive to the superconducting quasi-particle distribution. The quasi-particle distribution can only be measured in a contact between two superconductors, since then both sides have strong energy dependence in their excitation spectra.

This is the model used to fit the dynamic resistance observed on the W-Ta contacts of this thesis. The solution was incorporated into a nonlinear fitting routine and the dynamic resistance of all contacts could thus be characterized in terms of the BTK parameters (See chapter 3). These parameters were then used in further fitting routines to analyze the photoresponse of the contacts in Chapter 4 in terms of optically induced changes in Δ and the temperature of the metal.

2.2.5 Summary of IVC Parameters.

It is important to note the effect of each BTK parameter on the two main features of the IVC. These are the resistance minimum at $V=\Delta$ and flow of a bias-independent excess current $I_{excess} \sim \Delta R_N/e$ for $V_{bias} >> \Delta$. Changes in T smooth out the sharp features of the dynamic resistance but do not alter the excess current at large bias. Changes in Δ alter the position of the minima in the dynamic resistance and change the excess current by an amount linearly proportional to the change in Δ. The barrier parameter Z, which is proportional to the strength of the delta function barrier assumed for the ideal NS interface is of order 0.5 for most contacts. An increased Z means a larger barrier which means that the resistance peak at zero bias will increase in size, making the dynamic

resistance look more like the tunneling dynamic resistance. Increasing Z also decrease the excess current, and in the tunneling limit of very large Z ~10, the excess current is essentially zero. Finally, the parameter Γ accounts for inelastic scattering at the contact and is typically much less than Δ. The effect of Γ is to smooth the features in the dynamic resistance in a manner similar to the temperature. An increase in Γ will also decrease the flow of excess current, because this corresponds to a more strongly scattering barrier at the interface which pushes the dynamic resistance toward the tunneling limit.

---

[1] G. E. Blonder, M. Tinkham, and T. M. Klapwijk, Phys. Rev. B **25**, 4515, (1982).
[2] A. F. Andreev, Zh. Eksp. Teor. Fiz. **46**, 1823 (1964) [Sov. Phys.-JETP **19**, 1228 (1964)].
[3] Yu. V. Sharvin, Zh. Eksp. Teor. Fiz. **48**, 984, (1965) [Sov. Phys.—JETP **21**, 655, (1965)].
[4] H. Srikanth, and A. K. Raychaudhuri, Phys. Rev. B **46**, 14713, (1992).
[5] See for example R. Landauer, IBM J. Res. Dev. **1**, 223 (1957); Y. Imry, in *Directions in Condensed Matter Physics*, edited by G. Grinstein and G. Mazenko (World Scientific, Singapore, 1986); M. N. Wybourne et. al., Superlat. Microstuct., **20**, 110 (1996); I. I. Takayanagi, Surf. Sci. **302**, 200 (1996).
[6] J. C. Maxwell, *Treatise on Electricity and Magnetism* (Oxford: Clarendon) 1904; A. M. Duif, A. G. M. Jansen, and P. Wyder, J. Phys.: Condens. Matter **1**, 3157, (1989).
[7] G. Wexler, Proc. Phys. Soc. **89**, 927, (1966).
[8] See for example W. L. McMillan and J. M. Rowell, *Superconductivity*, edited by R. D. Parks (Marcel Dekker, New York), Vol 1 p. 561.
[9] K. K. Likharev and L. A. Yakobson, Zh. Eksp. Teor. Fiz. **68**, 1150 (1975) [Sov. Phys.-JETP **41**, 2301 (1975)].
[10] V. N. Gubankov, and N. M. Margolin, Pis'ma Zh. Eksp. Teor. Fiz. **29**, 733, (1979) [JETP Lett. **29**, 673, (1979)].
[11] S. N. Artemenko, A. F. Volkov, and A. V. Zaitsev, Pis'ma Zh. Eksp. Teor. Fiz. **28**, 637 (1978) [JETP Lett. **28**, 589 (1978)]; Zh. Eksp. Teor. Fiz. **76**, 1816 (1979) [Sov. Phys.-JETP **49**, 924 (1979)]; Sold State Commun. **30**, 771 (1979).
[12] A. V. Zaitsev, Zh. Eksp. Teor. Fiz. **78**, 221, (1980) [Sov. Phys. JETP **51**(1), 111, (1980)].
[13] See for example P. G. deGennes, *Superconductivity of Metals and Alloys*, (Addison Wesley: Advanced Book Classics) (1989).
[14] R. Kummel, Z. Phys. **218**, 472, (1969).

[15] J. Demers and A. Griffin, Can. J. Phys. **49**, 285, (1970); A Griffin, and J. Demers, Phys. Rev. B **4**, 2202, (1977).
[16] O. Entin-Wohlman, J. Low Temp. Phys. **27**, 277, (1977).
[17] G. E. Blonder and M. Tinkham, Phys. Rev. B **27**, 112, (1983).
[18] See for example J. Vrba and S. B. Woods, Phys. Rev. B **3**, 2243, (1971); and refs 6-10 in A. Plecenik et. al., Phys. Rev. B **49**, 10016, (1994).
[19] H. Srikanth and A. K. Raychaudhuri, Physica C **190**, 229, (1992).
[20] A. Plecenik, M. Grajcar, Š. Benačka, P. Seidel, and A. Pfuch, Phys. Rev. B 49, 10016 (1994).
[21] R. C. Dynes, J. P. Garno, G. B. Hertel, and T. P. Orlando, Phys. Rev. Lett. **53**, 2437 (1984).

Chapter 3

Finite Bias Resistance Peaks

Introduction

The last chapter described the BTK theory of conductance through Normal-metal Superconductor (NS) interfaces. Current flow is modeled as scattering off of an idealized delta function barrier potential and step function pair potential resulting in a resistance dip at a contact bias voltage equal to the gap and an excess current in addition to the ohmic current at large bias. Both of these effects are due to the extra current carried by Andreev scattered electrons in the metal, which reflect as holes at the NS interface with the creation of a Cooper Pair in the superconductor. The intuitive BTK picture has been very successful in describing quantitatively the dynamic resistance of real NS interfaces, and this chapter will show that the model accurately describes the dynamic resistance of the Ta-W point contacts of this thesis for bias voltages $V \sim \Delta$.

There are however NS interfaces exhibiting deviations from the BTK current voltage characteristic (IVC) that are qualitatively different from this basic picture. The deviations fall into two main categories: Finite bias and zero bias. The zero bias deviations result from the breakdown in the assumptions of a simple barrier between the superconductor and the metal assumed by BTK. The primary zero bias deviation is a minimum (instead of a maximum) in the resistance at zero bias which can be much smaller than the largest BTK resistance drop of 50%. Models of this feature involve, for

example, the assumption that the surface oxides near the interface must be treated as a region of depressed superconductivity, making the interface N-S'-S rather than the simple NS interface assumed by BTK.

The finite bias deviations from BTK theory are associated with suppression of Andreev scattering at the NS interface, usually by destruction of the superconductivity at bias voltages large enough to destabilize the superconductor in the high current flow region near the contact. Other finite bias structure, including quantum resonances, can then result from the characteristics of the barrier region that results after the transition.

This chapter will focus on observations and modeling of finite bias resistance peaks observed in the Ta-W SNPCs of this thesis. A zero bias resistance minimum was also observed on some of the contacts, but was not be explored in depth. These observations and their implications are discussed in Appendix B.

The finite bias resistance peaks occur in a class of small area (estimated diameter less than 10nm; see discussion below), high resistance ($R>10\Omega$) Ta-W SNPCs formed between a sharpened tungsten whisker and bulk superconducting tantalum at symmetric voltages far in excess of Δ ($V>10\Delta$). To our knowledge this is the first report of resistance peaks in such contacts. As in the work of other authors discussed below, the peaks can be attributed to a decrease of excess current arising from Andreev reflection. Of special interest in the present work is the linear dependence of the resistance peak voltage on the square root of the measured contact resistance. As will be shown below, this dependence can be analyzed by considering the magnetic field produced by current flow through the contact and treating the contact as a wire of nanoscale dimensions. The

resistance peaks occur when the magnetic field due to current flow reaches the critical level for a wire of radius equal to the contact radius estimated from the theory of ballistic contacts. The model is found to explain the dependence of resistance peak voltage on contact resistance and also to be in quantitative agreement with the data.

3.1 Previous Observations of Finite Bias Structure

To place the present work in context, this section will discuss previous observations of finite bias conductance which deviates from BTK behavior. Finite bias resistance peaks have been seen in the dynamic resistance of other types of NS nanoconstrictions showing BTK behavior. All of these have considerably larger area and/or have different geometries than the Ta-W SNPCs examined in the present study. Each study considered different mechanisms for the above gap structure, but all of the explanations connect the resistance peaks to a decrease in excess current arising from Andreev scattering at the NS interface(s).

The measurements of Xiong et. al.[1] considered the conductance through an NS interface between thin films of Nb and Ag which were grown to overlap along one edge by a controllable amount. The dimensions of these NS contacts were thus adjustable in one dimension from 10-2500nm and were fixed in the other dimension at 28μm. These authors observed a single finite bias peak similar to those discussed in this chapter. (They also observed a zero bias resistance minimum; see Appendix B.) The peak was observed at various finite bias voltages in a range from 3.5 to 17mV. They recorded the temperature dependence of the peaks and found that it had the same temperature

dependence as the gap regardless of how large the voltage of the peak was at low temperature. They also recorded the magnetic field dependence of the peak voltage and found that, again, regardless of peak voltage at H=0, the peak voltage decreased in value in the same way with increasing H field. These authors did not give a quantitative explanation of the mechanism producing the peaks, but noted that because the peak voltage's temperature dependence is the same as the gap, the peak may occur at a critical current density. A high enough current density in a superconductor can be "de-pairing" and cause the superconductor to become normal in the vicinity of the contact. This mechanism was consistent with their observation, since the critical current density is linear in the superconducting gap[2].

Another NS interface that exhibited finite bias resistance peaks were the point contacts studied by Hahn et. al.[3,4,5]. These were formed by growing a thin film of Ag on a bulk crystalline sample of Ta and creating a nanoshort by subjecting the Ag-Ta interface to a voltage pulse. The contact resistances were very small ($R<1\Omega$); the authors estimated a contact radius from the Sharvin resistance formula (discussed in the last chapter) of 70nm. The zero bias structure of these contacts was fairly well described by the BTK theory although some deviations were observed near zero bias. At large bias voltages (3-6mV), a sharp transition was observed which showed considerable voltage hystersis. The sharp transition was accompanied at higher bias by several additional resistance peaks whose shape and number varied from contact to contact. The first sharp transition was attributed by these authors to the destruction of superconductivity at the contact by thermal effects, however they did not present a quantitative explanation of the

destruction mechanism. The suppression of superconductivity extends into the sample some distance, and the conductance structure at high bias was then related to quantum interference inside this bubble of normal Ta near the contact. The bubble forms a quantum box in which one side is the barrier potential at the Ag-Ta interface, and the other side is the pair potential of the NS interface inside the superconductor. Normal reflection occurs at the first interface and Andreev reflection at the second. As computed by Hahn[4], the transmission and reflection coefficients of this box then determine the conductance structure as a function of bias. A complication of this model is that the bubble changes in size as the bias voltage is increased. Lack of knowledge regarding this "melting depth" as well as the exact geometry of the contact resulted in some discrepancies between theory and data, but the general structure of the conductance followed the model. The dynamic resistance of these contacts was also studied in the presence of a magnetic field, and additional oscillations were found to occur at large biases. This behavior was explained by adding a supercurrent component to the normal current flowing at the NS boundary. The supercurrent was modulated by the magnetic field generated by the current flow, and this created the additional oscillatory component in the dynamic resistance.

Finite bias peaks have also been seen in Superconductor-Semiconductor (S-Sm) nanostructures[6]. These were formed by growing 15nm thin film of InAs and then depositing a thin film of Nb on top of this layer. The Nb film was interrupted by an AlSb barrier. A voltage was applied across the Nb on either side of the barrier and current flow occurred through the interface between the Nb-InAs barrier, then through the thin In As

layer under the Al Sb barrier and back into the other Nb film through a second Nb-InAs S-Sm interface. These authors observed a single resistance peak at a bias voltage much larger than the gap as well as a resistance dip at zero bias. They found that the temperature dependence of the voltage of this peak was the same as the gap. The conductance was explained by considering the effect of multiple reflections of electrons off of the S-Sm interface as they propagate down the 15nm channel of InAs. Multiple reflections resulted in a greatly increased Andreev scattering rate, and this caused the large dip in resistance (peak in conductance) near zero bias. The explanation of the finite bias peaks then followed by considering the trajectory of Andreev reflected holes. These holes normally recombine with electrons in the InAs, but with sufficient quasi-particle injection into the superconductor, they recombined with these excitations, canceling out the increased excess current resulting from the multiple reflections of electrons.

3.2 Experiment

Ta-W point contacts were formed between an electrochemically etched tungsten whisker and a mechanically polished tantalum (99.95% pure) post. The etching procedure* consisted of an AC etch using either 3N or 2N KOH. The whisker was connected to a variac AC voltage source and submerged in the KOH solution. An AC voltage of 2-6Vrms was applied to the submerged tip. Etching continued for approximately 1 second and then the tip broke, preventing further current flow. The

* Although this standard procedure was adequate, a refined method was also examined. By etching the whisker down to ~1μm, raising the whisker so that the meniscus surrounded the 1μm diameter region, and repeating the AC etch, tips of 10nm radius could be produced much more readily.

sharpness of the tip resulted from this fast switching off of the etch. The procedure produced tips with radii in the range 10-200nm as seen in SEM micrographs.*

The contacts were formed as in Fig. 3.1. Before etching, the whisker was bent into an L shape. Half of the L was used as a spring to press the tip into the tantalum. Contacts were formed in superfluid He at 1.8K with a mechanical approach mechanism driven by a motor outside the dewar. At this temperature the Ta is superconducting (T_c=4.5K) and the W remains normal.

The dynamic resistance was measured by recording the AC voltage developed on the contact through a voltage divider as shown in Fig 3.2. This voltage is proportional to the dynamic resistance, dV/dI, of the contact. It was measured with a lock-in amplifier at a frequency of 1-10kHz. A bias voltage was imposed on the contact through another resistor. The dynamic resistance vs voltage (RVC) curves were generated by plotting AC voltage vs bias voltage. The current flowing through the contact was also recorded by measuring the voltage across the bias resistor. The slope of this current with respect to the bias voltage was used to measure the absolute resistance of the contact. The dynamic resistance signal could then be normalized to this value.

The ability to change the force on the contact via the L-shaped spring allowed stable contacts in the range from 10-1000ohms. After initial contact, increased force produced a series of jumps to lower resistance, yielding a series of RVCs with decreasing contact resistance

* Caution had to be used in forming the SEM image of very sharp tips (10s of nm). Overexposure dulled these tips within 10s of seconds.

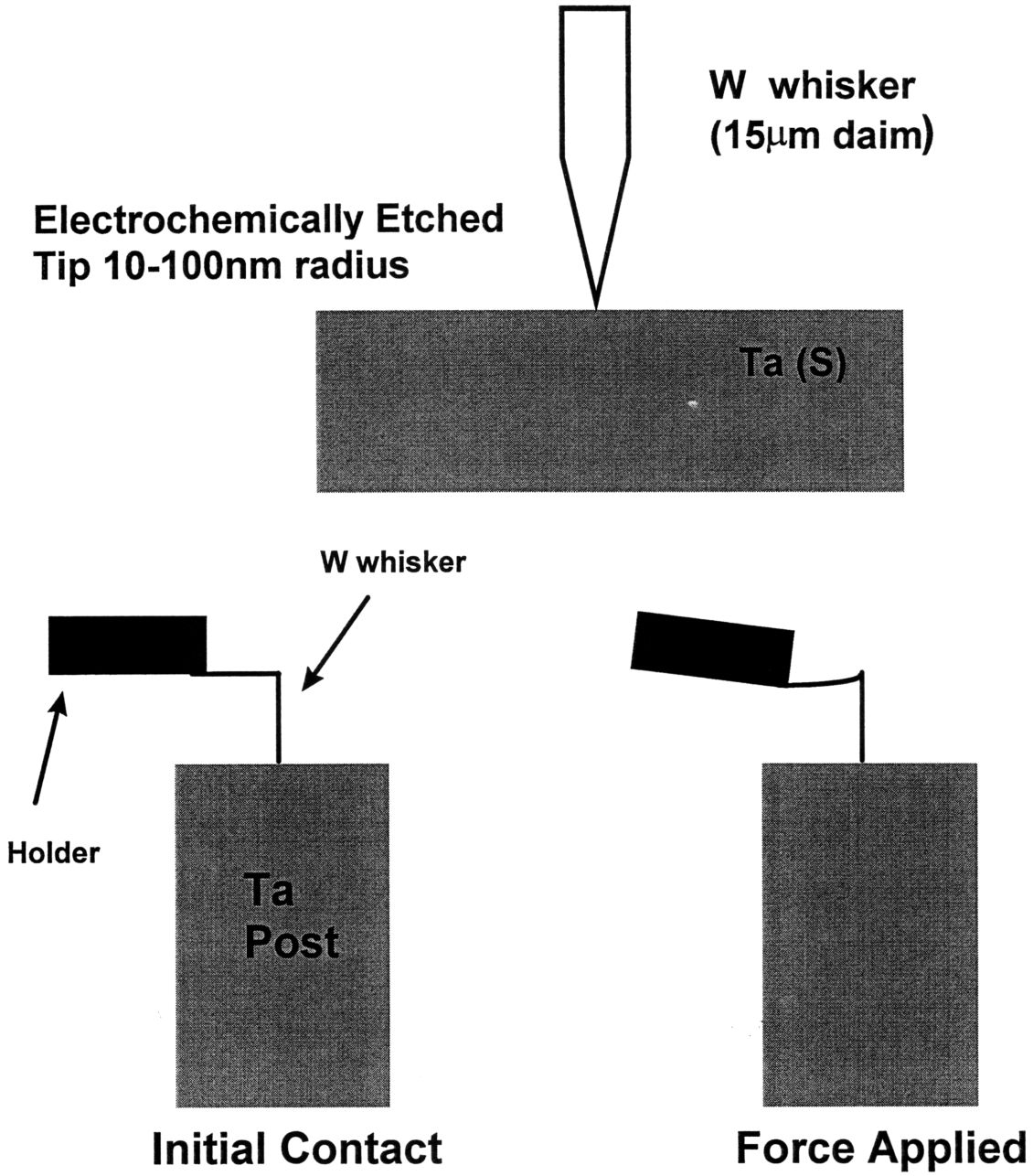

Fig. 3.1 Ta-W Point Contacts. The point contacts of this thesis were formed in superfluid He by pressing a sharpened tungsten whisker into a polished Ta post with a mechanical positioning device. The whisker was bent into an L before etching and the top half of the L was used to gradually increase the force on the contact until current flowed from the W to the Ta. Increased force produced a series of decreasing contact resistances. The top picture shows a schematic of the contact area with dimensions.

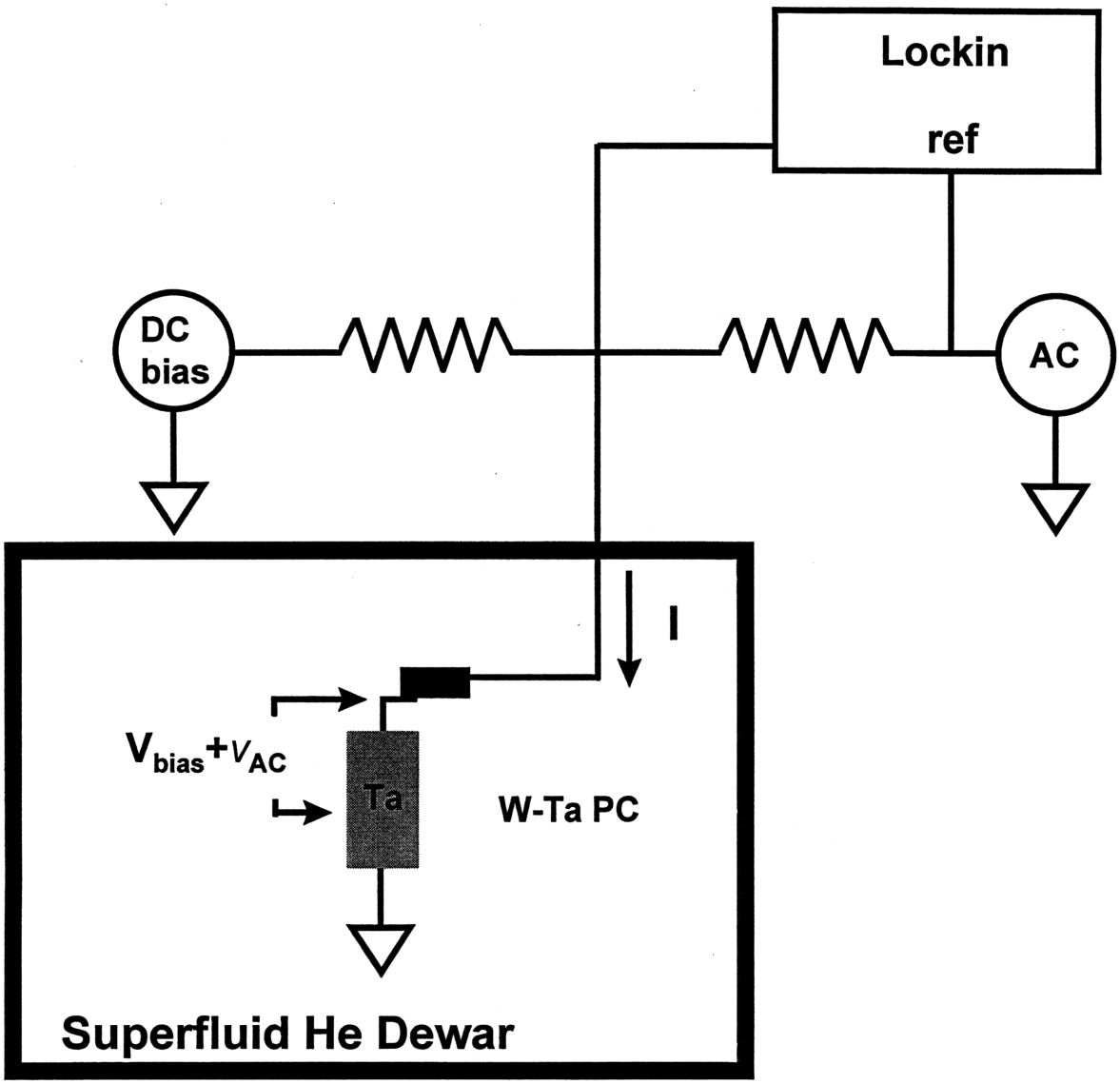

Fig. 3.2 Measurement of Dynamic Resistance. The Ta-W point contact resistance was measured by recording the AC voltage developed on the contact through the voltage divider arangement shown.. A bias voltage was also coupled to the contact and recorded along with the AC voltage. The DC current was also measured across the bias resistor

Fig. 3.3 Dynamic Resistance of Ta-W Superconductor Normal-metal Point Contacts. Normalized dynamic resistance vs bias voltage from Ta-W point contacts at 1.8K. Data from four contacts is shown. Each series of decreasing contact resistance is generated by increasing the force on the contact. The dynamic resistance is normalized to 1 at a bias voltage of 5mV. Each division corresponds to a change of 0.2 in normalized dynamic resistance. The curves are offset for clarity.

3.3a (curves offset for clarity)

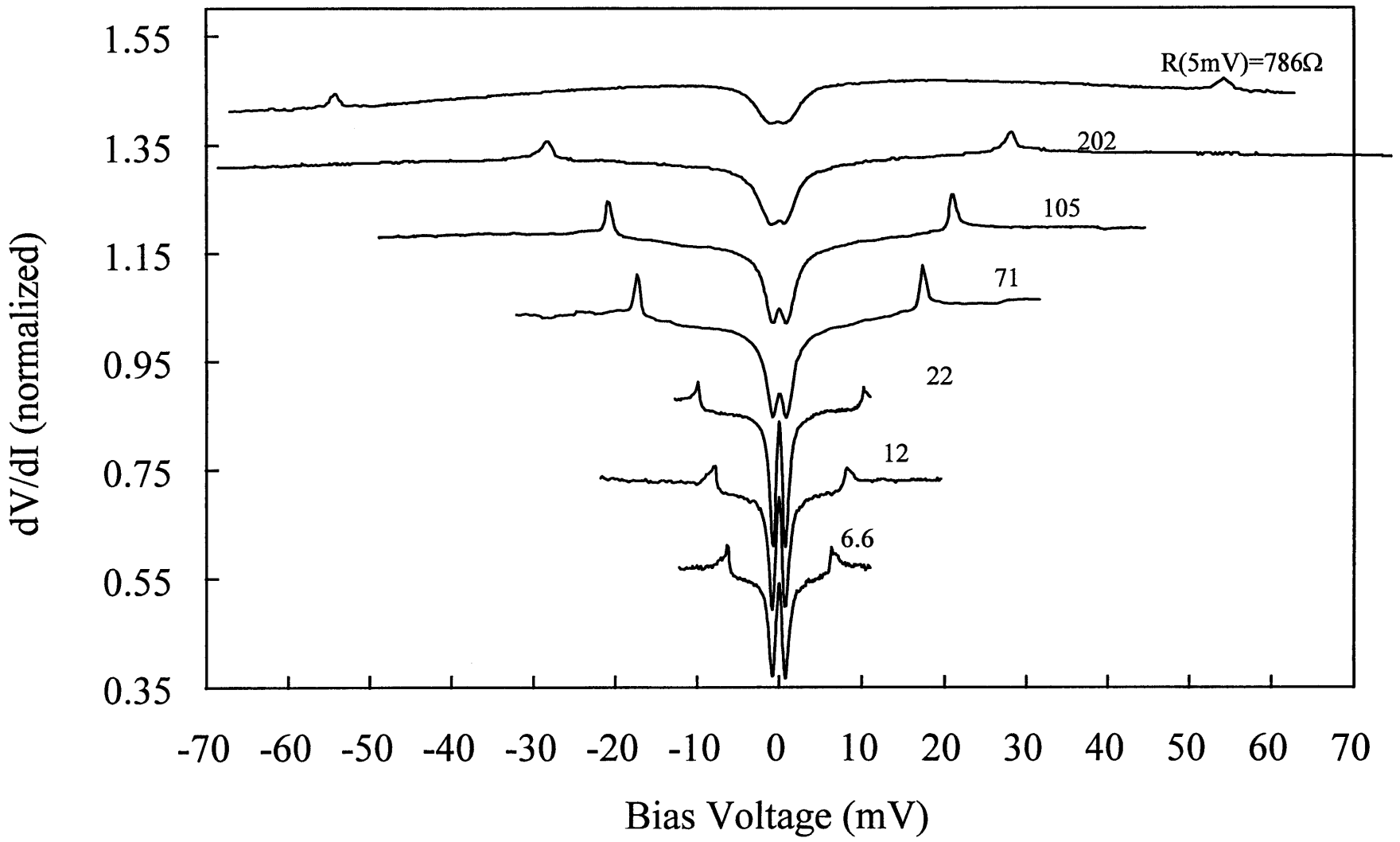

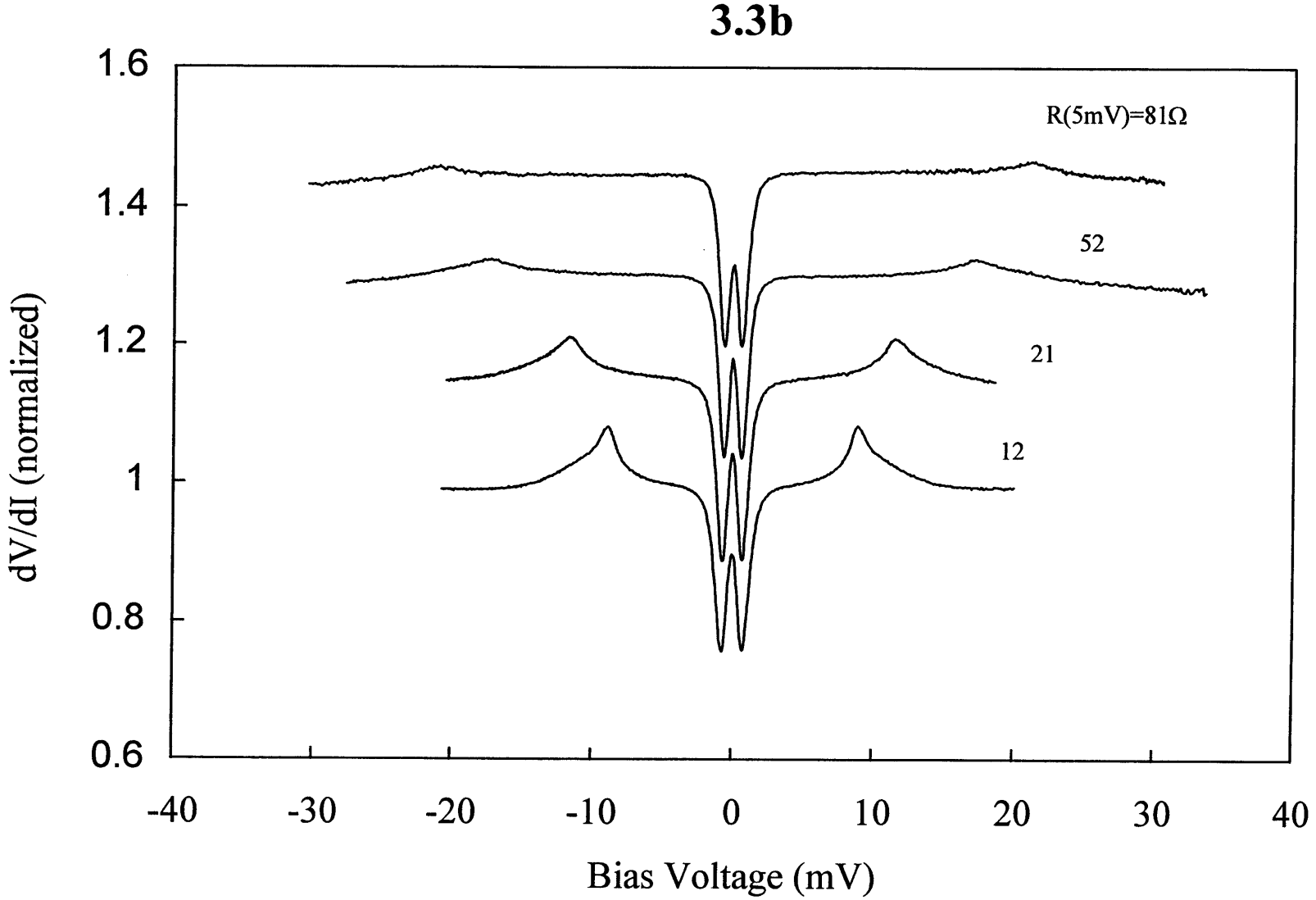
3.3b
R(5mV)=81Ω
52
21
12
dV/dI (normalized)
1.6
1.4
1.2
1
0.8
0.6
-40
-30
-20
-10
0
10
20
30
40
Bias Voltage (mV)

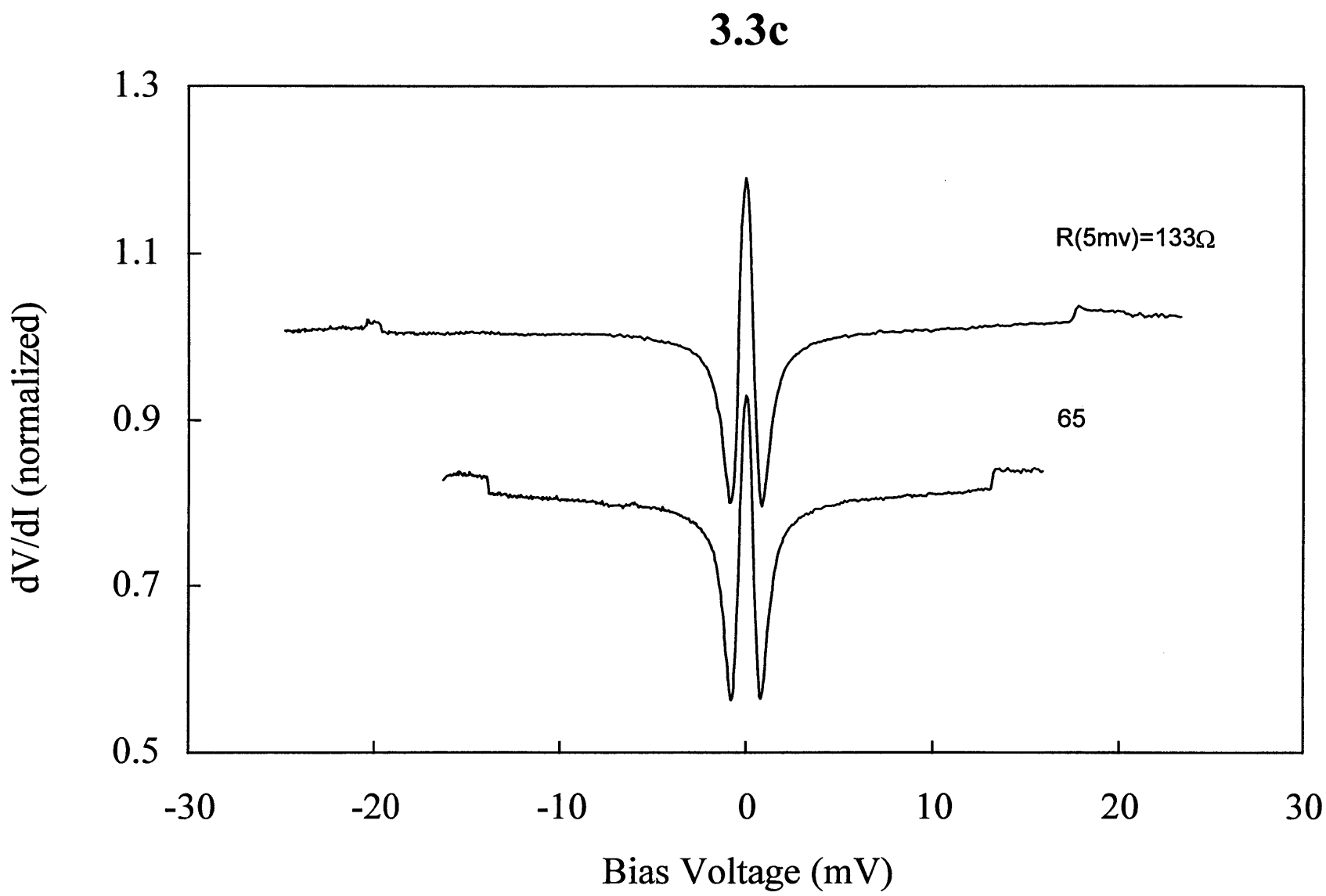
3.3c
1.3
1.1
0.9
0.7
0.5
dV/dI (normalized)
R(5mv)=133Ω
65
-30
-20
-10
0
10
20
30
Bias Voltage (mV)

3.3d

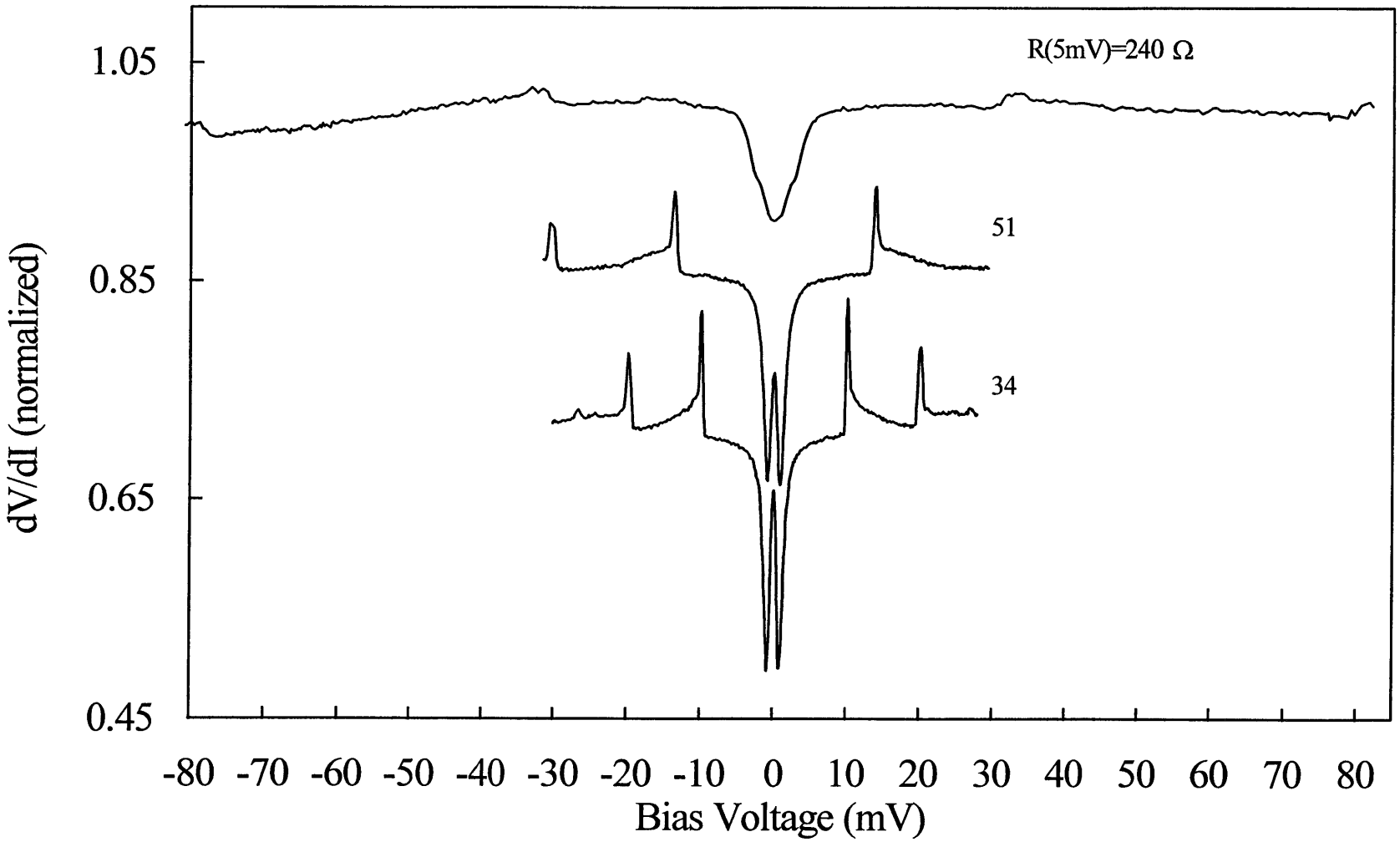
R(5mV)=240 Ω
51
34
1.05
0.85
0.65
0.45
dV/dI (normalized)
-80 -70 -60 -50 -40 -30 -20 -10 0 10 20 30 40 50 60 70 80
Bias Voltage (mV)

3.3 Results and BTK Modeling

3.3.1 Dynamic Resistance

Fig. 3.3 shows four series of RVCs generated in this manner. Each plot shows the curves generated on a given contact by increasing the force on the contact. The curves are shown in order of decreasing resistance (increasing force). The resistance of each RVC measured at a bias voltage of 5mV is shown next to the curve and each curve is normalized to unity at 5mV. The curves are offset for clarity, but the scale is the same for each. The decreases in resistance are produced by increasing the force on the contact as described in the last section. The high bias peaks always occur in symmetric pairs. Very little hysteresis is observed in scanning the bias voltage both ways over the finite bias peak. The peaks can be both sharp or broad. For each contact the voltage at which the peaks occur, V_{peak}, is linear in the square root of contact resistance R (see Fig. 3.4):

$$V_{Peak} = k\sqrt{R} + V_o . \qquad (3.1)$$

Where k~1.8mV/$\sqrt{\Omega}$ on average and varies by 30% between contacts and V_o is 3mV on average.

Although most contacts showed one peak, a few showed no peaks. The peak may have been too broad to be observed in these contacts. The contacts could also show more than one peak as in Fig 3.3d. The higher order peaks also fall on a line. The values of k and V_o for the second set of peaks in Fig. 3.3d is 4.6mV/$\sqrt{\Omega}$ and -4.5mV. Fig. 3.4 plots the dynamic resistance peak voltage V_{peak} vs the square root of the contact resistance for the resistance peaks of all of the plot of Fig 3.3.

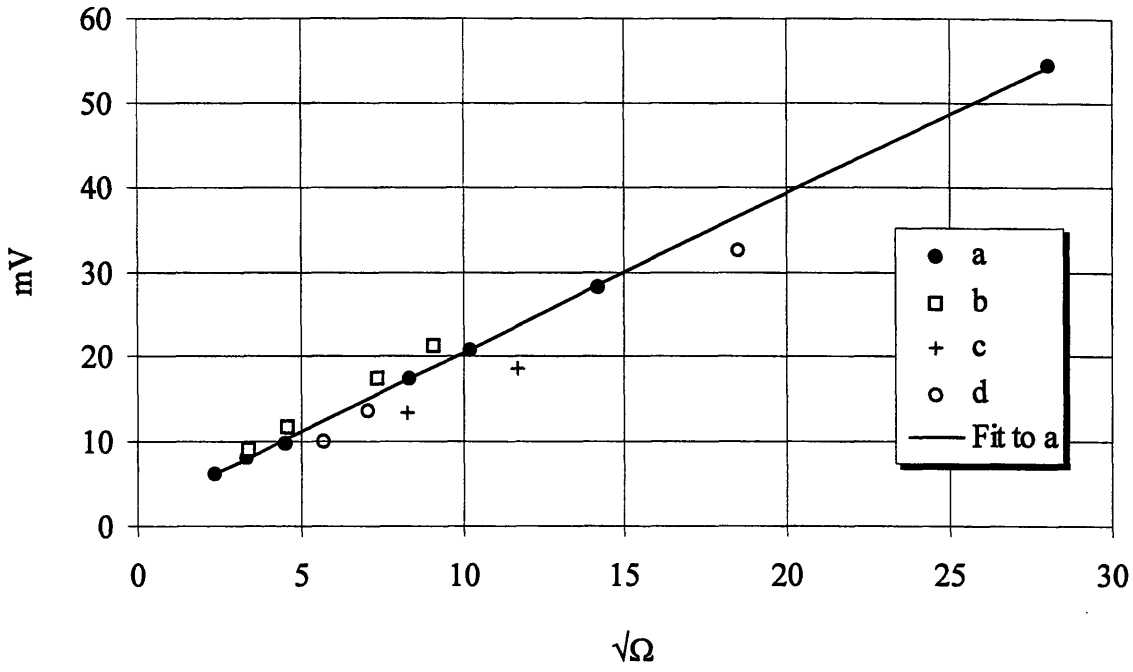

Fig. 3.4 Resistance Peak Voltage vs Contact Resistance. Bias voltage of dynamic resistance peaks (V_{peak}) plotted vs the square root of the contact resistance ($\sqrt{R_N}$). The series of points are taken from Fig. 3.3 and have the same letter. The line shows a linear fit to series a.

3.3.2 BTK fit of the Dynamic Resistance

The zero bias structure for all of the RVCs is well fit to the BTK model including finite quasi-particle lifetime parameter, Γ, which was described in the last chapter. The temperature was recorded during the run to be 1.8K. This value was fixed during the fitting procedure and the BTK parameters Δ, Z and Γ were varied to produce the best fit. The method used was a standard nonlinear least squares technique performed with the Levenberg-Marquardt method[7]. Fig. 3.5 shows the fits to all of the curves of Fig 3.3. The quality of the fits is excellent for R<200Ω and less accurate for R>200Ω. The fits show that as the contact resistance decreases, the BTK barrier strength Z tends to increase slightly and the lifetime parameter Γ tends to decrease. For instance, in the curves in Fig.

3.3a, Z and Γ range from 0.47 and 1mV (R=780Ω) to 0.67 and .05mV (R=6.6Ω); the curves in Fig. 3.3d yield Z and Γ ranging from 0.34 and 1.2mV (R=240Ω) to 0.60 and 0.14mV (R=34Ω). This trend is consistent with earlier measurements of contact resistance as a function of the force on the contact, and is discussed in Appendix A. The accuracy of the BTK model in describing the current flow through the W-Ta point contacts will be exploited in the next chapter when a model of the photoresponse of these contacts is developed. In this model, the BTK parameters derived from this fitting procedure will be used to compute the current increment induced by light.

3.3.3 Ballistic Conductance and Contact Radius

The accuracy of the BTK fit is strong evidence that conduction through these contacts is ballistic (contact radius, a, less than electron mean free path, ℓ_e) since the BTK theory assumes ballistic conduction and is modified in the diffusive regime[8,9]. Moreover, the barrier parameter Z is ~0.5 for most contacts. This means that the contacts all have low barriers and are very transmissive*. As a result the resistance is determined almost entirely by the size of the contact.

Relating this resistance to the contact radius provides further proof that the conduction through these contacts is ballistic. As discussed in the previous

* The BTK transmission coefficient[9] is $T=(1+Z^2)^{-1}$.

Fig. 3.5 BTK Fit of the W-Ta SNPC Dynamic Resistance. Solid line: data; Dashed line: fit. The dynamic resistance vs bias voltage from Fig 3.3 is plotted along with the best fit dynamic resistance curve using a modified BTK conductance model that includes the effects of inelastic scattering near the contact via the lifetime parameter Γ.

3.5a

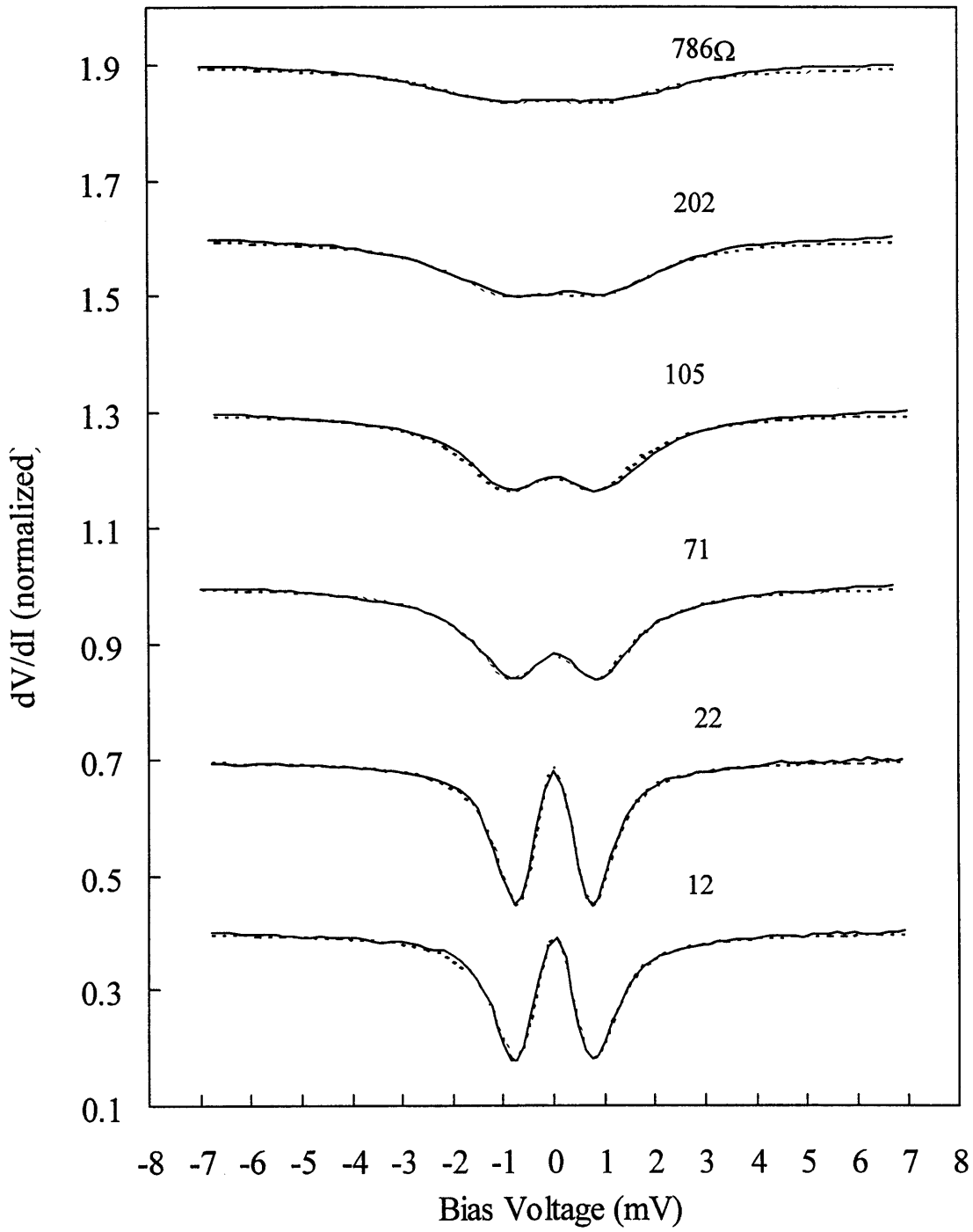
786Ω
202
105
71
22
12
1.9
1.7
1.5
1.3
1.1
0.9
0.7
0.5
0.3
0.1
dV/dI (normalized)
-8 -7 -6 -5 -4 -3 -2 -1 0 1 2 3 4 5 6 7 8
Bias Voltage (mV)

3.5b

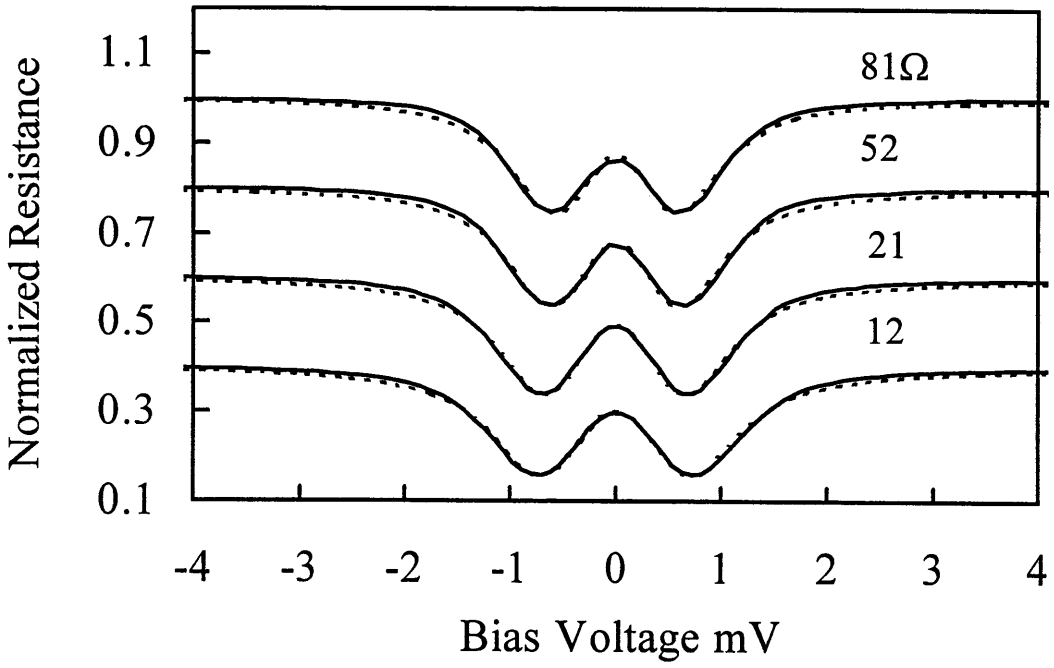
Normalized Resistance
1.1
0.9
0.7
0.5
0.3
0.1
81Ω
52
21
12
-4
-3
-2
-1
0
1
2
3
4
Bias Voltage mV

3.5c

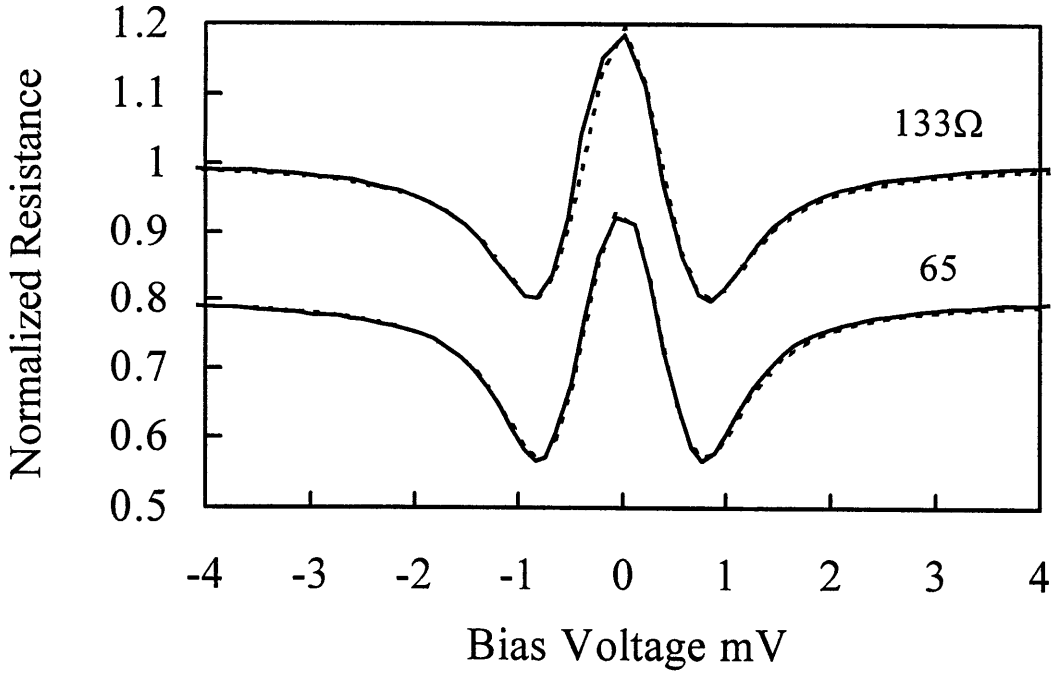
Normalized Resistance
1.2
1.1
1
0.9
0.8
0.7
0.6
0.5
133Ω
65
-4
-3
-2
-1
0
1
2
3
4
Bias Voltage mV

3.5d

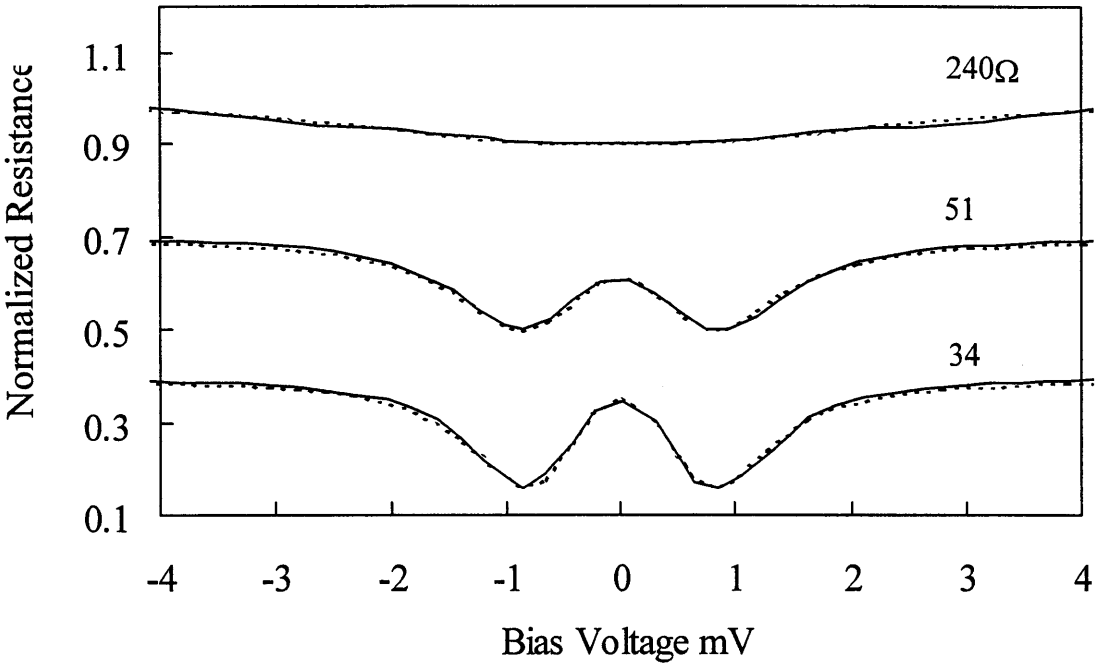

chapter, $a \ll \ell_e$, the resistance is related to the contact radius, a, by the ballistic BTK-Sharvin resistance formula*:

$$R_{Sh} = \frac{1+Z^2}{2N(0)e^2 v_F \frac{\pi}{4} a^2},$$

and, if $a \gg \ell_e$, by the diffusive, or Maxwell resistance formula:

* The formula is the same as the Sharvin resistance for ballistic constrictions except for the factor $(1+Z^2)$ which accounts for reflection off of a residual oxide barrier. See Chapter 2.

$$R_{Maxwell} = \frac{\rho}{2a}$$

Only one of these formulas will give a consistent value of the contact radius. For a contact resistance of 10Ω, the two formulas give R_{Sh}=7nm (with values of the density of states[10], and Fermi velocity[11], N(0)=1.6x10^{28}states/eVm^3, and v_F=8.9x10^{5}m/s) and $R_{Maxwell}$=0.05nm (with a high estimate[12] for the low temperature resistivity of tungsten, ρ_W=0.1μΩcm). Clearly, the contact resistance is too large to be well described by the diffusive conductance formula. It is therefore assumed in the next section, that the BTK-Sharvin formula can be used to relate the contact resistance and the contact radius.

Since Z is approximately the same for most contacts, the product $\sqrt{R_{Sh}a^2}$ is approximately constant for all contacts, and the BTK-Sharvin resistance formula can therefore be converted into a useful relation to estimate the contact radius from the measured contact resistance:

$$\sqrt{R_{Sh}a^2} = \sqrt{\frac{1+Z^2}{2N(0)e^2v_F\frac{\pi}{4}}}$$

With values for N(0) and v_F for tungsten as given above, and taking Z=0.5, $\sqrt{R_{Sh}a^2}$ =19nm$\sqrt{\Omega}$. Using this relation, the inferred contact radius, *a*, for the RVCs in Fig. 3.3 ranges from 1nm to 10nm.

As can be expected, these contact radii for current flow are less than the geometrical tungsten whisker tip radius of 10-200nm measured in an SEM micrograph.

This difference results from the plastic deformation that the W tip undergoes when it pierces the native oxide layers (~1nm of Ta_2O_5 [Ref 13]; ~one monolayer of WO_3 [Ref. 14]) and forms the low barrier electrical contact with the Ta sample (See Refs 14,15, and Appendix A). The result is a blunted W tip of radius 10-200nm, and a 1-10nm contact for current flow formed when the initially much sharper W tip, or an asperity on a blunted tip, pierces the oxide layers.

3.4 Model of Finite Bias Resistance Peaks

3.4.1 Destruction of Superconductivity

The finite bias resistance peaks can be understood by considering the Andreev scattering that occurs at the Normal-metal Superconductor (NS) interface between the tungsten and tantalum. As discussed in Chapter 2, Andreev reflection at the NS interface results in an excess current for bias voltages far above the superconducting gap, Δ. The resulting current voltage characteristic in the region of the resistance peaks ($V>>\Delta$) is:

$$I(V >> \Delta) = \frac{V}{R_N} + I_{excess}. \qquad (3.2)$$

I_{excess} is independent of voltage, and $I_{excess}R_N \sim \Delta/e$. When superconductivity is destroyed at the contact the excess current is reduced, and the resulting shift in the IVC appears as a peak in the dynamic resistance. This process is depicted in Fig 3.6 which shows how a finite bias resistance peak corresponds to a decrease in excess current just as the resistance minimum at $V=\Delta$ corresponds to the build up of excess current. This argument

in indirect, however, section 4.5 of this thesis presents a direct optical measurement of the destruction of superconductivity when the finite bias peak occurs.

The model of the finite bias peaks considered here assumes that superconductivity is destroyed by the magnetic field produced by current flow through the contact. The dependence of resistance peak voltage V_{peak} on contact resistance R_N then follows by considering the critical current of the constriction formed by the contact and the relationship between the radius of the contact and its resistance.

Since the RVCs have large resistance and are well described by the BTK theory (see section 3.3.3) one can reasonably estimate the contact radius from the measured resistance in the absence of superconductivity using the ballistic BTK-Sharvin result:

$$R_N = \frac{1+Z^2}{2N(0)e^2 v_F \frac{\pi}{4} a^2} \tag{3.3}$$

Therefore:

$$a \propto \frac{1}{\sqrt{R_N}}.$$

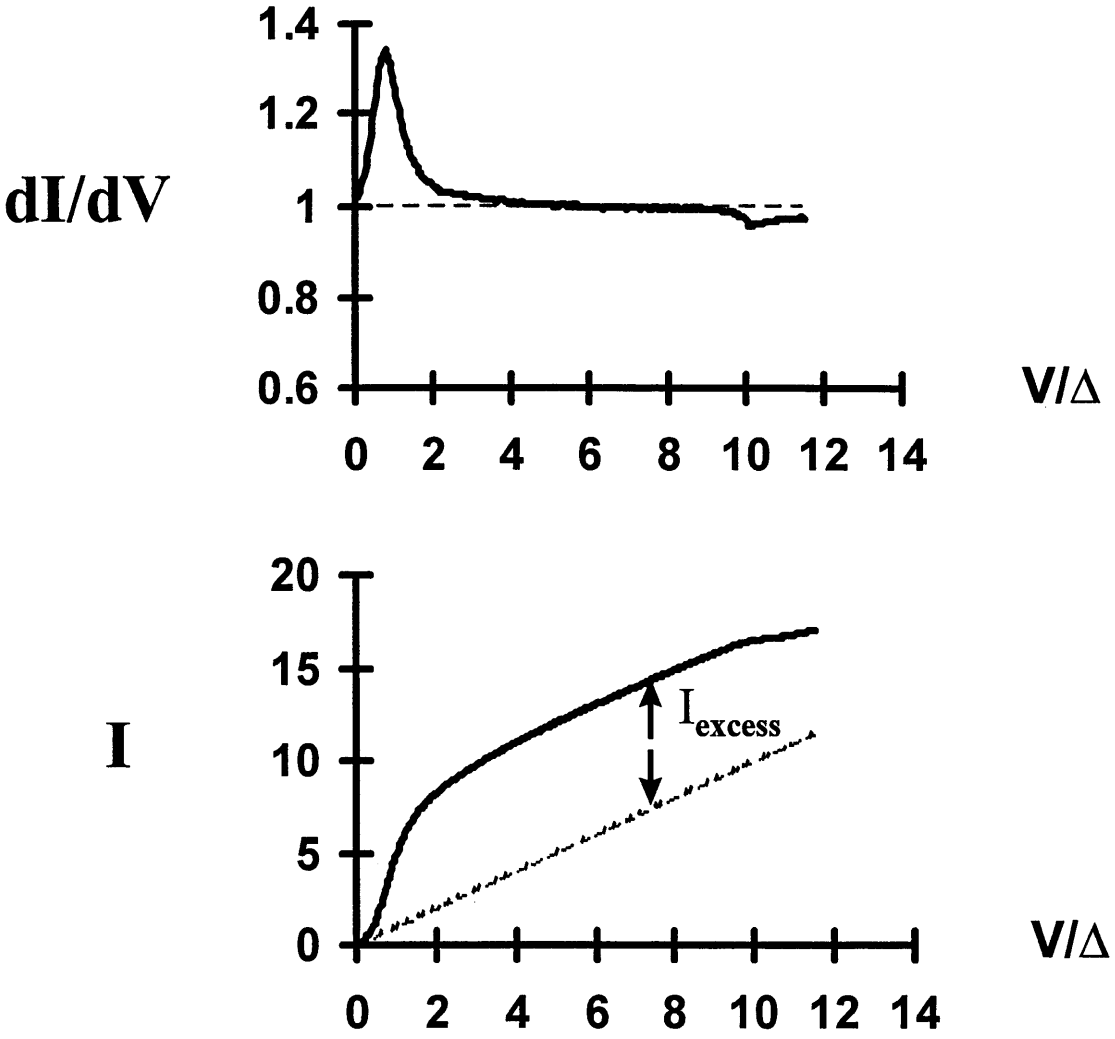

Fig. 3.6 **Connection between Resistance Peaks and Excess Current.** The bottom plot shows a greatly exaggerated graph of the IVC associated with the dynamic resistance of the top plot. The dashed lines correspond to the ohmic current and constant dynamic resistance when both sides of the contact are normal metals. These plots show that the resistance peak corresponds to a decrease in excess current flowing through the contact, and must therefore be related to destruction of superconductivity at the contact.

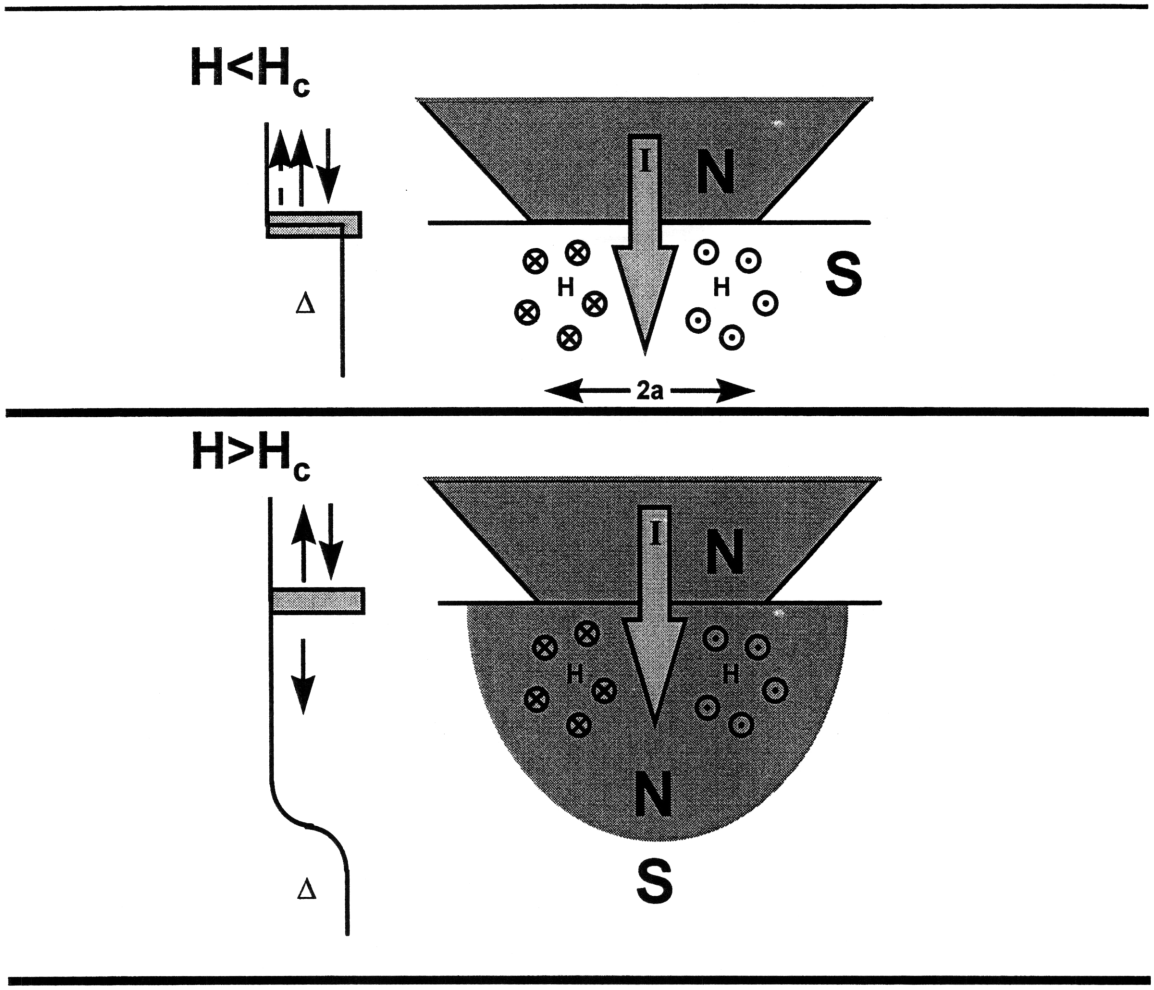

Wire Model: $H_c=I_c/2\pi a$

Fig. 3.7 **Model of Resistance Peaks.** The figure depicts the onset of the critical field near the contact which results in destruction of superconductivity at the contact. The result is a switching off of excess current due to Andreev reflection which manifests itself as a peak in the dynamic resistance.

3.4.2 Critical Current

Current flow through the contacts is restricted to a region of radius a and length of order quasi-particle elastic mean free path ℓ_e. This current will be encircled by a magnetic field whose maximum value can be computed as in a wire of radius a: $H_{max}=I/(2\pi a)$. Therefore the critical current for such a constriction should be:

$$I_c = 2\pi a H_{c1}, \tag{3.4}$$

where H_{c1} is the superconducting critical field. Previous measurements[16] on 99.95% pure tantalum showed that it was a type II superconductor. A type II superconductor expels magnetic flux up to a field H_{c1} and supports a mixed state up to a field H_{c2}. Beyond this is a surface superconducting state that exists up to a field H_{c3}. This surface superconductivity, though, exhibits no gap[17]. Therefore the appropriate critical field for Eq 3.4 is H_{c1}, when magnetic flux first penetrates the superconductor and alters the Andreev scattering at the NS interface. A diagram depicting the onset of the critical field is shown in Fig 3.7.

3.4.3 Dependence of V_{peak} on R_N.

Combining equations 3.3 and 3.4 gives the correct dependence of V_{Peak} on R_N:

$$V_{Peak} = \left(2\pi a H_{c1}\right)R_N - I_{excess}R_N = k\sqrt{R_N} + V_o \tag{3.5}$$

$I_{excess}R_N \sim \Delta/e$ and does not depend the contact radius.

The constant V_o is negative in this formula, however the measured value of V_o is in fact positive. (See Fig 3.4) This can be accounted for by including the Maxwell correction[18] to R_N via Eq. 2.7 of the last chapter:

$$R_N = \frac{1+Z^2}{2N(0)e^2 v_F \frac{\pi}{4}a^2}\left(1+\frac{3\pi}{8}\Gamma(K)\frac{a}{\ell_e}\right)$$

where $K=\ell_e/a$. The coefficient $(3\pi/8)\Gamma(K)$ is close to unity* for all values of K and so an approximate form for this result may be used:

$$R_N = R_{Sh}\left(1+\frac{a}{\ell}\right)$$
$$\ell \cong \ell_e$$

$$R_{Sh} = \frac{1+Z^2}{2N(0)e^2 v_F \frac{\pi}{4}a^2} \tag{3.6}$$

This refinement gives the same k as before but changes V_o:

$$V_{Peak} = k\sqrt{R_N} + V_o + O\left(a/\ell_e\right), \tag{3.7}$$

where

$$k = 2\pi H_{c1}\sqrt{R_{Sh}a^2} \tag{3.8}$$

and

*$(3\pi/8)\Gamma(K)$ varies from 0.817 in the Sharvin limit K>>1 to 1.18 in the Maxwell limit K<<1. See Chapter 2.

$$V_o = \frac{\pi H_{c1}\left(R_{Sh}a^2\right)}{\ell} - I_{excess}R_N \qquad (3.9)$$

The measured value of k=1.8mV/√Ω., along with the value of $\sqrt{R_{Sh}a^2}$ ~19nm√Ω computed in section 3.3.3 implies a value of H_{c1}=1.53x10^{4}A/m=193gauss. This may be compared with the value of H_{c1} from the measurement of Ref. 16 on 99.95% tantalum which was H_{c1}=375gauss at 1.8K. The discrepancy between these values can be due to impurities, which reduce the value of H_{c1} in a type II superconductor[19]. A decreased H_{c1} can also result from ohmic heating at the contact, an effect discussed in the next section.

As a check of consistency, the mean free path ℓ_e may be estimated from the value of V_o, which was ~1mV in most of the contacts. The value $I_{excess}R_N$ varied between contacts due to the variation of Z and Γ. This quantity was determined from the measured current vs voltage, as well as an integral over the properly normalized dynamic resistance. These two methods agreed, and on average $I_{excess}R_N$~0.3mV. Taking these values, the above formula gave a mean free path ℓ_e~13nm. This value is consistent with the assumption of a ballistic microconstriction, since the values of R_N implied contact radii of 10nm or (in most cases) less.

3.5 Discussion

3.5.1 Effect of local heating.

At large enough bias voltages, one expects to see an effective temperature increase of the superconductor in a small volume near the contact due to power

dissipation in this region. This increase in temperature depends only on the power dissipated in the contact and results in a decreased critical field H_{c1}, which is consistent with the low value inferred from the model of section 3.4. It is important to note that the dependence of V_{peak} on R_N implies that the power dissipated in the contact when the peak occurs is always the same(neglecting the small offset V_o):

$$V_{peak} \propto \sqrt{R_N} \Rightarrow V_{peak}^2/R_N = \text{constant} \sim 4\mu W.$$

This means that the increase in effective temperature near the contact will be the same for all contacts. As a result, the same reduced value of H_{c1} applies for all values of R_N on a given contact, in agreement with observation.

To estimate the heating in the contact we assume that the quasi-particles injected into the bulk tantalum sample form a region with an elevated effective temperature T* of dimension equal to the quasi-particle diffusion length, L_{qp}. A simple rate equation argument shows that the steady state increase in density of quasi-particles in this region is proportional to the power P dissipated in the contact: Most of the dissipated energy is distributed among the quasi-particles, with very little excess energy in the phonons[20]. The dissipated power divided by the average quasi-particle energy ($\sim\Delta$), is thus the rate of quasiparticle creation. Multiplying this rate by the lifetime of a quasiparticle τ_R (the time for two quasi-particles to recombine), and dividing by the volume of the region of increased quasi-particle density, L_{qp}, then gives the excess density*:

$$\delta N_{qp} \sim (P/\Delta)(\tau_R/L_{qp}^3).$$

* This result uses an average value for the pair recombination time $\tau_R(T^*)$ and $L_{qp}(T^*)$

The effective temperature T* can then be estimated from the relationship between the total number of quasi-particles and the temperature[21]:

$$\delta N_{qp} \sim N_T = 4N(0)\left[\pi\Delta(T)k_B T/2\right]^{1/2} e^{-\Delta(T)/k_B T}. \qquad (3.10)$$

The typical dissipated power at V_{peak} is 4μW. The exact value of L_{qp} and τ_R are not known for these contacts, but taking typical values of L_{qp}=5μm and τ_R=2x10^{-8}sec (See Chapters 4 and 5) a temperature increase of order 1K results. According to Ref. 16, this would decrease the critical field to ~200 gauss consistent with the value inferred from the model of the finite bias peaks.

3.5.2 Temperature Dependence of Finite Bias Peaks.

The temperature dependence of V_{peak} was also measured. The helium in which the contact was immersed was allowed to slowly warm from 1.8K through the superfluid to normal He transition at 2.15K and up to 4.3K while the dynamic resistance was continuously scanned. Fig. 3.8 shows the finite bias peak of Fig 3.3b at several temperatures. These measurements showed that V_{peak} decreased by about 10% before flattening to nothing at a temperature of ~3K.

These observations can be qualitatively understood by considering the effect of both heating and magnetic field at the contact. The resistance peak voltage V_{peak} is linear in the critical field H_{c1} (See Eq 3.8 and 3.7.), however H_{c1} depends on the effective temperature due to power dissipation at the contact as well as the thermal bath

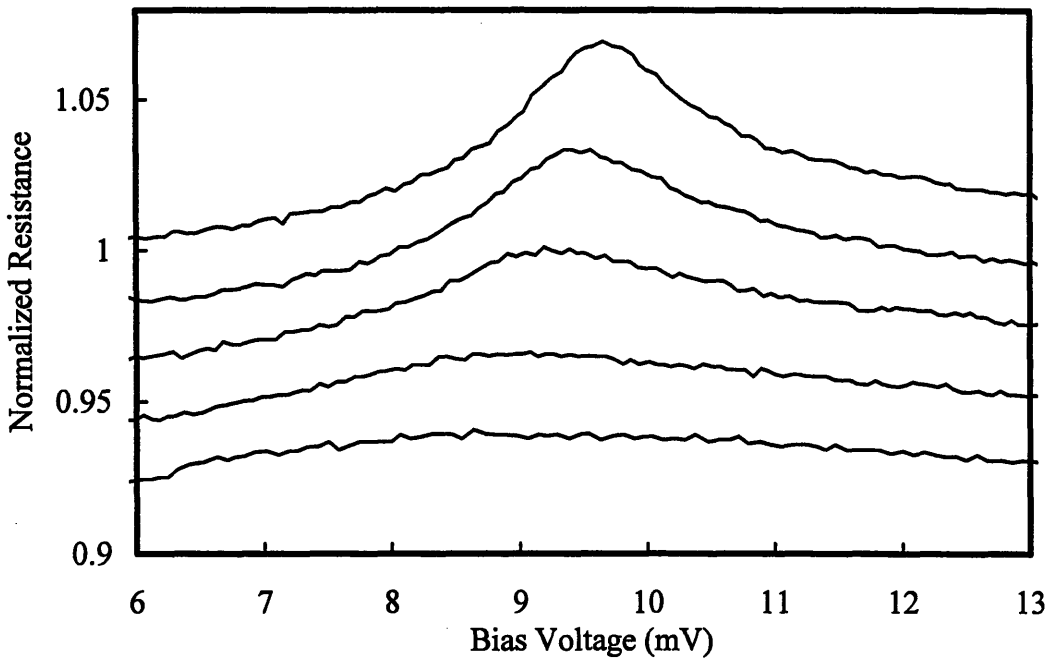

Fig. 3.8 **Temperature Dependence of Finite Bias Resistance Peaks.** Each dynamic resistance curve has the same scale but is offset for clarity. Each curve has a different temperature. Starting with the top curve, T=2.00K, 2.28, 2.56, 2.82, 3.06.

emperature. The weak temperature dependence results if the quasi-particle density generated by power dissipation at V_{peak} is much larger than the initial thermal quasi-particle density. In this case the effective quasi-particle temperature when the bias voltage equals V_{peak} depends mainly on the dissipated power V_{peak}^2/R_N, and so V_{peak} will have a weak dependence on thermal bath temperature. Moreover, at a high enough bath temperature, one expects heating to destroy the superconductivity via a smooth 2nd order transition before the magnetic field is large enough to destroy superconductivity. This is also observed in Fig 3.8.

Above 3K the contact of Fig 3.8 showed occasional sharp peaks at bias voltages near the finite bias peak. These could originate from resonances inside the normal region in a manner similar to the mechanism of Hahn[4]. The peaks may also be due to changes in the liquid He: These temperature measurements could be complicated by the superfluid to normal helium transition at T=2.15K. Additional, unwanted temperature dependence due to the turbulence and altered thermal conduction in the normal helium can not be ruled out.

3.5.3 Comparison with Previous Work.

Having inspected other mechanisms for the finite bias peaks, the following are inconsistent with the observations of the point contacts of this thesis: As mentioned above, simple heating of the contact would cause a gradual transition, inconsistent with the sharp change in I_{excess}. Mechanisms that involve a critical current density, such as depairing current density, J_c are ruled out because of the dependence of V_{peak} on R_N: If the peak always occurred at a critical current density value, J_c, then, neglecting I_{excess}, $V_{peak}=R_N J_c \pi a^2$, and since $R_N \propto 1/a^2$, V_{peak} would not change as R_N changed. This would exclude the depairing current density mechanism considered in Ref 1. Also, the mechanism of reabsorption of Andreev holes proposed as an explanation for the RVC peaks in the S-Sm-S structure of Ref. 6 has little applicability in the W-Ta SNPCs used here since it relies on current confinement in a thin planar region bounded by the superconductor. The quantum interference which is discussed in Ref 4 does not easily explain the dependence of V_{peak} on R_N. Instead, the W-Ta PCs of this thesis seem to

show only the first rapid decrease in excess current observed in Ref. 5, and none of the subsequent interference oscillations observed by these authors.

3.5.4 Flux Quantization.

A calculation of the magnetic flux surrounding the current implies that each peak corresponds to a single flux quantum:

$$\Phi_o = \frac{hc}{2e} = 2.07 \times 10^{-7}\,\text{gauss} - \text{cm}^2$$

A single flux quantum carrying a field equal to the critical field must be approximately 100nm in radius. This is of order the contact radius and implies that field destroying superconductivity at the contact is contained in a single flux quantum. This dimension is of order the penetration depth λ of magnetic fields in the Ta. Note that this is not the dimension of the region where superconductivity is destroyed at the contact. The dimensions of the destroyed region are of order the coherence length ξ of Ta, which is much small than the penetration depth. Both of these lengths have been measured in crystalline Ta samples[22] at low temperature and found to be λ~100nm and ξ~31nm. The added impurities in the 99.95% polycrystalline Ta of this thesis would make λ go up and ξ go down, which is in closer agreement with dimensions of the vortex which is expected to form in these contacts when superconductivity is destroyed at the contact. If the coherence length of the tantalum is small enough, a single flux quantum may not be enough to completely eliminate the SN boundary. Therefore when the current increases

enough to produce another quantum of flux a further decrease in excess current, and corresponding resistance peak, will be observed as in Fig. 3.4d.

3.6 Summary

Above gap RVC peaks have been observed in high impedance, small area W-Ta SNPCs. The voltage of these peaks is linear in the square root of the contact resistance. This observation points to a model in which the RVC peak corresponds to a destruction of superconductivity near the contact from a critical field produced by current flow through the contact. Multiply peaked RVCs and the small size of the contact point to the conclusion that each peak appears when a single additional magnetic flux quantum encircles the current. When heating at the contact is included, the model is in quantitative agreement with observation, the critical field H_{c1} being reduced by heating. The mechanism at work in these contacts is different from those considered in other systems with above gap structure, however these systems have different geometries and larger contact area than the SNPCs in the present study.

---

[1] P. Xiong, G. Xiao, and R. B. Laibowitz, Phys. Rev. Lett. 71, 1907 (1993).
[2]See for example M. Tinkham, *Introduction to Superconductivity*, (Krieger), p 119 (1975).
[3] A. Hahn, and H. Lerchner, in *Prodeedings of the 17th International Conference on Low Temperature Physics, Karlsruhe, 15-22 August 1984,* edited by U. Eckern, A. Schmid, W. Weber, and H. Wühl (North-Holland, Amsterdam, 1984), pt. II, DL 9, p. 803.
[4] A. Hahn, and K. Humpfner, Phys. Rev. B 51, 3660, (1995).
[5] A. Hahn Phys. Rev. B **31**, 2816, (1985).
[6] C. Nguyen, H. Kroemer, and E. L. Hu, Phys. Rev. Lett. 69, 2847, (1992).
[7] W. H. Press, S. A. Teukolsky, W. T. Vetterling, and B. P. Flannery 1992, *Numerical Recipes in C* 2nd Ed. (Cambridge University Press) p. 681.
[8] G. E. Blonder and M. Tinkham, Phys. Rev. B **27**, 112, (1983).
[9] G. E. Blonder, M. Tinkham, and T. M. Klapwijk, Phys. Rev. B **25**, 4515, (1982).

[10] S. V. Vonsovsky, Yu. A. Izyumov, and E. Z. Kurmaev, *Superconductivity of Transition Metals, Their Alloys, and Compounds*, (Spring-Verlag) p 203, (1982).
[11] D. A. Papconstantopoulos, *Handbook of the Band Structure of Elemental Solids* (Plenum Press) p. 176 (1986).
[12] Desai, et. al., J. Phys. Chem. Ref. Data **13**(4), p 1091, (1984).
[13] H. J. Mathieu, M. Datta, and D. Landolt, J. Vac. Sci. Technol. A **3**(2), p. 331 (1985).
[14] H. D. Riccius and K. J. Siemsen, Appl. Phys. A **35**, p. 67 (1984).
[15] K. C. Liu, MIT PhD Thesis, P. 51 (1979).
[16] F. T. J. Smith, and H. C. J. Gatos, Appl. Phys., 39, 3793, (1968).
[17] P. G. deGennes, *Superconductivity of Metals and Alloys* (Addison Wesley: Advanced Book Classics), p. 11 (1989).
[18] A. G. M. Jansen, A. P. van Gelder, and P. Wyder, J. Phys. C 13, 6073 (1980); A. M. Duif, A. G. M. Jansen, and P. Wyder, J. Phys.: Condens Matter 1, 3157 (1989).
[19] See for example M. Tinkham, *Introduction to Superconductivity*, (Krieger), p 111-114 (1975).
[20] W. H. Parker, Phys. Rev. B, 12, 3667, (1975)
[21] W. H. Parker and W. D. Williams, Phys. Rev. Lett. **29**, 924 (1972).
[22] T. J. Greytak, and J. H. Wernick, J. Phys. Chem. Solids **25**, 535 (1964).

Chapter 4

Photoresponse of Ta-W Point Contacts

Introduction

Optical methods have been used extensively to study the nonequilibrium dynamics of both superconductors and normal metals. The most commonly used systems in these studies are thin film tunnel junctions between two superconductors or between a metal and a superconductor. The conductance properties of such tunnel junctions have been well understood since the early 60s. This theoretical understanding makes experiments on tunnel junctions easy to interpret and is the basis for their utility in studying nonequilibrium effects as well as the basic parameters of superconductors and metals, such as the superconducting gap and the electron phonon interaction.

In contrast to this, there have been almost no optical studies using visible or near-infrared radiation on cryogenic point contacts between a sharpened tip and a bulk material where one or both sides are superconducting. In part, this is due to the fact that, as discussed in previous chapters, the conductance properties of these nanoscale point contacts, in which the tunneling barrier is very low or nonexistent, have only been well understood in the last 15 years using the theory of Blonder et. al. (BTK) and its refinements. (See Chapter 2.) Optical measurements of point contacts are promising for several reasons: They are sensitive to the nonequilibrium properties of the irradiated nanoscale tip as well as the bulk material; they should also be useful as a probe of the conductance properties of the contact; finally, point contacts can be formed with materials

that cannot easily be grown in thin films such as certain novel superconductors and crystalline materials.

This chapter presents photoresponse measurements of the superconductor normal-metal point contacts (SNPCs) formed between a nanoscale tungsten metal tip and bulk superconducting tantalum which were described in the last chapter. Optical illumination of these point contacts affects both the metal tip and the bulk superconductor: The effect of light on the superconductor is to induce a nonequilibrium quasi-particle density, which manifests itself as a change in gap of the superconductor; the effect of light on the metal tip can be described by an increase in the effective temperature of the metal electrons. Therefore the photoresponse depends on only two parameters: The changes in the gap of the superconductor, $\delta\Delta$, and the change in the effective temperature of electrons in the metal tip, δT. The photoresponse signal is then proportional to the optically induced current increment resulting from the change in these two parameters and can be computed from the BTK theory of the current voltage characteristic. A fit of the data to this model then yields values of the superconductor gap decrease and metal electron temperature increase as a function of laser intensity. These results will be used in this chapter and the next to describe several novel effects and applications: 1) The photoresponse can be used as an electron thermometer to determine the increase in effective electron temperature of the tungsten metal tip. The dependence of electron temperature on laser intensity points to a previously unobserved mechanism of heat transfer between the irradiated nanoscale W tip and the superfluid He. 2) Since the photoresponse measures the change in gap of the superconductor, the photoresponse can be used as a probe of the flow of excess

current in the contact. As will be shown in this chapter, this probe is very useful in verifying aspects of the model of the finite bias resistance peaks discussed in the previous chapter. 3) Finally, the fact that the photoresponse is sensitive to the optically induced quasi-particle density will be used in the following chapter in a real-time measurement of the quasi-particle recombination time in Ta.

In view of the extensive background section which follows, a brief summary of this chapter will be given: The background section will review theoretical and experiment treatments of nonequilibrium effects in both metals and superconductors. This will be followed in section 4.2 by a description of the photoresponse experiment and presentation of the photoresponse data. In section 4.3 the model of the photoresponse will then be developed and the fit of this model to the photoresponse data will be described. Finally, sections 4.4-4.6 describe the implications of the fit of the model to the photoresponse data. Section 4.4 discusses the linearity of $\delta\Delta$ with power. Section 4.5 discusses use of the photoresponse as a probe of the SNPC conductance mechanisms. Section 4.6 examines the dependence of δT on laser intensity.

4.1 Background

4.1.1 Optically Induced Nonequilibrium Superconductivity

The nonequilibrium state of a superconductor irradiated by visible light was first studied by Testardi[1] in 1971 who performed measurements of the resistance of thin superconducting films irradiated by pulsed Argon ion laser light at 514nm. These early measurements showed that superconductivity could be destroyed by light and, more

importantly, that the nonequilibrium state of an irradiated superconductor could not be described by simple heating of the quasi-particle and phonon distributions. Following this early work, many experimental and theoretical examinations of the problem of an irradiated superconductor have greatly improved our understanding of the interaction between light and superconductors. This work has been part of a larger effort to understand the properties of nonequilibrium superconductivity: The thermal equilibrium state of a superconductor is sensitive to many perturbations such as quasi-particle or phonon injection, microwave radiation, and high energy particles as well as visible and infrared radiation. This section will focus only on the nonequilibrium state induced by visible and infrared radiation. The general topic of nonequilibrium superconductivity has been treated extensively in several works[2,3,4] and a review of the interaction of light with superconductors has also been published[5].

Absorption of Photons. Since visible and infrared photons have energy far in excess of the superconducting gap (1eV>>1meV), their effect on the superconductor is simply to break Cooper pairs resulting in highly excited quasi-particle excitations. These excitations decay very rapidly via electron-electron and then electron-phonon scattering to energy levels of order Δ. These very fast processes are similar to those occurring in a metal since the energy scales are much larger than the gap energy. However, as the quasi-particles relax to energies near the gap edge, the dynamics become fundamentally different from that of an irradiated metal. This is because the ground state of a superconductor is of course fundamentally different from that of a metal: One must to take into account the pair condensate as well as the quasi-particle excitations and the

phonons. In a superconductor, a high energy or "pair-breaking" phonon with $E>2\Delta$ can break a Cooper pair resulting in the addition of two quasi-particles to the condensate. Two quasi-particles can also recombine into a Cooper pair resulting in the emission of a high energy phonon. Low energy phonons can only scatter inelastically or elastically off of quasi-particles as in a metal. There are therefore, three intrinsic time scales that characterize nonequilibrium steady state of an optically illuminated superconductor: the quasi-particle recombination time τ_R, the phonon pair breaking time τ_B, and the inelastic electron-phonon scattering rate τ_{in}. A fourth time scale is the time for a phonon to escape the sample, and is dependent on sample size and configuration. For instance, in thin superconducting films, phonons can escape directly into an underlying insulating substrate.

Model Distributions: μ^* and T^*. Although the steady-state nonequilibrium distribution of quasi-particles in an irradiated superconductor must in general be computed using kinetic theory, there are two limiting cases in which the nonequilibrium quasi-particle distribution can be described simply by a Fermi distribution with changes in either the chemical potential or temperature of the quasi-particles. These are known as the μ^* and T^* models. The μ^* model was first proposed by Owen and Scalapino[6]. It assumes that quasi-particle recombination is the slowest step in the relaxation process of the irradiated superconductor and that the phonons are strongly coupled to the surrounding thermal bath. In this model the phonons and quasi-particles equilibrate to the bath temperature, but the quasi-particles do not equilibrate with the condensate, resulting in a quasi-particle distribution described by the bath temperature and a chemical potential,

μ^*, different from that of the condensate. This model applies best to very thin films at low temperatures since the phonons are strongly coupled to the thermal bath of the substrate and the recombination time for quasi-particles is very long at low temperatures due to the small density of quasi-particles present at low T. An important consequence of the μ^* model is that if the rate of quasi-particle generation is high enough the superconductor will undergo a 1st order phase transition to the normal state. This prediction was confirmed[7] by experiments on thin film tunnel structures using current injection to drive the superconductor out of equilibrium.

If, on the other hand, the phonons are weakly coupled to the surrounding thermal bath and the recombination time is relatively fast, then the energy relaxation will be dominated by quasi-particle recombination and generation with emission and absorption of pair-breaking phonons. In this case the quasi-particles will be in thermal equilibrium with the pair-breaking phonons and both distributions will be described by an effective temperature T*. The low energy phonons will remain at the bath temperature since they can only exchange energy with the quasi-particles via the much slower process of inelastic scattering. The T* model was first proposed by Parker[17] and is applicable in most experiments since phonon escape rates, even in thin films, are often slow compared to the quasi-particle recombination times for temperatures above ~1K.

In a bulk superconductor, such as the Ta used in this thesis, the phonon escape time is long due to the low surface area to volume ratio and low transmission rate of phonons across the Ta superfluid-He boundary. In this case inelastic scattering of high energy phonons to low energies ($E<2\Delta$) becomes the dominant relaxation mechanism of

the high energy phonons. The inelastic scattering rate is typically much less than the pair-breaking time[8]. Therefore very little energy is transferred from the high energy to the low energy phonons and the T* model will be applicable.

An important consequence of the weak coupling of phonons to the bath is the effect known as "phonon trapping". The phonon resulting from the recombination of two quasi-particles is more likely to break a Cooper pair than to escape from the sample or scatter inelastically to $E<2\Delta$. The result is that the effective lifetime of a quasi-particle is enhanced by the factor $1+\tau_{es}/\tau_B$, since the recombination phonons regenerate quasi-particles an average of τ_{es}/τ_B times before the escaping. This effect will be apparent later in this chapter and in the next when the dynamics of the quasi-particle and phonon densities is discussed.

Kinetic Theory Calculations. It is important to mention briefly that these two models are in reasonable agreement with more involved calculations using kinetic theory, but that these more complete treatments also predict new phenomena when the superconductor is strongly perturbed from equilibrium. As mentioned above, in general the quasi-particle and phonon distributions f(E) and $F(\Omega)$ must be calculated from kinetic theory using the electron phonon interaction $\alpha^2(\Omega)F(\Omega)$. Such calculations have been performed for superconductors under optical illumination[9,10]. For weak coupling of phonons to the thermal bath, these calculations show that optical radiation results in a quasi-particle distribution intermediate between the T* and a simple heating model[11]. This result is in agreement with experiment[12]. The deviation from T* is to be expected since the low energy phonons will experience some heating under these conditions, but

not as much as the high energy phonons which can interact more directly with the quasi-particles via pair breaking. For strong coupling to the thermal bath, kinetic equation calculations have been carried out by Elesin[13] and show that for certain values of the temperature and phonon trapping factor τ_{es}/τ_B the gap can be multivalued. Therefore a mixed state results. Many of the predictions of Elesin have been observed[14] however questions remain concerning the mixed state[15,16]. Note however that the prediction of a multivalued gap is in qualitative agreement with the μ^* model prediction of a 1st order phase transition.

Nonequilibrium Dynamics. As will be seen below, the photoresponse measurements of this chapter are not sensitive to the exact quasi-particle distribution induced in the superconductor because they are performed on superconductor normal-metal point contacts rather than contacts between two superconductors. The photoresponse of an SNPC gives information only about the change in gap of the irradiated superconductor. It is therefore important to understand the connection between the change in gap and changes in the quasi-particle distribution. Parker[17] showed that *for small departures from equilibrium, the decrease in gap is proportional to the increase in the total number of quasi-particles*. The relationship is the same for both the μ^* and T^* distributions as well as intermediate distributions. For this reason it is not necessary to examine the time evolution of the full quasi-particle and phonon distributions: Only the dynamics of the total quasi-particle density is important.

The time evolution of the total quasi-particle density was first addressed by Rothwarf and Taylor[18]. They took into account the fact that the dynamics of the quasi-

particles is coupled with that of the pair breaking phonons and developed coupled rate equations for the total densities of quasi-particles and pair breaking phonons. These rate equations take into account all of the processes discussed above: quasi-particle recombination, pair breaking, inelastic electron-phonon scattering and phonon escape from the sample, as well as external sources of quasi-particles and phonons such as optical illumination or quasi-particle currents. A modification to the original equations is the inclusion of diffusive terms to account for spatial variation of the quasi-particle and phonon densities[19]. With all of these considerations Rothwarf and Taylor's equations take the form:

$$\left(\frac{\partial}{\partial t} - D_{qp}\nabla^2\right)N_{qp} = I_{qp} - 2RN_{qp}^2 + \frac{2}{\tau_B}N_{ph}$$

$$\left(\frac{\partial}{\partial t} - D_{ph}\nabla^2\right)N_{ph} = I_{ph} + RN_{qp}^2 - \frac{1}{\tau_B}N_{ph} - \frac{N_{ph} - N_{ph}^T}{\tau_{es}}$$

In these equations, N_{qp} is the total number of quasi-particles, N_{ph} is the total number of pair-breaking phonons (phonons with $E>2\Delta$), and N_{ph}^T is the number of pair-breaking phonons present in thermal equilibrium. As mentioned above, τ_B is the time for a phonon to break a Cooper pair and τ_{es} is the time for a phonon to leave the sample or scatter inelastically to $E<2\Delta$, where they can no longer break Cooper pairs and are no longer included in the density N_{ph}. The rate τ_{es}^{-1} appearing in these equations is in fact equal to the sum of the phonon escape rate and the rate of inelastic scattering to low phonon energies $E<2\Delta$. The terms I_{ph} and I_{qp} are source terms for quasi-particles and phonons. The recombination time does not appear explicitly in these equations because the rate of decrease of the total number of quasi-particles due to recombination is proportional to the

number of pairs of quasi-particles present and hence to the square of N_{qp}. For small deviations from thermal equilibrium, however, the quasi-particle density decay rate is linear in the increase in quasi-particle density N_{qp}-N_{qp}^{T}, and the decay time is $\tau_R=(2RN_{qp}^{T})^{-1}$, where N_{qp}^{T} is the number of quasi-particles present in thermal equilibrium in the superconductor. These equations also include diffusive terms with diffusion constants D_{qp} and D_{ph}. The diffusion terms are generally left out in the treatment of thin films, but are important in describing the evolution of the quasi-particle density in the bulk superconducting samples of this thesis.

It should be noted that these rate equations can be derived from energy averages over the appropriate coupled Boltzmann equations[10]. The Rothwarf Taylor equations are valid because, at low temperatures, $k_BT<<\Delta$, most of the quasi-particles and pair-breaking phonons have energy $E_{qp}\sim\Delta$ or $E_{ph}\sim2\Delta$, therefore one may use energy averaged relaxation rates and densities.

4.1.2 Optically Induced Nonequilibrium in Metals

The non-equilibrium state of an irradiated metal can be described by considering the flow of energy between the electron, phonon and bath reservoirs. In this picture one considers the dynamics of the total energy of the electrons and phonons. The electrons and phonons are described by effective thermal distributions, but are not necessarily at the same temperature. Optical illumination couples to the electron energy reservoir and this energy is transferred to the phonons by inelastic electron-phonon scattering. Wellstood et. al.[20] have shown both experimentally and theoretically that the rate of energy transfer

from the electrons to the phonons is, in the absence of diffusion: $\Sigma(T_e^5-T_{ph}^5)$, where Σ is the thermal contact parameter, T_e is the effective electron temperature and T_{ph} is the effective phonon temperature. These authors have also shown how this temperature dependence is modified by diffusive effects due to the temperature dependence of the inelastic mean free path of electrons.

The phonon energy couples from the metal to a surrounding insulator or cryogenic liquid via a thermal boundary resistance. The flow of phonon energy across a boundary between a metal and either an insulator or metal has been treated by many authors since Kapitza[21] first observed a thermal resistance at such boundaries. The origin of the thermal resistance is the acoustic mismatch between the phonons in the two materials which results in a finite phonon reflectivity at the boundary. The resulting heat flux was calculated by Khalatnikov[22] for metal superfluid He boundaries and by Little[23] for metal insulator boundaries to be: $J=\sigma_{ph}(T_{ph}^4-T_{bath}^4)$. The T^4dependence arises from an energy integral over the product of the phonon density of states $F(\Omega)\sim\Omega^2$, and the phonon energy Ω. The observed T dependence differs from the ideal, and many modifications have been considered[24] including inelastic scattering of electrons off of a surface oxide, effects of surface roughness, and interaction of electrons directly with the He.

Recent studies have shown how sample size plays a role in determining which energy transfer rates dominate the energy relaxation and how the effective temperatures of the electrons and phonons are related to the power driving the metal out of thermal equilibrium[25,20]. Such measurements have been performed on thin film and wire geometries. The metal is driven out of thermal equilibrium by applying an E field and

temperature measurements are made by measuring changes in noise[20] or in current-voltage characteristic (IVC) of the microstructure[26]. Optical measurements have also been used to study non-equilibrium properties of metals both at room T and at cryogenic temperatures. These measurements have been performed primarily on thin film tunnel junctions between a normal metal and a superconductor and have provided information on the non-equilibrium state of both the superconductor and normal metal. As in the study of nonequilibrium superconductivity, very few measurements[27] have been performed to examine the nonequilibrium properties of cryogenic metals using the optical response of point contacts at cryogenic temperatures. As will be seen below, the photoresponse of a superconductor normal-metal contact acts as a thermometer of the effective temperature of electrons in the metal tip, and provides another tool for studying heat transfer mechanism between metals and superfluid He.

4.2 Photoresponse Experiment

Fig. 4.1 shows the experimental setup used in measuring the photoresponse of the Ta-W superconductor normal-metal point contacts (SNPCs). These were previously described in Chapter 3: The 15μm tungsten whisker was etched to a 10-100nm radius tip and the Ta was polished to an optical flat. Light at 860nm from a Ti:Sapphire laser was focused through a window in the cryogenic dewar and was centered on the contact. The angle of incidence of the laser beam was ~15° to the surface normal of the Ta (near normal incidence on the Ta). The laser power was 10-1000μW, and the laser spot diameter was either 15 or 26μm. The laser intensity at the contact was therefore between

Fig. 4.1 Photoresponse Experiment

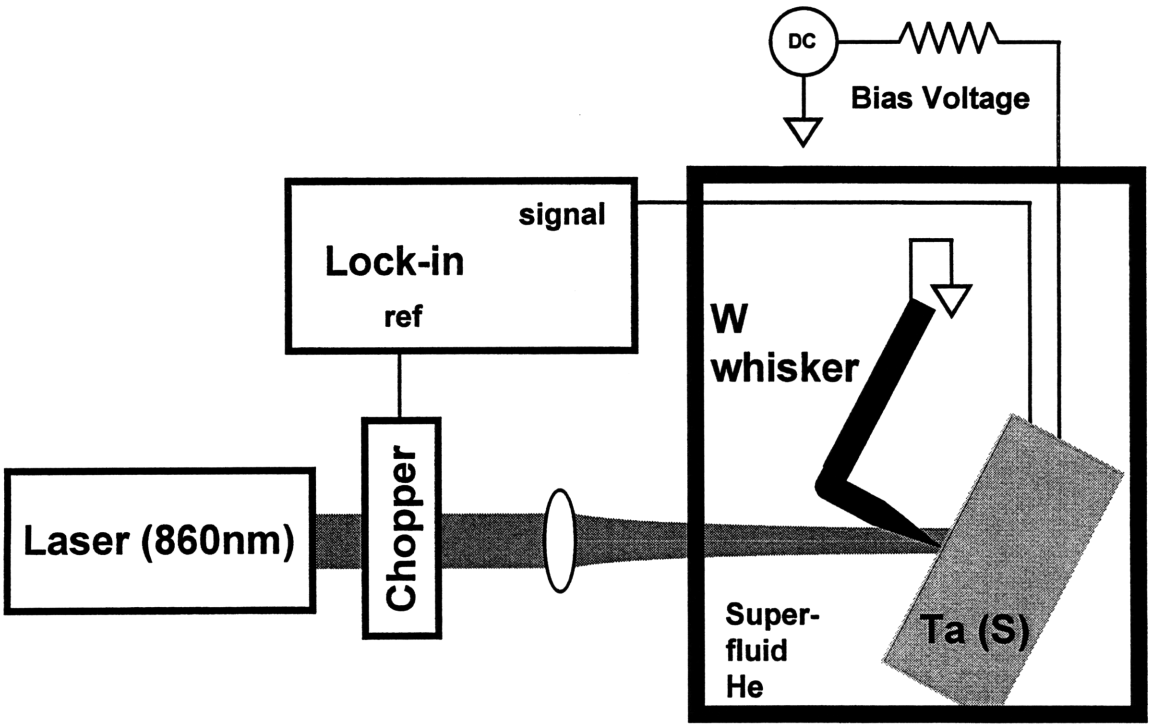

Fig. 4.1. Photoresponse Experiment. Light is focused through a window in the He dewar onto the W-Ta normal-metal superconductor point contact, which is immersed in superfluid He. The light is chopped on and off at 1kHz and the change in voltage on the contact is detected by the lock-in. A bias voltage is coupled to the contact with a bias resistor. This voltage is scanned and recorded along with the lock-in signal yielding a photoresponse plot vs bias voltage. (See Fig. 4.2.)

one and a few hundred W/cm^2. The light was chopped at 1kHz in one set of measurements and modulated sinusoidally at 50% in another using an AOM. (Fig. 4.1 shows only the chopper.) The change in voltage on the contact was measured with a lock-in amplifier. As in the dynamic resistance measurements, a bias voltage was coupled to the contact through a resistor and measured with an opamp (not shown). The bias voltage was scanned and recorded along with the photoresponse, generating a plot of

photoresponse vs bias voltage across the contact. Fig. 4.2 shows 4 sets data. Fig. 4.2a and 4.2b used chopped light and Figs 4.2c and 4.2d used the 50% modulated light.

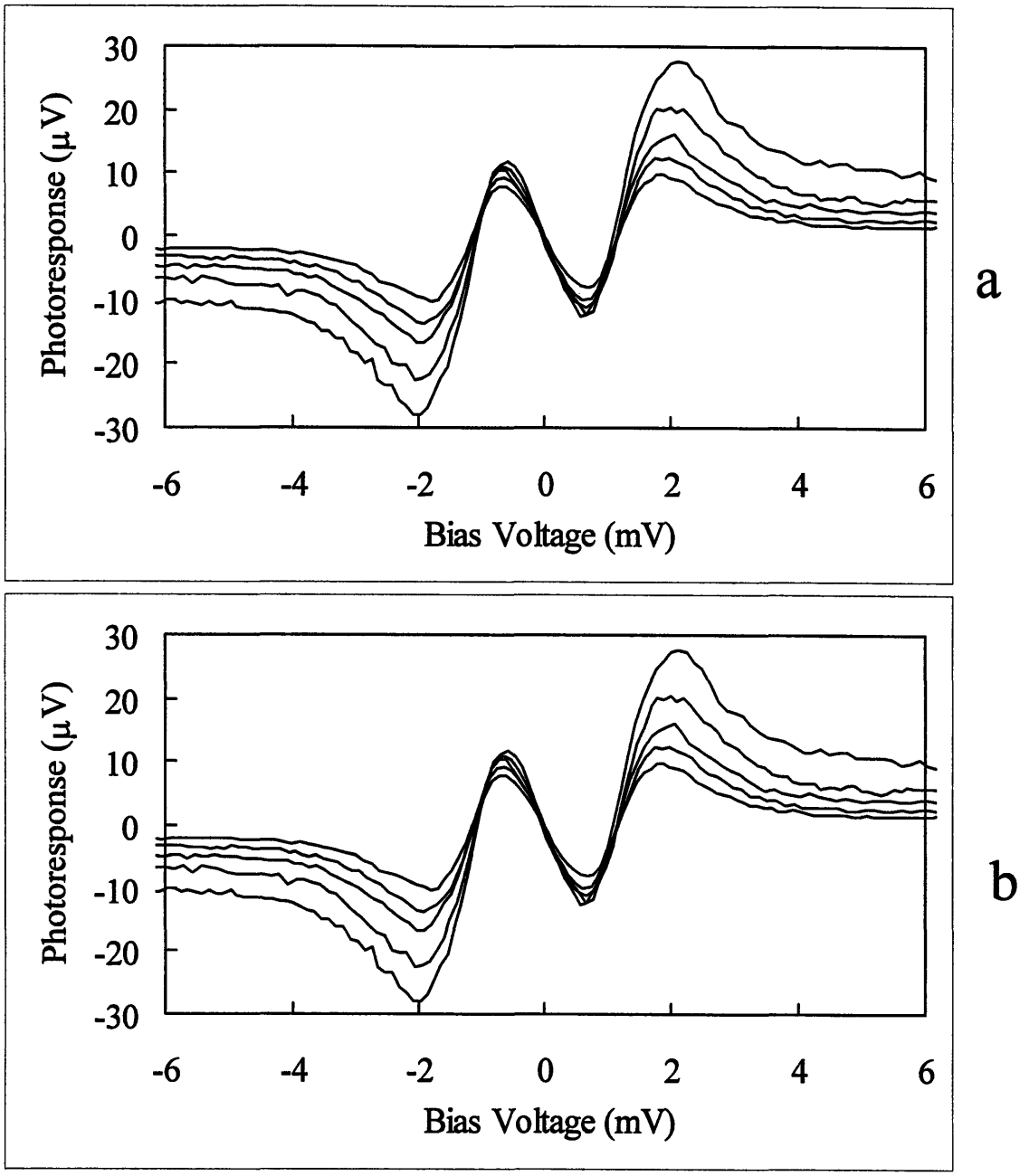

Fig. 4.2 Photoresponse vs Bias Voltage. Four data sets generated with the setup of Fig. 4.1. Each curve was generated with a different laser intensity. Plots a and b were generated with chopped light. The laser intensities, in W/cm^2, starting with the smallest plot are: (a) 45, 83, 89, 199 (b) 14, 24, 30, 39, 50, 58, 71, 86. Plots c and d were generated with 50% sinusoidal modulation. The peak to peak laser intensity swings are: (c) 32, 65, 132, 254; (d) 108, 184, 214, 222, 399, 403, 849.

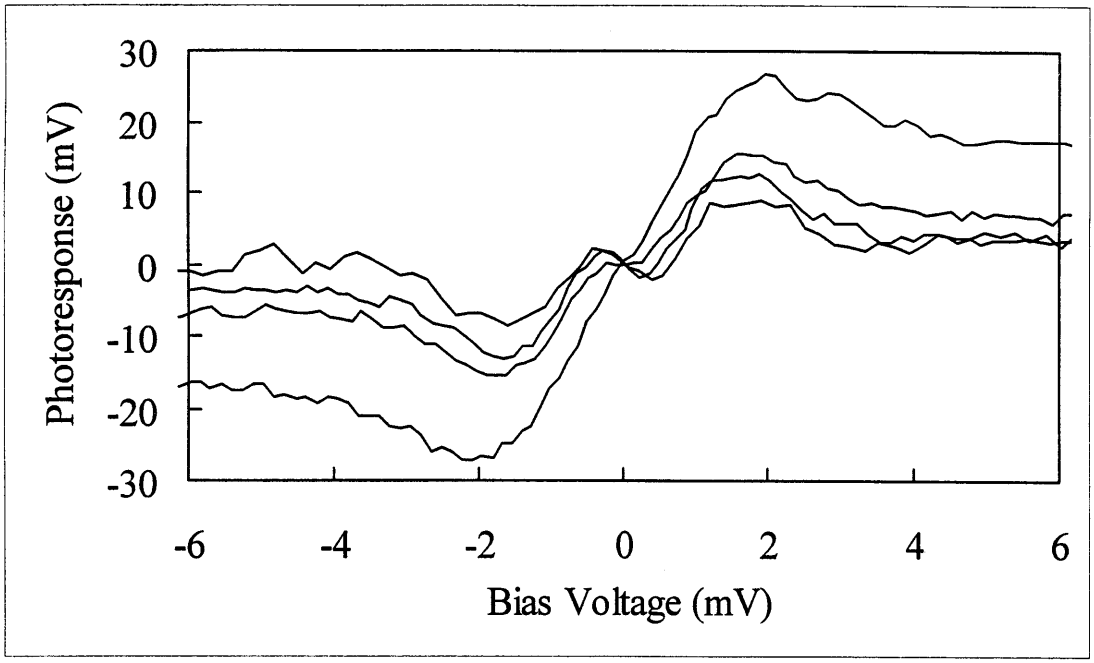

c

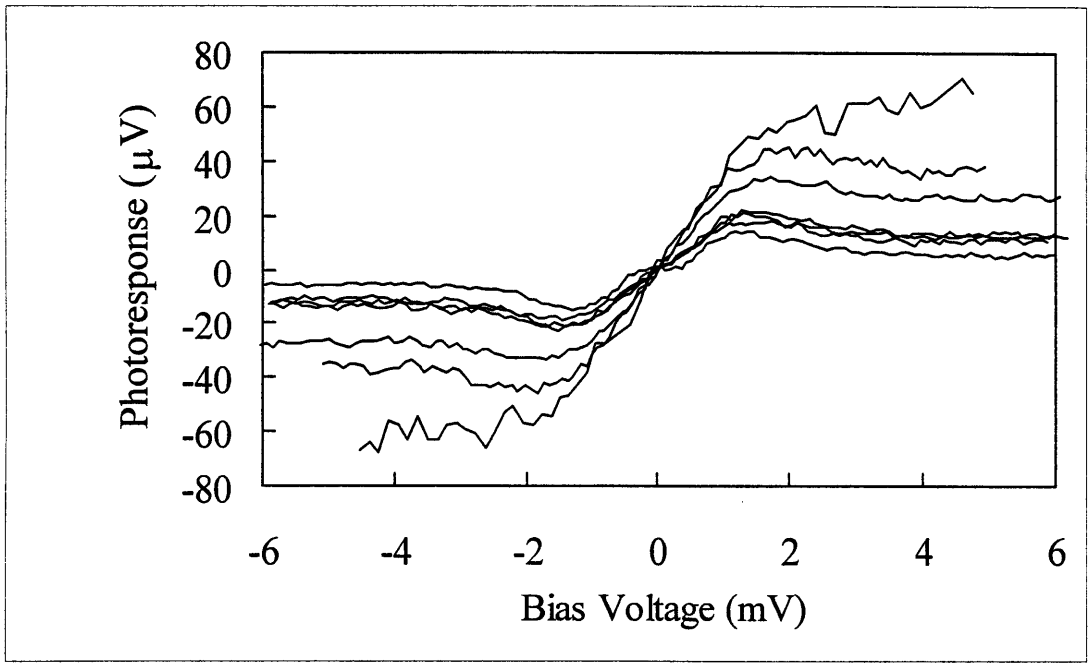

d

Fig. 4.2 (cont.)

4.3 Photoresponse Model

The SNPC photoresponse can be understood by considering the change in the IVC of the irradiated point contact. As previously discussed, the BTK current through a ballistic contact between a normal metal and a superconductor is:

$$I = k\int dE\left[f(E-eV,T)-f(E,T)\right]\cdot\left[1+A(E,\Delta,Z,\Gamma)-B(E,\Delta,Z,\Gamma)\right], \qquad (4.1)$$

where A is the probability of Andreev reflection and B is the probability of normal reflection at the NS boundary, Δ is the superconducting gap, T is the temperature of the metal (the superconductor temperature enters only via the gap), V is the bias voltage across the contact, Z is proportional to the small, residual barrier at the contact, and Γ takes into account the finite lifetime of quasiparticles in the superconductor. As discussed in the last chapter, the BTK parameters Δ, T, Z, and Γ vary between contacts, and must be determined for each contact by performing a least-squares fit of the dynamic resistance of the contact to the theoretical BTK dynamic resistance. See Chapter 3.

To understand the photoresponse, the effect of irradiation on both the tungsten tip as well as the bulk tantalum must be taken into account. The effect of irradiation on the tungsten metal tip is to increase locally the effective electron temperature in a region extending up the tip a length equal to the laser spot size. Due to diffusion of electrons, this region will extend beyond the laser spot a length of order the electron diffusion length. The effect of irradiation on the bulk superconductor is to break Cooper pairs in the superconductor, resulting in an increase in the density of quasi-particles and corresponding decrease in the superconducting gap in a region at the surface of the

superconductor of depth equal to the diffusion length of quasi-particles in the superconductor. The diffusion length scales of both quasi-particles and metal electrons are large compared to the elastic mean free path of electrons impinging on the NS boundary. This means that current flow in the irradiated SNPC will be well described by a BTK IVC with different values of the superconductor gap and effective metal electron temperature which take into account the laser irradiation. The resulting photoresponse is then proportional to the difference of the unirradiated and irradiated IVCs:

$$\text{Photoresponse} \propto \delta I = I(V,T+\delta T,\Delta-\delta\Delta,Z,\Gamma)-I(V,T,\Delta,Z,\Gamma). \qquad (4.2)$$

The parameters Z and Γ are not expected to change appreciably because they depend mainly on impurities near the contact (See chapter 2), and these are unaffected by non-equilibrium changes in the quasi-particle and metal electron distributions. Moreover, it is not clear how changes in Z and Γ could result in the observed linear dependence on laser power of the finite bias photoresponse signal. (See below and Fig. 4.6)

Further evidence that Z and Γ do not change in the illuminated IVC were obtained from a study of the temperature of the dynamic resistance. As mentioned previously, the effect of light is similar to an effective heating, so the dependence of Γ and Z on T should be similar to their dependence on laser intensity. Dynamic resistance measurements were performed as the temperature of the He was gradually allowed to increase from 1.8K to 4.3K, the boiling point of He under a few atms of pressure. The temperature was recorded on a thermal diode and the series of RVCs were all fit using the BTK model to obtain the temperature dependence of the parameters $\Delta(T)$, Z(T), and $\Gamma(T)$. The results

for one of the runs are shown in Fig. 4.3. The gap shows the characteristic decrease with temperature, but Z and Γ remain approximately constant. The only trend is that Γ decreases slightly with temperature. A decrease in Γ, though, cannot account for the observed signal, since a decrease in Γ results in increased excess current flow (See Chapter 2) and hence an increase in the finite bias signal which was not observed.

Fig. 4.4 shows graphically how the photoresponse is equal to an optically induced current increment. The top half of the figure shows an irradiated and unirradiated BTK current voltage curve, greatly exaggerated for the purpose of argument, and the bottom figure shows a photoresponse and the best fit δI from the model.

Fitting Procedure. The actual signal voltage measured by the lock-in amplifier is equal to this change in current divided by the conductance of the contact:

$$\text{Photoresponse} = (I(V,T+\delta T,\Delta-\delta\Delta)-I(V,T,\Delta))/(dI/dV) \qquad (4.3)$$

Fig. 4.5 shows the fits of the model to the curves of Fig. 4.2. The curves are easy to fit "by hand,", and this was fully adequate for the purpose of comparing data and model. The reason for this is that the constant photoresponse signal at large bias depends only on the change in gap δΔ. This is clear from Fig. 4.4, which shows that this signal arises only from the change in excess current which is proportional to the gap of the superconductor. (See Chapter 2). Changes in the metal tip temperature only smear out the photoresponse signal, but do not affect the finite bias signal. The manual fit therefore had two steps: Adjust δΔ to match the observed photoresponse signal at large bias and then adjust δT to

a

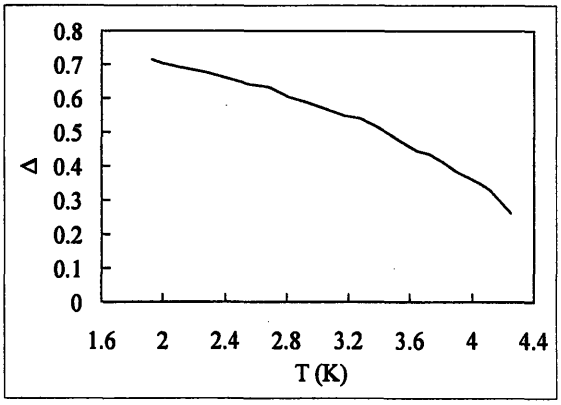

b

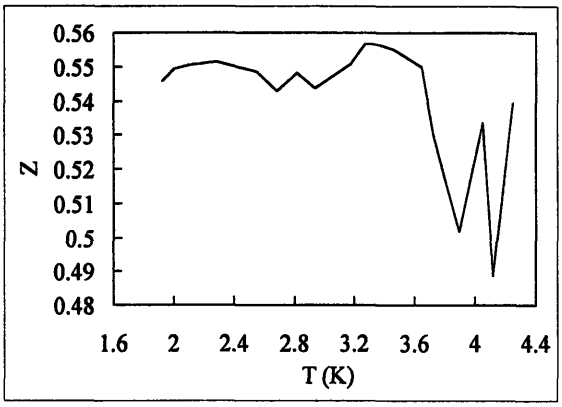

c

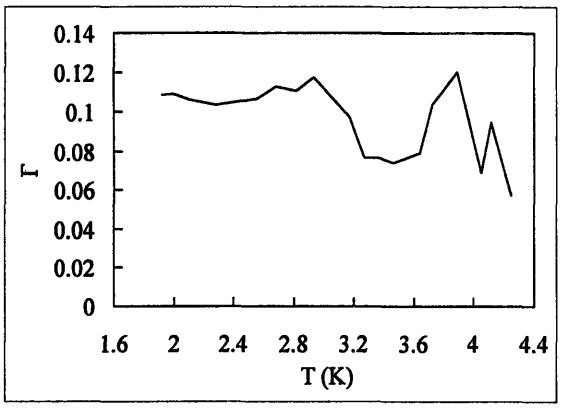

Fig 4.3 Temperature Dependence of the Parameters Δ, Z, and Γ. (a) Δ vs T shows the characteristic decrease with T; (b) Z vs T; (c) Γ vs T. The weak T dependence of Γ and Z, especially for low T, is strong evidence that these parameters do not change under laser illumination.

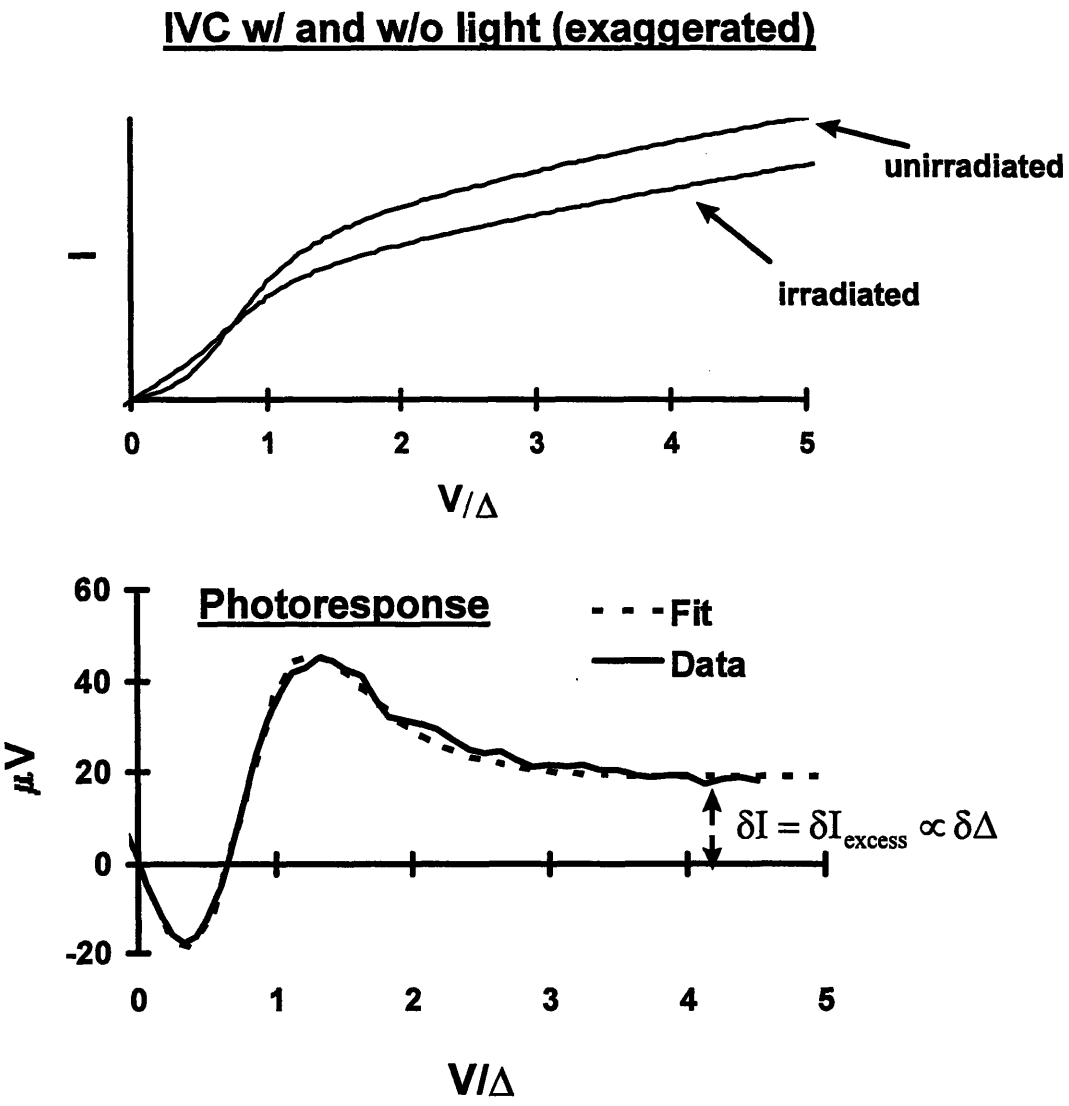

Fig. 4.4 Model of Photoresponse. The point contact photoresponse is proportional to the change in current induced by light. The top plot shows an irradiated and an unirradiated IVC (exaggerated). The bottom plot shows the model curve generated by taking the difference of two such BTK IVCs along with an actual photoresponse curve. The effect of light is taken into account by using an irradiated IVC that has an increased effective metal electron temperature, T+δT, and a decreased gap value, Δ-δΔ.

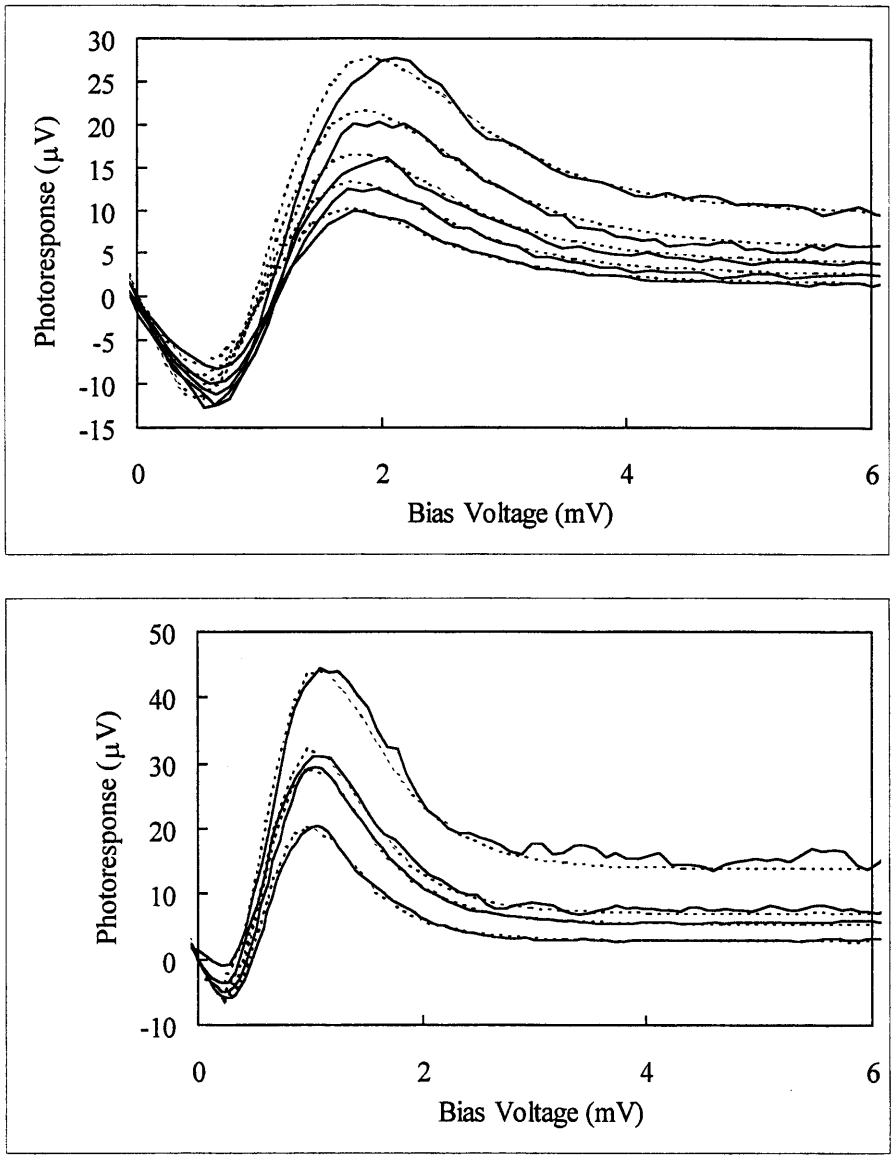

Fig. 4.5 Fits of the Photoresponse Model to Data. Each plot shows the curves from Fig. 4.2 along with the best fit photoresponse model curve. Negative bias voltages are left out for clarity. Each data set has the same letter as in Fig. 4.2. The photoresponse model curves are given by: $(I_{BTK}(V,\Delta-\delta\Delta,T+\delta T,Z,\Gamma)-I_{BTK}(V,\Delta,T,Z,\Gamma))/(dI/dV)$. The fit is performed by adjusting $\delta\Delta$ and δT, while Δ, T, Z, and Γ are held fixed at values determined by the BTK fit to the dynamic resistance of the contact.

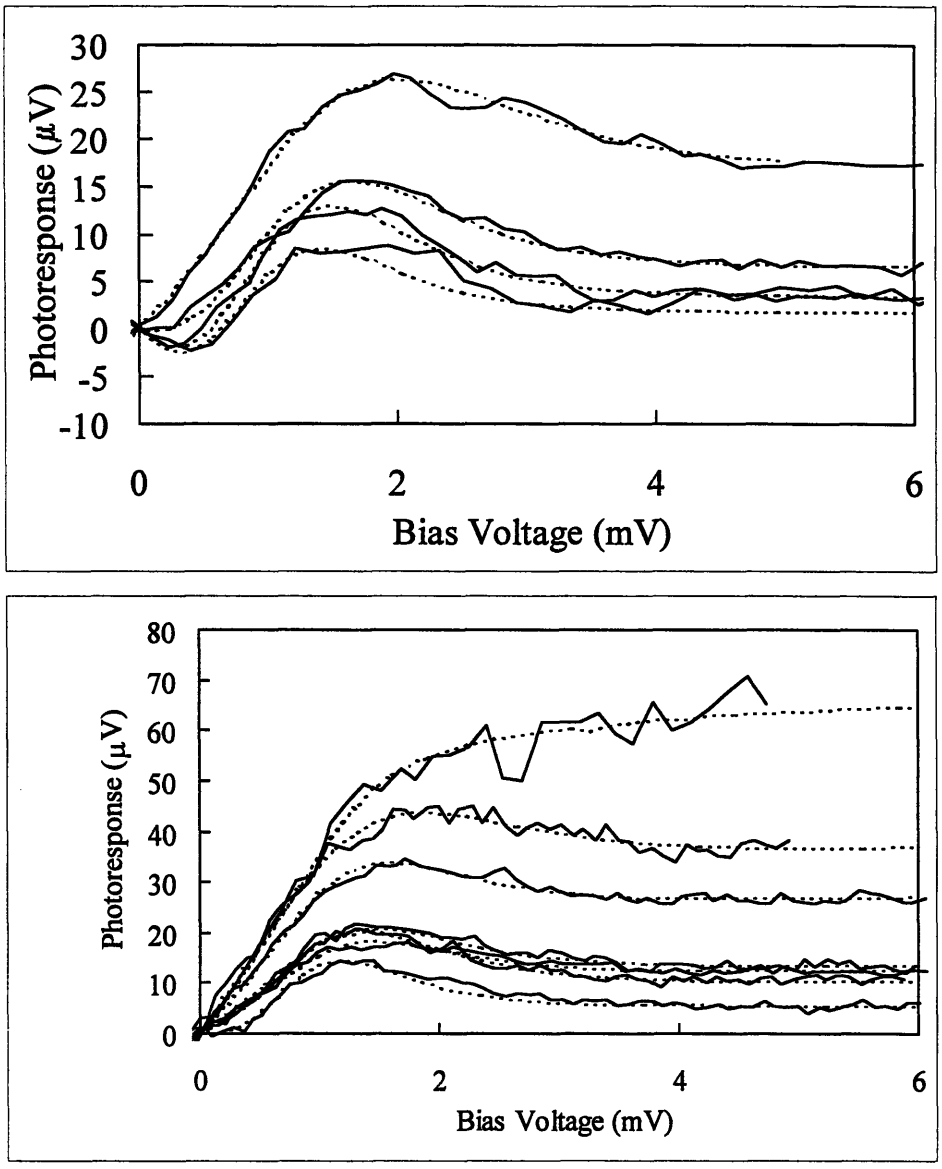

Fig 4.5 (cont.)

fit the structure at zero bias. Changes in δT affected only the height of the maxima and minima near V=Δ. The values of Δ, Γ, and Z used in the fitting procedure were determined by fitting the dynamic resistance of that same contact to the BTK model as

described in Chapter 2. The value of T was measured during the experiment. The 50% data required adjustment of both T and δT to account for the DC laser intensity.

Fig. 4.6 shows plots of the fit values δΔ and δT taken from the photoresponse curves of Fig. 4.2. These are plotted vs incident laser intensity. The plots show that δΔ is linear in the laser intensity. The temperature change was not linear in laser intensity. Instead, the irradiated metal temperature is related to the laser intensity by: $T_{eff\,metal}^{n}-T_{He\,bath}^{n}\sim J_{laser}$, where is 3 in all the plots except 5a, in which n=4 The next three sections will discuss the significance of these results.

4.4 Change of Gap Under Laser Illumination

The linear dependence of the decrease in gap δΔ on laser power follows from 1) Parker's result[17] relating the decrease in gap to the increase in quasi-particle density and 2) a solution of the linearized Rothwarf and Taylor equations. Specifically, Parker's result states that, if δΔ is small, then δΔ/Δ is proportional to the excess quasi-particle density induced by the light:

$$\delta\Delta/\Delta=-2\delta N_{qp}/(4N(0)\Delta) \qquad (4.4)$$

Fig. 4.6a: $\delta\Delta/\Delta$ vs Laser Intensity

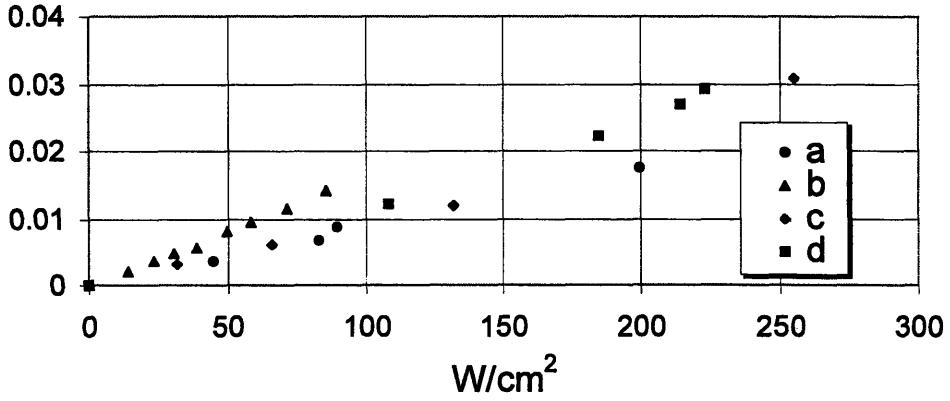

Fig. 4.6b: δT vs Laser Intensity

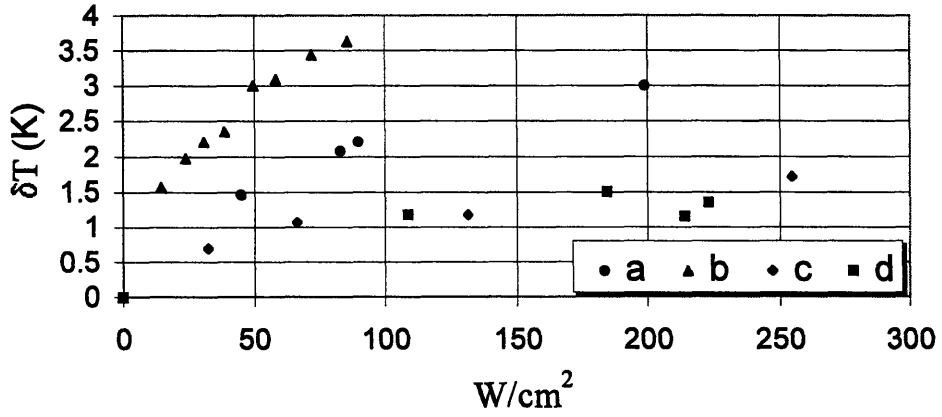

Fig. 4.6 Fit Values of $\delta\Delta$ and δT vs Incident Laser Intensity. Values of $\delta\Delta$ and δT vs laser intensity taken from the fits of Fig. 4.5. Each data set has the same letter as in Figs. 4.2 and 4.5.

$$\delta N_{qp}/(4N(0)\Delta)<0.1 \qquad (4.5)$$

Where N(0) is the single spin density of states at the Fermi energy. Parker showed that this result is approximately independent of the exact non-equilibrium quasi-particle

distribution as long as the change in quasi-particle density does not exceed the limit set by Eq. 4.5. This result is to be expected since the superconducting order parameter is a measure of density of Cooper pairs in the superconductor, and so a small increase in the number of quasi-particle excitations (broken Pairs) should be reflected in a decrease in the Cooper pair density.

The relationship between the laser intensity and the induced quasi-particle density follows from a solution of the Rothwarf-Taylor equations with diffusion included. As discussed in the background section these equations are:

$$\left(\frac{\partial}{\partial t} - D_{qp}\nabla^2\right)N_{qp} = I_{qp} - 2RN_{qp}^2 + \frac{2}{\tau_B}N_{ph}$$
$$\left(\frac{\partial}{\partial t} - D_{ph}\nabla^2\right)N_{ph} = I_{ph} + RN_{qp}^2 - \frac{1}{\tau_B}N_{ph} - \frac{N_{ph} - N_{ph}^T}{\tau_{es}} \qquad (4.6)$$

where, if $N_{qp}{}^T$ is the number of quasi-particles in thermal equilibrium, then $(2RN_{qp}{}^T)^{-1}$ is the recombination time, τ_R; N_{qp} is the total number of quasi-particles of all energies, N_{ph} is the total number of "pair-breaking" phonons, i.e., those with $E_{ph}<2\Delta$, τ_B is the time for a phonon to break a Cooper pair (averaged over energy), τ_{es} is the time for a phonon to leave the sample or equilibrate without breaking cooper pairs, D_{qp} and D_{ph} are the diffusion constants, and I_{qp} and I_{ph} are source terms.

The equations imply that, N_{qp}, the density of quasi-particles is in general nonlinearly related to the laser power, which is proportional to the quasi-particle source term, I_{qp}. However, as can be seen in Fig 4.6, the observed $\delta\Delta$ is linearly related to the incident laser intensity. Therefore, using Eq. 4.4 δN_{qp} varies linearly with I_{qp} and the

linearized version of these equations is sufficient to analyze the data. A linear solution of the equations will be valid as long as the increase in quasi-particle density is small compared to the thermal number of quasi-particles in the superconductor.

In addition to the linearity assumption, two other assumptions can be made in solving these equations: 1) The phonon diffusion length and time are small enough that the phonon density follows the quasi-particle density adiabatically[19] (i.e. phonons break Cooper pairs before diffusing appreciably). This assumption follows from the fact that the phonon velocity (v_{sound}~$2x10^3$m/s) is much less than the quasi-particle velocity (v_{fermi}~10^6m/s), and that the phonon pair breaking time is of order the phonon elastic scattering time[8]. The space and time derivatives in the second Eq of 4.6 are then zero, resulting in a relationship between N_{qp} and N_{ph} that can be used to eliminate N_{ph} from the first equation of 4.6. 2) The laser spot is large enough (25μm) compared to the quasi-particle diffusion length that the one may assume one dimensional diffusion in the direction normal to the surface (x-direction).

Under these assumptions, the linearized equation for the steady state value of $\delta N_{qp}=N_{qp}-N_{qp}^T$ results:

$$D_{qp}\frac{\partial^2 \delta N_{qp}}{\partial x^2} = I_{qp} - \frac{2}{\tau_R\left(1+\tau_{es}/\tau_B\right)}\delta N_{qp} \qquad (4.7)$$

Note that in this equation the recombination time τ_R is enhanced by the phonon trapping factor $(1+\tau_{es}/\tau_B)$, resulting from the fact that the phonons emitted in quasi-particle

recombination generate more quasi-particles by breaking pairs before they escape or relax via other mechanisms.

The quasi-particle source term I_{qp} is related to the incident laser power as follows. The incident light decays exponentially into the sample with decay constant α. The rate of creation of quasi-particles can be computed from the Poynting vector of the optical field by using conservation of energy:

$$S(x) = S_o e^{-\alpha x} \tag{4.8}$$

$$\vec{\nabla} \cdot \vec{S} = -\frac{\partial u}{\partial t} \Rightarrow \alpha S(x) = Q(x) \tag{4.9}$$

Q is the volume rate at which energy is deposited in the superconductor due to the Poynting vector S. Since the average energy of quasi-particles is of order Δ, the rate of energy deposition is related to the source term I_{qp} as $I_{qp}(x)=Q(x)/\eta\Delta$, where η is of order 1 and takes into account the fact that the average energy of quasi-particles is slightly larger than Δ and that the laser energy is held largely by the quasi-particles as opposed to the phonons[17]. The value of the Poynting vector at the surface of the superconductor is related to the reflectivity of the tantalum and the incident laser power/area: $S_o=S_{inc}(1-R)=(P_{laser}/A_{beam})(1-R)$. Therefore the source term has the form:

$$I_{qp}(x) = \frac{S_{inc}(1-R)}{\alpha\eta\Delta} e^{-\alpha x} \tag{4.10}$$

The linearized equation can then be solved with the boundary condition that no quasi-particles flow across x=0: $dN_{qp}/dx|_{x=0}=0$. The solution of the linearized equation is then the sum of two exponentials:

$$N_{qp}(x)-N_{qp}^{T}=\frac{\alpha S_{inc}(1-R)}{\eta\Delta}\frac{1}{D\alpha^{2}-\tau^{-1}}\left(\alpha\sqrt{\tau D}e^{-x/\sqrt{\tau D}}-e^{-\alpha x}\right) \tag{4.11}$$

In this equation $\tau=\tau_R\,(1+\tau_{es}/\tau_B)/2$ is half the enhanced recombination time and D is the diffusion coefficient for quasi-particles. The optical penetration depth, $1/\alpha$, is very small compared to the quasi-particle diffusion length diffusion length, $\sqrt{\tau D}$, and this makes the solution essentially an exponential with a decay length equal to $\sqrt{\tau D}$:

$$N_{qp}(x)-N_{qp}^{T}\cong\frac{S_{inc}(1-R)}{\eta\Delta}\sqrt{\frac{\tau}{D}}e^{-x/\sqrt{\tau D}} \tag{4.12}$$

Current flow through the contact is only sensitive to the value of this solution within a quasi-particle mean free path (~10nm) of the contact. Since this is much smaller than the quasi-particle diffusion length, this expression may be taken at x=0 and related to the observed change in gap:

$$\frac{\delta\Delta}{\Delta}=2\frac{(N_{qp}(0)-N_{qp}^{T})}{4N(0)\Delta}\cong\frac{2}{4N(0)\Delta}\frac{S_{inc}(1-R)}{\eta\Delta}\sqrt{\frac{\tau}{D}} \tag{4.13}$$

This slope of $\delta\Delta/\Delta$ vs $S_{inc}(1\text{-}R)$ may be compared with the graphs of Fig. 4.6a. Taking parameters for Ta: $N(0)=7\text{x}10^{28}$states/eVm^3, Δ=0.7meV, τ=40nsec (see next chapter), $v_F=0.6\text{x}10^{6}$m/s, and $\ell_{elastic}$=10nm, the slope becomes $1.3\text{x}10^{-3}$m^2/W. This is very close to the average observed value of $1.7\text{x}10^{-3}$m^2/W. The agreement is very good considering

that parameters such as $D=(1/3)v_{Fermi}\ell_{elastic}$ and the enhanced recombination time τ are not known with great accuracy for the sample.

To address the assumption of linearity one can calculate the value $\delta\Delta/\Delta$ for which the total number of quasi-particles is equal to the thermal number of quasi-particles. The total density of quasi-particles in a superconductor at temperature T is calculated from the quasi-particle distribution and density of states and is:

$$N_{qp}^{T} = 4N(0)\Delta\left(\frac{\pi k_B T}{2\Delta}\right)^{1/2} e^{-\Delta/k_B T}$$

Using this result, for T=1.8K, the maximum value of $\delta\Delta/\Delta$ is

$$\delta\Delta/\Delta|_{max}=2N_{qp}{}^{T}/(4N(0)\Delta)=0.013 \qquad (4.14)$$

Many of the measurements are below this value, although linearity is observed above this value.

4.5 Use of Photoresponse as a Probe of SNPC Conductance

As discussed in chapter 2, the excess current flow through an SN contact at bias voltages above Δ is proportional to the gap of the superconductor. Since the constant photoresponse signal at bias voltages greater than the gap is proportional to the change in gap, it can be viewed as a probe of excess current flow through the contact. This probe can be used to directly verify one of the assumptions of the model of the finite bias peaks of the last chapter: The destruction of superconductivity at the finite bias peak can be directly observed with the photoresponse, because, if the superconductivity is destroyed

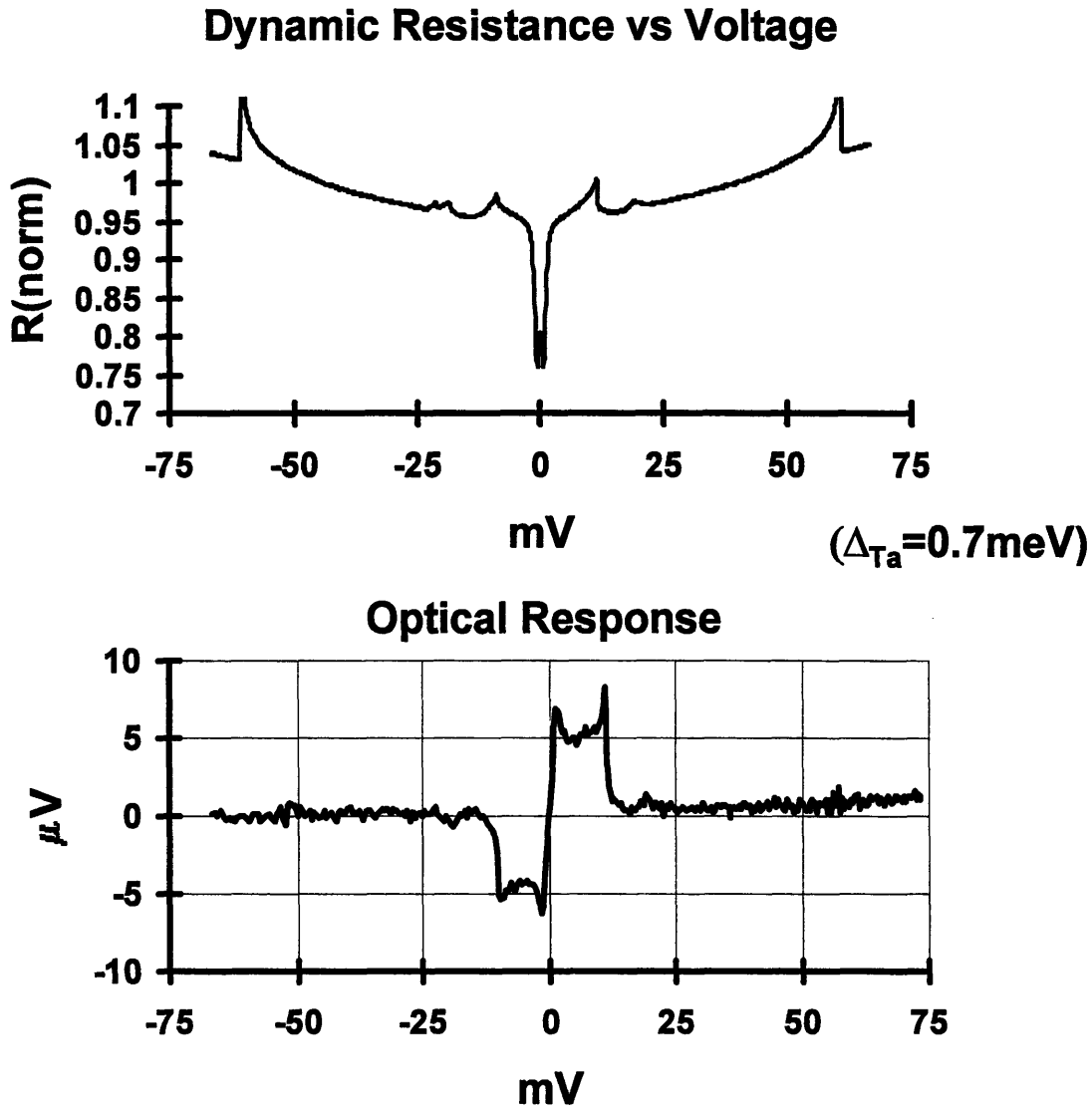

Fig. 4.7 Optical Probe of the Transition at the Finite Bias Resistance Peak. The top curve shows the dynamic resistance of an SNPC with three finite bias peaks. The lower curve shows the photoresponse of this contact. The photoresponse signal at bias voltages $V>>\Delta(=0.7mV)$ is proportional only to the optically induced change in gap, $\delta\Delta$. The fact that this signal is constant up to the first peak and then vanishes provides convincing evidence that the first finite bias peak corresponds to a destruction of superconductivity at the contact (making $\Delta=0$) while the higher voltage peaks must arise from a different mechanism. (See model of Chapter 3.)

then the gap goes to zero in the vicinity of the contact. This should be observable as a sudden decrease in the photoresponse signal. In fact, in some contacts, where there is more than one finite bias peak, this probe of the excess current will distinguish whether

the gap goes to zero in steps, or whether the higher order peaks have some other origin. Fig 4.7 shows both the dynamic resistance and the photoresponse of such a contact. The photoresponse signal goes to zero at the first finite bias peak, indicating that the gap near the contact as well as the excess current have gone to zero after the first peak. The higher order peaks result from other processes such as quantum interference. This is the first direct observation of this effect, and clearly points to applications of light as probe of conductance mechanisms in other systems with NS interfaces such as, for instance, the systems discussed in Chapter 3 that displayed finite bias peaks.

4.6 Electron Temperature vs Laser Power

The raw temperature data of Fig. 4.6b can be understood by plotting the change in temperature according to the formula $(T_e^3-T_{bath}^3)=aI_{laser}$. When the light is chopped on and off, this formula may be applied directly and the laser intensity will be linear in the difference of the cubes of the temperature. This is shown in Fig. 4.8b. (4.8a is plotted as in 4.8b, but with the fourth powers and will be discussed below.) For the 50% sinusoidally modulated light, the data cannot be plotted as a straight line. Instead the temperature changes can be plotted vs: $(2aI_{laser}+T_{bath}^3)^{1/3}-(aI_{laser}+T_{bath}^3)^{1/3}$. This formula has the same single adjustable parameter, a, and takes into account the 50% intensity modulation of the light. The first term is the temperature with light at its maximum value, and second term is the temperature with the light at its minimum. The peak-to-peak amplitude of the oscillating laser intensity is still I_{laser}. Figs. 4.8c and 4.8d show the data of series c and d from Fig. 4.6 along with a fit using this formula. Clearly Figs 4.8b and 4.8c follow this T^3 law quite well. Fig. 4.8d is very noisy, but also follows the law

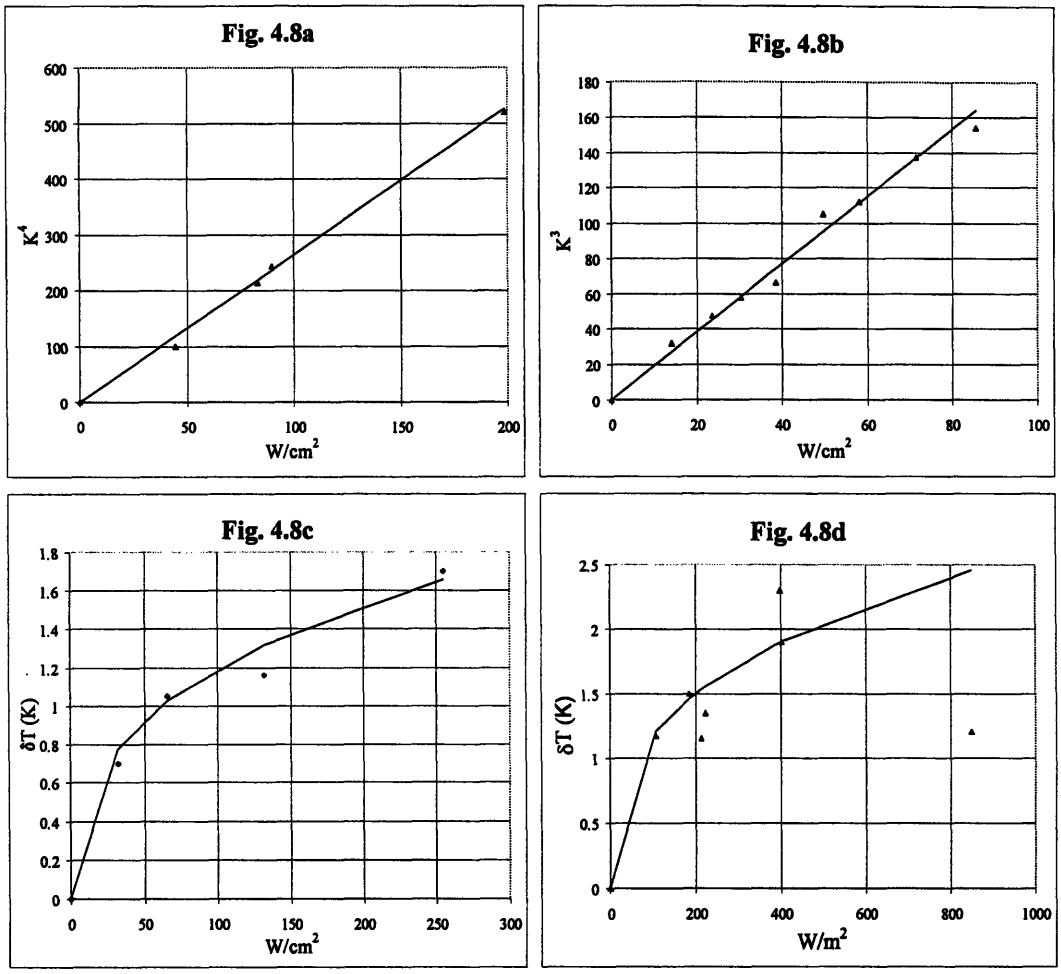

Fig. 4.8 Fit of δT vs Intensity to Model. Each plot shows one of the sets of data points of Fig. 4.6 along with a fit (line) to the model: $T_e^n - T_{bath}^n = aI_{laser}$, where n=3 for all the curves except (a), and $T_e = T_{bath} + \delta T$. (δT is taken from the fit of the photoresponse to the model.) Each curve has the same letter as Fig. 4.6. The model curve in each figure is: (a) $T_e^4 - T_{bath}^4$ vs I_{laser}; $a = 2.6 cm^2 K^4 W^{-1}$; (b) $T_e^3 - T_{bath}^3$ vs I_{laser}; $a = 1.9 cm^2 K^3 W^{-1}$; (c) $(2aI_{laser} + T_{bath}^3)^{1/3} - (aI_{laser} + T_{bath}^3)^{1/3}$; $a = 1.0 cm^2 K^3 W^{-1}$; (d) same fit equation and a value as (c). (The formula for (c) and (d) take into account the 50% modulated light used in these two measurements.)

approximately. One is thus led to consider mechanisms of heat transfer from the irradiated nanoscale W tip to the superfluid He that result in a flow of heat proportional to the difference of the cubes of the electron and He bath temperatures.

It was proposed by Little[23], that, in the presence of a oxide layer the conduction electrons can scatter inelastically off of the oxide layer, thereby transferring heat directly to the He Bath. The T^3 dependence then results from the two dimensional nature of the phonons in the surface oxide, since the flow of energy is an integral over the product of the surface oxide phonon density of states $F(\Omega) \sim \Omega$ and the energy transferred from the electron, which is equal to the phonon energy Ω. This mechanism is consistent with the small size of the contact it two ways. The contact size can be less than the cutoff wavelength for thermal phonons, greatly suppressing the usual phonon flow of heat due to bulk phonons (Kapitza effect; see background section.). Secondly, the tip size can be small compared to the inelastic mean free path of the electrons. This means that the high energy electrons excited by the light can only equilibrate by inelastic collisions with the oxide on the tungsten.

Another mechanism which can result in T^3 behavior, also proposed by Little[23], considers the effect of surface roughness on the normal phonon Kapitza effect which produces a heat flow proportional to the difference of the fourth powers of the temperature. Little showed that the presence of defects and other roughness can result in a phonon heat flow proportional to the difference of the cubes of the phonon and bath temperature. The T^3 dependence results from need to treat long wavelength phonons differently from short wavelength phonons. In the presence of roughness, the long

wavelength phonons see a smaller effective surface area. Taking the effective surface area to be $A(\Omega)\sim\Omega^{-1}$, the T^3 dependence results. However, because this mechanism relies on conduction via bulk phonons, which may be suppressed in the nanoscale tip region, this mechanism is likely to be weaker than the mechanism of inelastic scattering off the surface oxide.

To our knowledge this T^3 dependence has not been observed previously, and because of the tip's small size, may be much more efficient than the heat conduction mechanisms that are observed in bulk measurements. The magnitude of the heat flow can be compared with previous measurements on bulk Cu which also gave T^3 dependence. These measurements showed that $J_{heat}= \sigma(T_e^3-T_{bath}^3)$ where $\sigma=0.007 K^3cm^2/W$. To compare the present results with this work ones assumes that all of the power which is absorbed at the tip is flows out of the tip via this heat flux. The laser power absorbed in the tip is $I_{laser}(1-R)$, where R is the total power reflected from the W tip. The heat flux, J occurs over twice the area over which light is absorbed. Therefore: $J_{heat}=I_{laser}(1-R)/2$, and $\sigma=(1-R)/2a$, where a is the constant from the plots of Fig 4.8. Using the dielectric constant for tungsten at room temperature, which is not expected to be very different at cryogenic temperatures, $(1-R)\sim0.5$, and $\sigma=0.1$, 0.2 and 0.2 K^3cm^2/W for Figs 4.8b, 4.8c, and 4.8d respectively.

Another consequence of the small size of the tip is that the effect of diffusion is minimized near the contact. The region within one mean free path of the tip (~10nm) which is important for the conductance properties of the contact, is much smaller than the diffusion length in the metal. As a result the induced effective electron temperature is

uniform in this region, and the flow heat from this region due to diffusion can be small compared to the heat flux across the W-superfluid He boundary. The electron temperature distribution farther up the tip requires the solution of a set of coupled equations for the effective electron and phonon temperatures. The solution requires a complete knowledge of the geometry of the tip which is not known exactly in this experiment. The details of the electron temperature distribution farther away from the contact do not affect the optical response, though, since, as mentioned, the current voltage characteristic is sensitive only to the electron temperature near the contact.

Since the T^3 heat conduction mechanism occurs only when the tip is of small enough size, one expects to see deviations from the T^3 behavior for larger tips. Although current flow occurs through a nanoscale orifice, some tips have radii as large as 1μm, especially after the plastic deformation that occurs when a sufficiently large force is applied to the contact. For a large enough tip the bulk phonon Kapitza effect will begin to dominate and a heat flux out of the tip proportional to the difference of the fourth powers of the bath and W temperatures will be observed. This can be seen in the data Fig 4.8a which showed this T^4 behavior.

4.7 Conclusion

In summary, the photoresponse of SNPCs has been accurately modeled by assuming that the effect of light can be described by two changes in the BTK IVC of the contact: A optically induced decrease in the superconducting gap, and an optically induced increase in the effective electron temperature of the metal tip. The observed

linear change of gap with laser power is shown to be consistent with theory. The sensitivity to the gap leads to use of the photoresponse as a probe of the flow of excess current in the contact. This probe was used to observe directly the destruction of superconductivity at the contact which was assumed in the model of Chapter 3. The photoresponse was also used in a novel measurement of the effective non-equilibrium change in electron temperature of a nanoscale W metal tip. The dependence of the effective electron temperature on laser power indicates that heat is conducted away from the tip region via inelastic electron scattering off of the surface of the metal tip in the constricted region. The inelastic electron scattering is expected to dominate because of the decreased dimension of the tip, which can be less than the thermal phonon wavelength and electron inelastic scattering length for electrons in W at 1.8K.

---

[1] L. R. Testardi, Phys. Rev. B **4**, 2189 (1971).
[2] Nonequilibrium Superconductivity, Editors D. N. Langenberg, and A. I. Larkin, Elsivier Science Publishers (1986).
[3] Nonequilibrium Superconductivity, Phonons, and Kapitza Boundaries, Editor K. E. Gray, Plenum Press (1981).
[4] D. N. Langenberg LT 14 Conference Ed. M Krusius and M. Vuorio (1975).
[5] A. Gilabert, Ann. Phys. Fr. **15**, 255 (1990).
[6] C. S. Owen, and D. J. Scalapino, Phys. Rev. Lett. **28**, 1559 (1972).
[7] J. Fuchs, P. W. Epperlein, M. Welte, and W. Eisenmenger, Phys. Rev. Lett. **38**, 919 (1977).
[8] S. B. Kaplan, C. C. Chi, D. N. Langenberg, J. J. Chang, S. Jafarey, and D. J. Scalapino, Phys. Rev. B, **14**, 4854, (1976).
[9] V. F. Elesin, and Yu. V. Kopaev, Sov. Phys. Usp. **24**, 116 (1981).
[10] J. J. Chang, and D. J. Scalapino, Phys. Rev. **B15**, 2651 (1977).
[11] J. J. Chang, W. Y. Lai, and D. J. Scalpino, Phys. Rev. **B20**, 2739 (1979).
[12] A. D. Smith, W. J. Skocpol, and M. Tinkham, Phys. Rev. B, **21**, 3879 (1980).
[13] V. F. Elesin, V. E. Kondrashov, and A. S. Sukhikh, Sov. Phys. Solid State **21**, 1861 (1979).
[14] R. Sobolewski, D. P. Butler, T. Y. Hsiang, and C. V. Stancampiano, Phys. Rev. B **33**, 4604 (1986).
[15] J. A. Pals, K. Weiss, P. M. T. M. van Attekum, R. E Horstman, and J. Wolter, Physics Reports **89**, 323 (1982)

[16] C. Vanneste, A. Gilabert, and D. B. Ostrowsky, Proc SPIE Technologies for Optoelectronics, R. F. Potter and J. M. Bulabois Editors, Vol 869 p. 2 (1987)
[17] W. H. Parker, Phys. Rev. B, **12**, 3667 (1975).
[18] A. Rothwarf, and B. N. Taylor, Phys. Rev. Lett, **19**, 27 (1967).
[19] N. E. Glass, and D. Rogovin, Phys, Rev, B, **45**, 7346 (1992).
[20] F. C. Wellstood, C. Urbina and J. Clarke, Phys. Rev. B, **49**, 5943 (1994).
[21] P. L. Kapitza, J. Phys. (U.S.S.R.) **4**, 181 (1941).
[22] I. M. Khalatnikov, and I. N. Adamenko, Zh. Eksp. Teor. Fiz. **63**, 746 (1972) [Sov. Phys. JETP **36**, 391 (1973)].
[23] W. A. Little, Can. J. Phys. **37**, 334 (1959).
[24]E. T. Swartz, and R. O. Pohl, Rev. Mod. Phys **61**, 605 (1989)
[25] J. P. Kauppinen and J. P. Pekola, Phys. Rev. B, **54**, R8353 (1996).
[26] M. Nahum and J. M. Martinis, Appl. Phys. Lett. **63**, 3075 (1993).
[27] O. P. Balkashin, I. I. Kulik, and I. K. Yanson, Fiz. Nizk. Temp. **16**(5), 389 (1990).

Chapter 5

Measurement of Quasi-particle Recombination Time Using the Photoresponse of a Ta-W Point Contact

Introduction

The previous chapter discussed how the nonequilibrium state of a superconductor can be characterized by the total number of excited quasi-particles and total number of pair breaking phonons ($E_{phonon}>2\Delta$). For small deviations from equilibrium, the quasi-particle density relaxes to its equilibrium value at a well defined rate. This quasi-particle density recombination rate is a function of only equilibrium parameters and the basic parameters of superconductivity, and is well approximated by the recombination time for individual quasi-particles with energy close to the gap energy Δ. The quasi-particle recombination time is important because it is often much longer than the other scattering processes for quasi-particles and is therefore often the limiting step or bottleneck in the dynamics of a nonequilibrium superconductor. The quasi-particle recombination time is also important because it is related to basic parameters in the microscopic theory of superconductivity, and so it provides a check on this theory.

In the description of the photoresponse of a superconductor normal-metal point contact (SNPC) given in the last chapter, it was discussed how the effect of light on a superconductor is to break Cooper Pairs, resulting in an increase in quasi-particle density and a corresponding decrease in gap. When the light is modulated on and off, this effect

is observed as an oscillating photoresponse voltage on the contact. It was shown that for bias voltages $V>\Delta$, this oscillating voltage is linearly related to the change in gap and therefore measures the optically induced quasi-particle density directly. When the modulation frequency of the laser intensity exceeds the relaxation rate of the quasi-particle density, (or equivalently, the inverse of the response time of the quasi-particle density) the photoresponse signal will be decreased from its value at low frequencies. This roll-off of the photoresponse signal can therefore be used to measure the quasi-particle recombination time which, as mentioned above, is the same as the relaxation rate of the quasi-particle density. This chapter will present a quasi-particle recombination time measurement using the roll-off of the photoresponse.

An important aspect of this measurement, described in this chapter, is the method used to measure the roll-off: Because the quasi-particle recombination time is very short, signals originating on the point contact at the roll-off frequency may be beyond the electronic detection bandwidth of the experimental setup. This bandwidth is limited by unavoidable stray lead capacitances and impedance mismatch between the contact and the coaxial cables carrying the signal to the lock-in amplifier. The measurement technique, which takes advantage of the nonlinearity of the SNPC current voltage characteristic, converts the signal due to the optically induced oscillating quasi-particle density to an intermediate frequency lying within the detection bandwidth. As will be shown below this intermediate frequency signal is proportional to the derivative of the photoresponse and can be used to determine the roll-off frequency.

The advantages and novelty of this roll-off measurement technique are threefold: 1) It utilizes the simplicity and versatility of point contacts, allowing measurements on any superconductor that can be used in a point contact configuration. This includes materials that can only be easily made in bulk form, such as crystalline and some ceramic high temperature superconductors. 2) It can be used to perform measurements of the quasi-particle recombination rate in real time even when the recombination rate is beyond the bandwidth of the front end electronic detection system used to measure signals on the point contact. 3) Since the photoresponse signal is linearly related to the induced quasi-particle density (see chapter 4), the real time relaxation rate measured by this method can be clearly related to the decay of the quasi-particle density.

Section 5.1 will review calculations of the quasi-particle recombination time from the theory of superconductivity. This will be followed by a review in section 5.2 of various techniques of measuring the quasi-particle recombination time which will serve to place the measurement of this chapter in the context of the large number of recombination time measurements performed over the past 30 years. Section 5.3 will describe the experimental method, showing how the intermediate frequency signal is generated. Section 5.4 will then show how the recombination time can be obtained from the roll-off of this signal as laser intensity modulation frequency is increased. The chapter concludes with a discussion in section 5.5 of sources of variation in the quasi-particle recombination time and fundamental quantum limits on the detection method discussed in this chapter.

5.1 Calculations Of The Recombination Time

The first calculations of the quasi-particle recombination time were done by Schrieffer and Ginsburg[1] using Golden Rule arguments to compute the rate at which two quasi-particles recombine to form a Cooper pair. More recently Kaplan[2] et. al. have published the most authoritative set of calculations of quasi-particle and phonon scattering rates in superconductors. These results are computed from the BCS theory of superconductivity using Green's function methods. Their results show that all of the quasi-particle scattering rates for a given superconductor are related to a basic time scale:

$$\tau_o = Z_1(0)\hbar/2\pi b(k_B T_c)^3 \qquad (5.1)$$

Where $Z_1(0)$ is the real part of the energy dependent renormalization parameter taken at zero energy. This parameter is approximately equal to 2 for metallic superconductors, and is 1.69 for Ta. The parameter b is the coefficient in the approximate expression for the electron phonon coupling parameter $\alpha^2(\Omega)F(\Omega)=b\Omega^2$ in which Ω is the phonon energy, $\alpha^2(\Omega)$ is the electron-phonon coupling constant, and $F(\Omega)$ is the phonon density of states. The approximate expression is valid for Ta up to phonon energies 2Δ, hence it is used by Kaplan et. al. in calculations of the Ta quasi-particle recombination time. For Ta the parameter b is $1.73\text{x}10^{-3}$ meV^{-2}. Using these parameters one finds that for Ta: $\tau_o = 1.78\text{x}10^{-9}$sec.

The parameter τ_o sets the scale for the recombination time, however, the actual recombination time also depends on the quasi-particle energy and the distribution of the quasi-particles. In thermal equilibrium the recombination time is therefore temperature

dependent. For quasi-particles with energy near $\Delta(T)$ and for low temperatures, Kaplan gives an approximate expression for the recombination time which is valid for the temperatures considered in this chapter:

$$\tau_R^{-1} = \tau_o^{-1}\pi^{1/2}\left(\frac{2\Delta(0)}{k_B T_c}\right)^{5/2}\left(\frac{T}{T_c}\right)^{1/2} e^{-\Delta(0)/k_B T}. \tag{5.2}$$

The temperature dependence in this expression results from averaging over a thermal quasi-particle distribution which is exponential due to the gap in the quasi-particle energy spectrum. This expression can be understood by considering the expression for the total number of quasi-particles in thermal equilibrium:

$$N_{qp}^{T}=4N(0)\Delta(\pi k_B T/2\Delta)^{1/2}\exp(-\Delta/k_B T) \tag{5.3}$$

The recombination rate is then proportional to the density of quasi-particles:

$$\tau_R^{-1}=2RN_{qp}^{T} \tag{5.4}$$

where R is known as the recombination coefficient. This result is also clear from the fact each recombination event requires two quasi-particles, and Eq. 5.4 was derived this way in the last chapter from the Rothwarf-Taylor equations.

The relaxation rate of an excess quasi-particle density is different from the recombination time of individual quasi-particles in two ways. Firstly, since the recombination time of a quasi-particle is dependent on energy, it must be averaged over quasi-particle energy to arrive at the recombination time for the quasi-particle density. However, at low temperatures, most of the quasi-particles will be at energies close to

$E=\Delta$, hence the relaxation rate of the quasi-particle density is well approximated by the recombination time of quasi-particles near the gap energy.

Another more important modification to the recombination time is the effect of phonon trapping, which was mentioned in the last chapter. When two quasi-particles recombine, they emit a phonon to conserve energy. This phonon will in turn create two new quasi-particles unless it scatters inelastically to an energy too low to break a Cooper pair ($E<2\Delta$) or escapes from the superconductor into a surrounding insulator. As a result, excess quasi-particle density will decay more slowly than an individual quasi-particle by a phonon trapping factor equal to $(1+\tau_{es}/\tau_B)$.

5.2 Review Of Recombination Time Experiments

Measurements of the quasi-particle recombination time were first performed in the late 60s, and have been repeated on many materials with many different techniques. All of the methods involve some means of changing the quasi-particle density, either electrically or optically, and some way of detecting the relaxation rate of the nonequilibrium quasi-particle density, either directly in real time or indirectly by inference from measurements of steady state nonequilibrium parameters. A brief review of these methods follows.

Early measurements[3,4,5,6] were all indirect and used thin film double superconductor-insulator-superconductor tunnel junctions in the configiuration: S-I-S-I-S. One tunnel junction was used to inject quasi-particles into the center superconductor and the resulting change in quasi-particle density was detected by measurements of the

voltage across the second tunnel junction. The steady state quasi-particle density was proportional to the injection rate times the recombination time and so the recombination time could be inferred from measurements of the injection current and voltage produced in the second junction. Direct measurements using current pulse methods were also employed with SIS tunnel junctions[5] using aluminum, which has a very long recombination time. The recombination time was inferred from the voltage transient produced by a current pulse through the tunnel junction.

A fundamentally different technique followed from the work of Schmid[7]. This method employs the fact that the kinetic energy of the pair current has associated with it a kinetic inductance (see Schmid). The kinetic inductance is inversely proportional to the London pair density, and so a time rate of change in the pair density generates an emf in the superconductor. A measurement of this emf can then be used to determine the dynamics of the London pair density in real time. This method was used by Peters[8] who measured the roll-off of such an emf as the frequency of a small RF driving voltage was increased. The method has more recently been used by Bluzer[9] to detect the dynamics of quasi-particle recombination and generation in an irradiated thin film. In Bluzer's method, a thin film of superconducting material is placed on the end of a cylindrical waveguide and irradiated with fast laser pulses. The resulting pulse of induced emf is then observed on a fast oscilloscope and is proportional to the change in quasi-particle density. Bluzer was able to observe the dynamics of both quasi-particle generation as well as quasi-particle recombination. Using a similar experimental setup, Johnson[10] was

able to measure the recombination time of quasi-particles in Niobium by examining the decay of optically induced emfs.

Other optical methods have also been used to measure the quasi-particle recombination time. Parker[11] and Jaworski[12] performed an indirect measurement of the recombination time by using the change in IVC of an SIS junction to infer the change in quasi-particle density induced by light in a thin film of Pb. Real-time optical measurements using SIS junctions have also performed. Care had to be taken to ensure that these junctions had a bandwidth sufficiently high to measure the recombination time. Finally, microwave reflectivity measurements[13] have also been used as a probe of the optically induced nonequilibrium. The reflectivity of a superconductor at frequencies less than the Δ/h (~10GHz for metallic superconductors) is strongly dependent on the value of the gap, which can be related to the quasi-particle density.

Since the discovery of high temperature superconductors it has become clear that new methods of measuring recombination times must be employed. Because the gap of these superconductors is significantly larger than the classical metallic superconductors, their recombination times are also much faster. The primary tool used to measure the fast recombination time of these materials has been pulsed radiation. Bluzer[9] has used the kinetic inductance technique mentioned above to measure quasi-particle dynamics in high temperature superconductors.

Other authors have used changes in optical reflectivity[14] caused by a laser pulse to probe the optically induced nonequilibrium. Light generation by high T_c superconductors

has also been used to observe the optically induced nonequilibrium[15]. The proper interpretation of these effects is still a subject of research.

Despite the many measurements of the recombination time discussed above a measurement of the recombination time of Ta was not found. The only previous measurement was of the branch imbalance[16] relaxation time for temperatures near T_c. This work therefore represents, to our knowledge, the first measurement of the quasi-particle recombination time in Ta at temperatures far from T_c.

All of the above measurements were performed on thin films of various thicknesses. This has presented a difficulty with some novel materials, such as the ceramic superconductors and also with crystalline materials, which can be difficult to form into thin films. Also, the primary tool in real time optical measurements has been pulsed excitation. Because the recombination times are very short for most superconductors (>1e-8 sec) pulsed techniques require novel detection methods or special coupling with the superconducting sample to ensure a high enough system bandwidth to accurately observe the system response. In some methods, the measured relaxation rate is not easily related to the fundamental recombination time. As will be described in the next section, the method considered in this chapter addresses these measurement issues: 1) use of bulk samples 2) limited signal bandwidth of superconducting structure studied, and 3) ease of interpretation.

5.3 Experimental Method

As discussed in the introduction and the previous chapter, optical illumination of an SNPC breaks Cooper pairs in the superconductor resulting in an increased quasi-particle density and a decrease in the gap. When the light intensity is modulated, the decrease in gap manifests itself as an oscillating photoresponse voltage on the contact. For bias voltages greater than gap, this oscillating signal is linearly related to the gap decrease. By Parker's result (Eq. 4.4 and Ref 17) the gap change is proportional to the amplitude of the oscillating optically induced quasi-particle density. Therefore the photoresponse voltage at large bias is proportional to the optically induced quasi-particle density. To measure the relaxation rate of the quasi-particle density and hence the quasi-particle recombination time, the laser intensity modulation frequency is increased until a roll-off is observed in the large bias photoresponse signal. Because the quasi-particle recombination time is very short the roll-off frequency is beyond the bandwidth of the lock-in detection system used to measure the photoresponse. At the frequencies of interest in this measurement (100MHz), this bandwidth is limited by two unavoidable factors: Stray lead capacitance at the contact; and the mismatch of the contact impedance, which varies between contacts (10-200Ω), to the characteristic impedance of the coaxial cables carrying signals from the contact to the lock-in amplifier.

Instead of detecting the photoresponse directly, then, the voltage resulting from the oscillating quasi-particle density must be converted to a frequency which lies within the bandwidth of the detection system. This is accomplished by coupling a local oscillator (LO) voltage to the contact which differs from the laser intensity modulation frequency by an intermediate frequency (<100kHz) that is within the detection

bandwidth. A signal at the intermediate frequency is then generated because of the nonlinearity of the photoresponse characteristic as a function of bias voltage and can be detected by referencing the lock-in to the intermediate frequency. As will be shown in the next section, the signal at the intermediate frequency is proportional to the derivative of the photoresponse, and integration of this signal recovers the information necessary to determine the roll-off of the induced oscillating quasi-particle density with modulation frequency. The derivative signal is also proportional to the LO voltage and therefore the LO voltage amplitude must be measured to determine the roll-off frequency. This measurement is also performed using the nonlinearity of the contact as described in section 5.3.3.

5.3.1 Optical Setup.

The experimental setup used in the measurement of the derivative photoresponse signal is shown in Fig. 5.1. As in the photoresponse measurement, light is coupled to the SNPC with a lens. The chopped power modulation used in the photoresponse measurement was replaced by sinusoidal power modulation for the derivative measurements. For frequencies below 10MHz direct sinusoidal modulation of the first sideband of an AOM was used. At 110MHz and 220MHz, sinusoidal modulation was produced by interfering two sidebands of the AOM. Care was taken to ensure that the overlap of the two sidebands was maintained a few meters before and after the contact. A portion of the modulated light was split off before entering the dewar and detected on a PIN diode to measure the intensity modulation depth and to generate the reference frequency for the lock-in, which is the intermediate frequency: $\Delta\omega = \omega_{mod} - \omega_{LO}$. The

reference was produced by mixing the local oscillator frequency, ω_{LO}, with the modulation frequency, ω_{mod}, detected on the PIN diode.

Fig. 5.1 Recombination Time Measurement

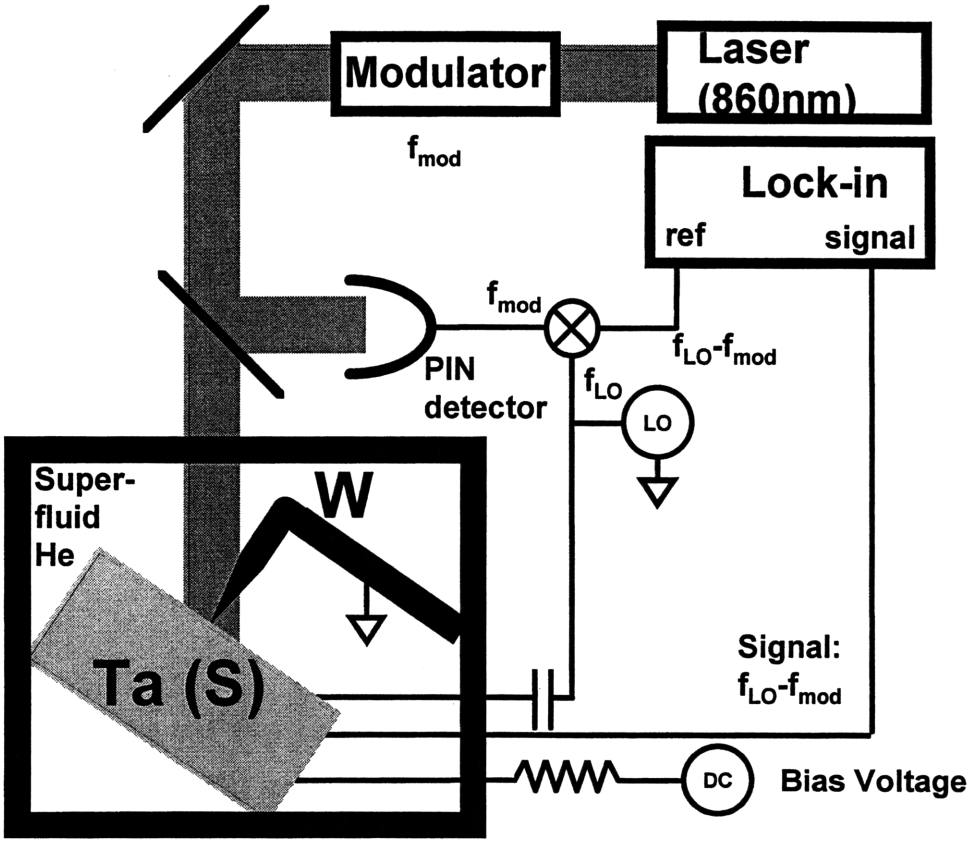

Fig. 5.1 Recombination Time Measurement. The recombination time is determined from the roll-off of the photoresponse at frequencies ω_{mod} which are beyond the signal detection bandwidth. A local oscillator is coupled to the contact and the lock-in is referenced to detect at the intermediate frequency ω_{mod}-ω_{LO} which is generated on the mixer. The nonlinearity of the contact then generates a signal at this difference frequency which can easily be detected. The roll-off is measured by increasing ω_{mod} while keeping ω_{mod}-ω_{LO} constant.

5.3.2 Electronics.

The electronics used in the derivative measurement are also shown in Fig 5.1. The point contact was formed as in the previous chapters. Voltages were sent to and carried away from the SNPC with separate micro-coax cables connected very close to the point contact to prevent unwanted signal rectifications by the lock-in and other components. As in the photoresponse measurements, the bias voltage was scanned as the lock-in signal was recorded, yielding in a plot of derivative signal vs bias voltage. The local oscillator was coupled to a double balanced mixer using a high frequency buffer. The other channel of the double balanced mixer was the laser intensity modulation signal detected on the PIN diode which was also coupled via a high frequency buffer. The difference frequency ω_{LO}-ω_{mod} was sent to the reference input of the lock-in. The same LO was also coupled to the contact via a capacitor.

5.3.3 Measurement of Local Oscillator Voltage.

The local oscillator voltage amplitude on the contact was measured using thenonlinearity of the SNPC IVC: The ~100MHz local oscillator was modulated at 1kHz and the rectified signal from the contact was measured with the lock-in as a function of applied bias voltage. The voltage could then be computed from the size of the rectified LO signal. The rectified LO signal is proportional to the second derivative of the IVC multiplied by the dynamic resistance of the contact*:

* This result is valid in the limit of $\omega_{LO} << \Delta$; see section 5.5.3 concerning quantum limits.

$$V_{rect} \sim \left(\frac{d^2I}{dV^2} \Big/ \frac{dI}{dV} \right) v_{LO}^2 \tag{5.5}$$

Plots of the measured LO signal as a function of bias voltage as well as fits using this bias dependence are shown in Fig. 5.2. The fit was performed by adjusting only the LO voltage amplitude v_{LO}. In the actual roll-off measurements, the LO voltage amplitude was adjusted so that this signal was the same in each measurement.

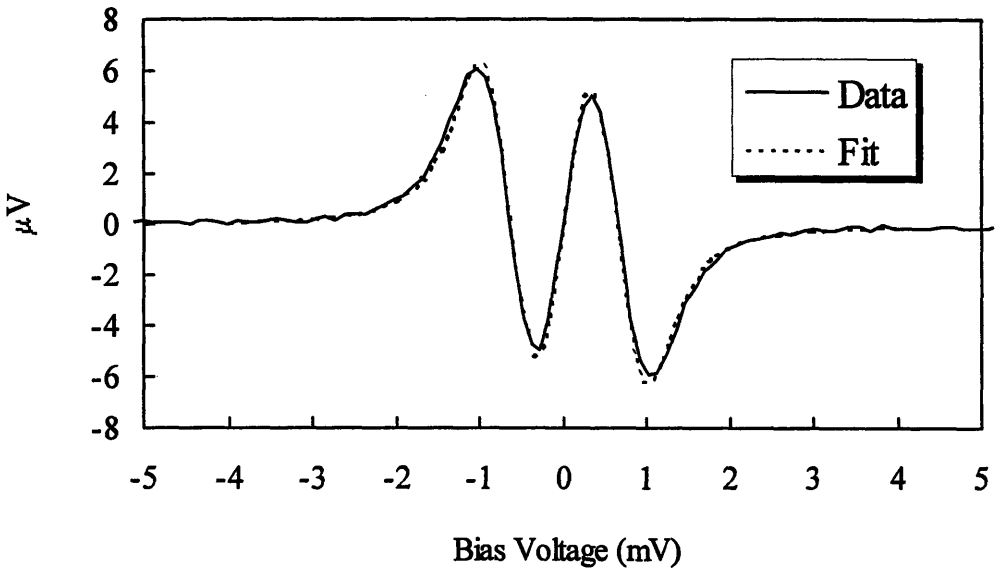

Fig. 5.2 Local Oscillator Recitification. The LO voltage on the contact is measured by modulating the LO and detecting the rectified voltage at the modulation frequency. The plot shows the rectified LO voltage and the best fit theoretical curve: $V_{LO} \sim (d^2I/dV^2)/(dI/dV)$. Accurate measurement of the LO voltage on the contact is necessary to measure the roll-off of the photoresponse signal.

5.3.4 Measurement Procedure

To procedure used to measure the roll-off was as follows: The derivative signal was recorded on a given contact for several laser intensity modulation frequencies. All

other parameters, local oscillator voltage amplitude, laser intensity modulation depth, and DC laser power remained the same between measurements. Any decrease in derivative signal was then due solely to the increased modulation frequency. Each measurement was performed for at least two realignments of the laser beam on the contact to eliminate any dependence on misalignment of the optics.

Derivative photoresponse signals vs bias voltage from 4 different contacts are shown in Fig. 5.3. In the first measurements (Figs 5.3a,b), modulation frequencies between 1 and 110MHz were used, and the modulation depth was 50%. These runs showed that there was little roll-off in derivative photoresponse signal up to 10MHz. Later runs (Figs. 5.3c and d) used 90% modulation depth and included only 0.1MHz as the low frequency modulation, and 110 and 220Mhz modulation to give a more accurate measurement of the roll-off.

5.4 Determination Of Recombination Time

5.4.1 Analysis of Derivative Signal

The first step in extracting the recombination time from the roll-off measurements is to show that the measured signal is proportional to the derivative of the photoresponse. This can be seen by writing the photoresponse signal as a function of a bias voltage plus a small local oscillator voltage term and Taylor expanding about the bias voltage:

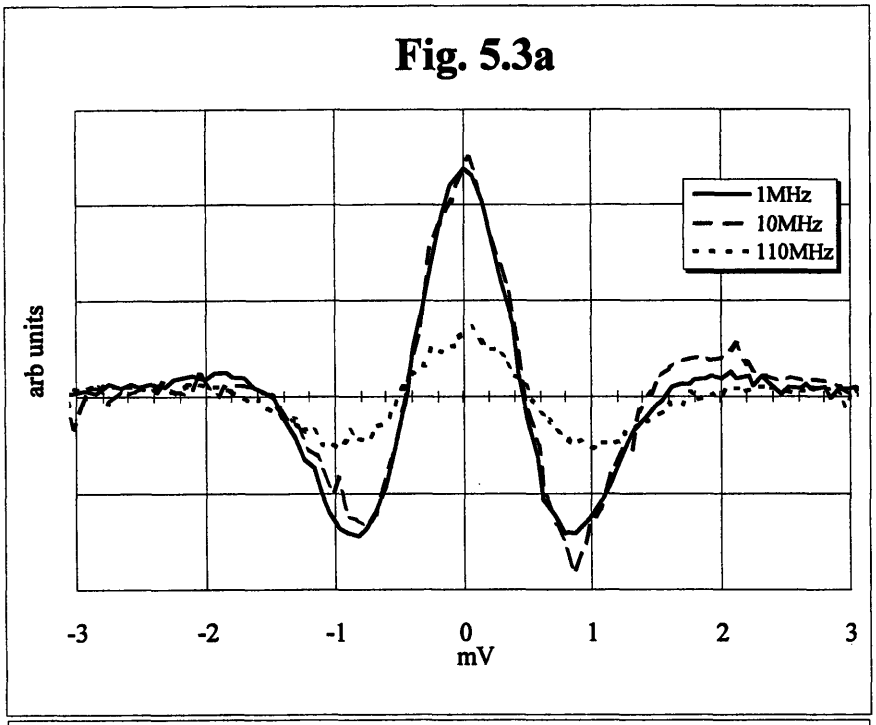

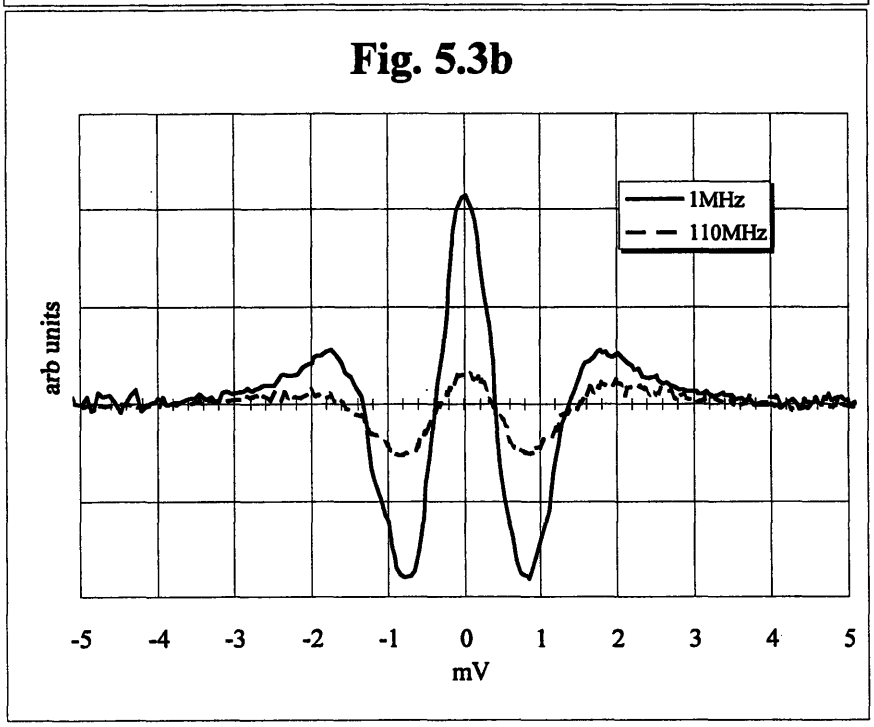

Fig. 5.3 Derivative Photoresponse Signals. These plots show four sets of derivative photoresponse measurements all taken on separate contacts with the setup of Fig. 5.1 This is the signal generated on the contact at the intermediate frequency, ω_{mod}-ω_{LO} when the light is modulated at ω_{mod} and a local oscillator voltage at frequency ω_{LO} is coupled to the contact.

Fig. 5.3c

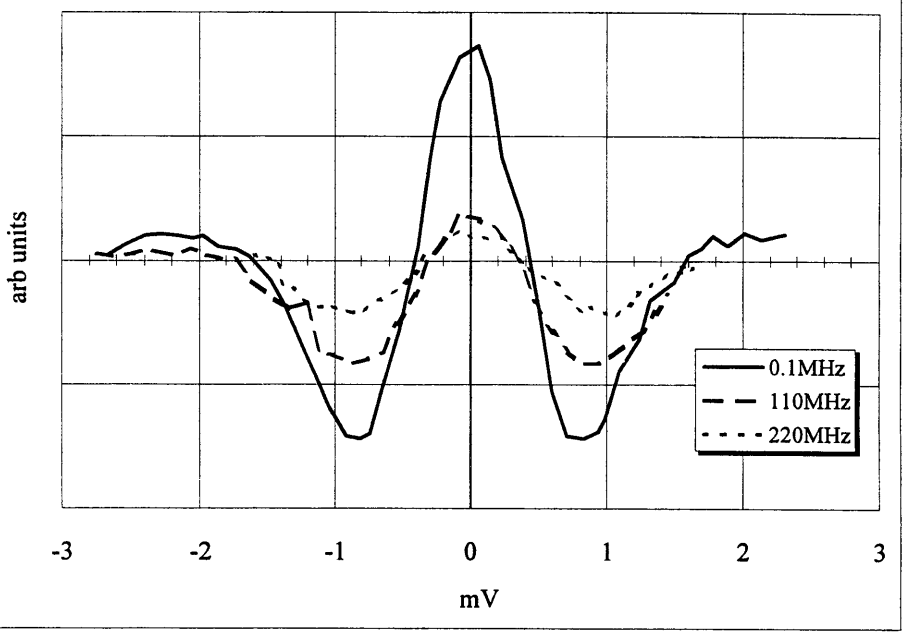

Fig 5.3d

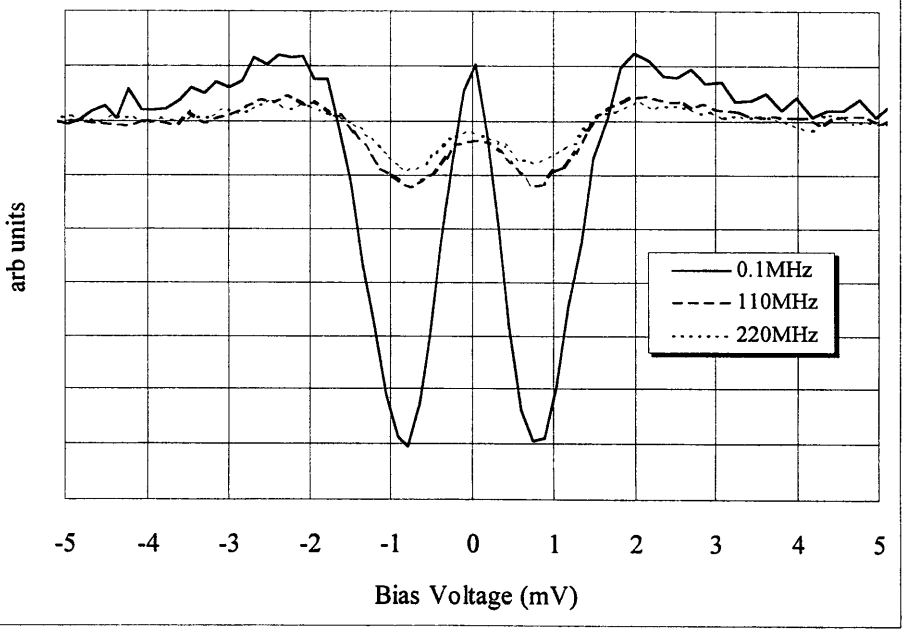

$$\delta I(V_{bias}+v_{LO}) \sim \delta I(V_{bias}) + (d\delta I/dV_{bias})v_{LO} \quad (5.6)$$

Each term in the Taylor series is proportional to the laser power which is modulated at ω_{mod}, and so the second term on the right hand side contains a term which oscillates at the intermediate frequency ω_{LO}-ω_{mod}. This is the derivative photoresponse signal which is detected by the lock-in amplifier. Eq. 5.6 therefore gives the bias dependence of the signal and shows that the underlying photoresponse signal (proportional to δI; see Chapter 4) is the integral of the derivative signal detected at the intermediate frequency.

Fig. 5.3 clearly shows a decrease in the derivative signal as ω_{mod} is increased, and these signals can be used in a rough estimate of the roll-off. However, this decrease may not be due solely to a decrease in the amplitude of the laser induced quasi-particle density. As discussed in Chapter 4, the photoresponse signal around zero bias is determined partly by the change $\delta\Delta$, which is proportional to the change in quasi-particle density, but also partly by δT in the metal tip temperature which is not related to the quasiparticle density. To be certain of measuring only the decrease in $\delta\Delta$, one computes the integral of the derivative signal with respect to bias voltage, which, as stated above, will be proportional to the photoresponse that would have been measured with the given laser intensity modulation. As shown in the last chapter, the finite bias value of the resulting photoresponse signal will be proportional only to the $\delta\Delta$ induced by the light and hence to the amplitude of the induced quasi-particle density. Fig. 5.4 shows plots of

integrals† of each curve in Fig 5.3 vs bias voltage. The plots clearly show that the induced quasi-particle density rolls off as the laser power modulation frequency increases.

5.4.2 Determination of Roll-off

Clearly the recombination time is of order $1/\nu_{roll\text{-}off}$. The exact relationship between the roll-off of $\delta\Delta$ and the recombination time follows from 1) the relationship between the laser-induced quasi-particle density and $\delta\Delta$, and 2) the relationship between the amplitude of the laser-induced quasi-particle density and the frequency at which the power of the laser is modulated.

A discussed in the last chapter, if $\delta\Delta$ is small, then $\delta\Delta/\Delta$ is proportional to the excess quasi-particle density induced by the light: $\delta\Delta/\Delta=-2\delta N_{qp}/(4N(0)\Delta)$, where N(0) is density of states at the Fermi energy. The result is approximately independent of the exact non-equilibrium quasi-particle distribution[17], and follows from the fact that Δ is a measure of the Cooper pair density.

The roll-off of $\delta\Delta$ with increasing laser intensity modulation frequency is computed by considering the dynamics of the total quasi-particle density under laser illumination. The incident light breaks Cooper pairs in a region of thickness equal to the light penetration depth. The quasi-particles and phonons generated by this process diffuse into the superconductor a distance of order the quasi-particle diffusion

† The derivative signals must be multiplied by dI/dV before integrating since the derivative photoresponse measured on the lock-in is actually proportional to $(d\delta I/dV_{bias})/(dI/dV_{bias})$.

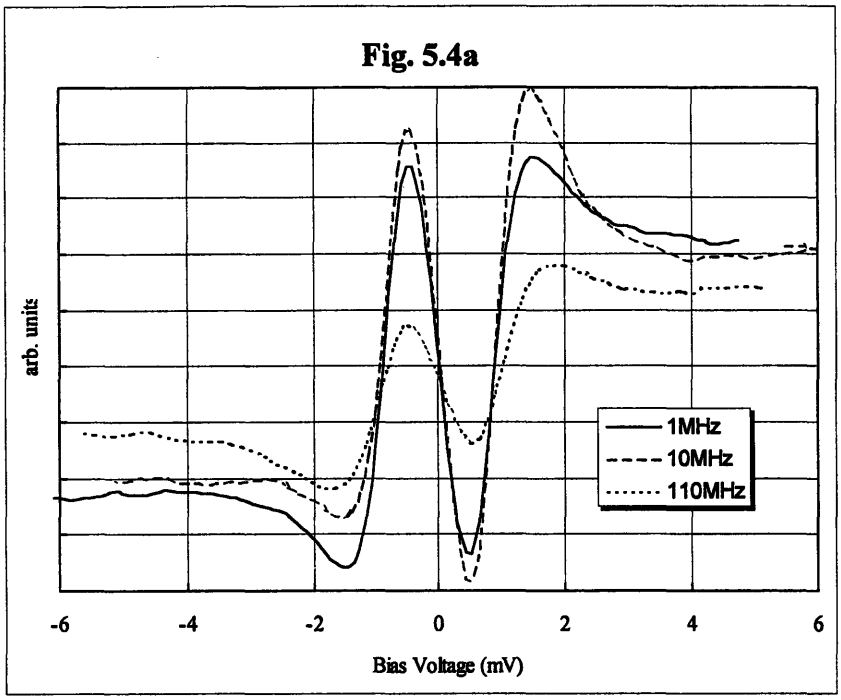

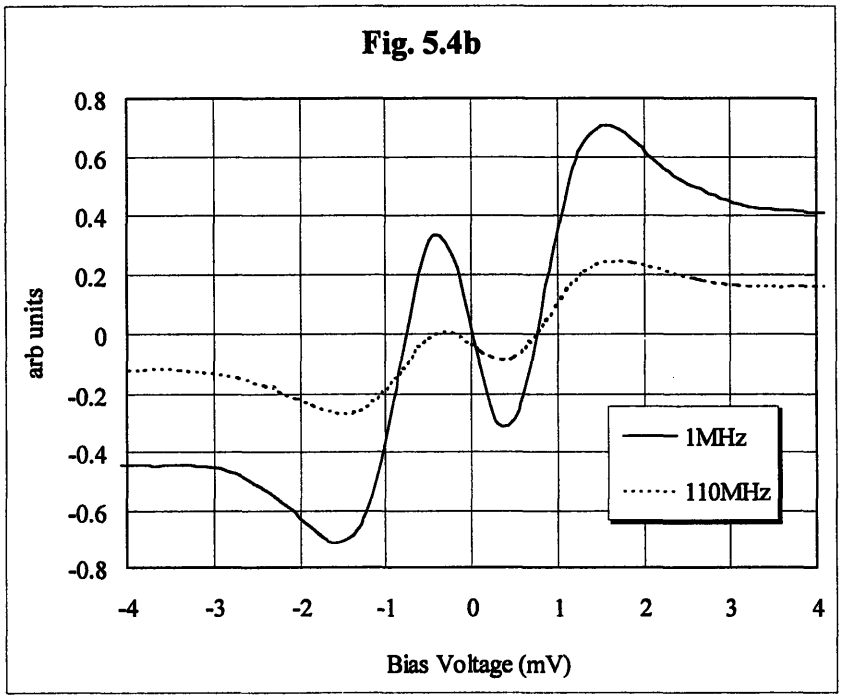

Fig. 5.4 Integral of the Derivative Photoresponse Signal. The plots are integrals of the curves in Fig. 5.3. The large bias value of these signals is proportional to the induced quasi-particle density. The roll-off of this quantity as laser modulation intensity yields the value of the quasi-particle recombination time.

Fig. 5.5c

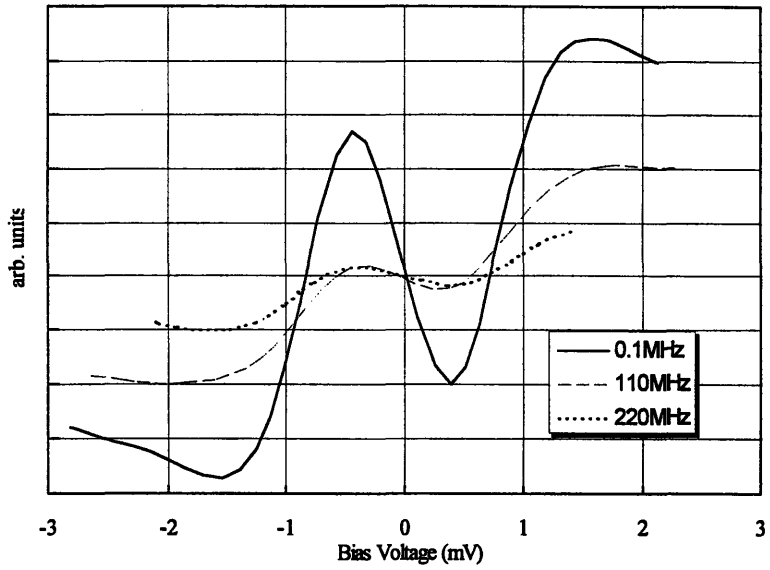

Fig. 5.4d

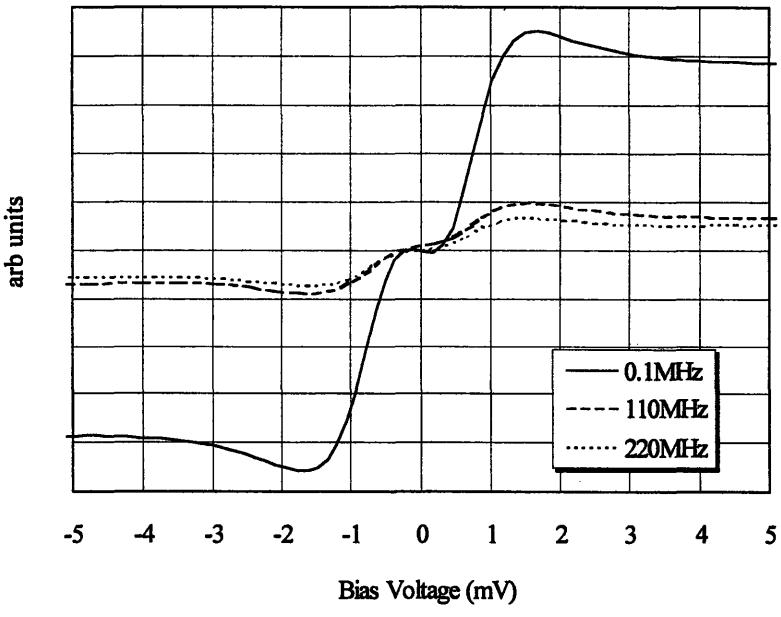

length. This region is characterized by a reduced gap which, as stated above, is determined only by the increase in total quasi-particle density in the region. The dynamics of the total quasi-particle density in this region is governed by the rate

equations of equations of Rothwarf and Taylor[18] with an added diffusive term[19] (See Chapter 4)

$$\left(\frac{\partial}{\partial t}-D_{qp}\nabla^2\right)N_{qp}=I_{qp}-2RN_{qp}^2+\frac{2}{\tau_B}N_{ph}$$
$$\left(\frac{\partial}{\partial t}-D_{ph}\nabla^2\right)N_{ph}=I_{ph}+RN_{qp}^2-\frac{1}{\tau_B}N_{ph}-\frac{N_{ph}-N_{ph}^T}{\tau_{es}} \qquad (5.7)$$

In these equations, if N_{qp}^T is the number of quasi-particles in thermal equilibrium, then, as stated in the introduction, $(2RN_{qp}^T)^{-1}$ is the recombination time, τ_R; N_{qp} is the total number of quasi-particles of all energies, N_{ph} is the total number of "pair-breaking" phonons, i.e., those with $E_{ph}<2\Delta$, τ_B is the time for a phonon to break a Cooper pair (averaged over energy), τ_{es} is the time for a phonon to leave the sample or equilibrate without breaking Cooper pairs, and D_{qp} and D_{ph} are the diffusion constants.

The equations can be linearized and solved by making the same assumptions as in Chapter 4: 1) The phonon diffusion length and time are small enough that the phonon density follows the quasi-particle density adiabatically (i.e. phonons break cooper pairs before diffusing appreciably); 2) the increase in quasi-particle density is small compared to the thermal number of quasi-particles in the superconductor; 3) the laser spot is large enough (25μm) compared to the quasi-particle diffusion length[‡] that the one may assume one dimensional diffusion in the direction normal to the surface (x-direction). Under these assumptions, a linearized equation for $\delta N_{qp}=N_{qp}-N_{qp}^T$ results:

[‡] $L_{qp}\sim\sqrt{(D_{qp}\tau_R)}=\sqrt{(v_F\ell_e\tau_R/3)}\sim 7\mu m$

$$\left(\frac{\partial}{\partial t} - D_{qp}\frac{\partial^2}{\partial x^2}\right)\delta N_{qp} = I_{qp} - \frac{2}{\tau_{eff}}\delta N_{qp} \tag{5.8}$$

As in the previous chapter, $\tau_{eff}=\tau_R(1+\tau_{es}/\tau_B)$. The enhancement factor $1+\tau_{es}/\tau_B$ is due to phonon trapping as discussed earlier.

The shape of the roll-off is determined by assuming that the incident laser intensity is a quasi-particle source of the form:

$$I_{qp}=I_o\exp(-\alpha x)(0.5)(1-\cos\omega_{mod}t). \tag{5.9}$$

Here α is the optical penetration depth which is very small compared to the quasi-particle diffusion length (α^{-1}~20nm). The roll-off of δN_{qp} with modulation frequency ω_{mod} can then be derived and related to the roll-off of $\delta\Delta$ using the linear relationship between $\delta\Delta$ and δN_{qp}. The resulting amplitude $\delta\Delta$ as a function of ω_{mod} is:

$$\delta\Delta(\omega_{mod})/\delta\Delta(\omega_{mod}=0) = (1+(\omega_{mod}\tau_{eff})^2)^{-1/4}. \tag{5.10}$$

This is the roll-off function for the finite bias photoresponse signal, and may be compared with the experimental results to obtain the recombination time.

5.4.3 Recombination Time of tantalum.

The recombination time is determined by fitting Eq. 5.10 to the measured roll-off functions taken from the integrated curves of Fig. 5.4. The measured roll-off function for a given set of curves in Fig 5.4 is obtained by taking the large bias value of the integral of each derivative photoresponse signal, and plotting these values vs modulation

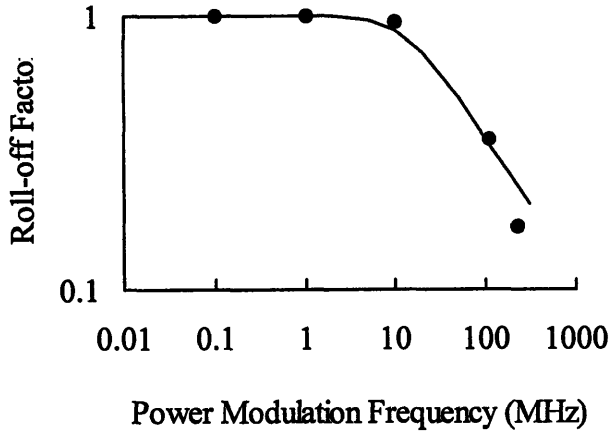

Fig. 5.5 Roll-off. The plot shows the average roll-off function deduced from the four measurements of Fig. 5.2. This is plotted along with a theoretical curve which takes diffusion into account.

frequency. The lowest modulation frequency in each data set was always chosen to be well below the roll-off frequency. Early measurements showed little roll-off up to frequencies of 10MHz (See Fig. 5.3a), and therefore every run included a data point at either 1 or 0.1 MHz. All data points in a given run were normalized to this value to obtain the roll-off function. Fig. 5.5 shows a plot of the measured roll-off function averaged over all five measurements along with the expected roll-off function of Eq. 5.10. The value of the quasi-particle recombination time, averaged over all four measurements was τ_{Reff} 50nsec. The values ranged between about 10 and 100nsec. The theoretical value of τ_R for tantalum at 1.8K was computed by Kaplan et. al.[2] to be τ_R=5nsec. Therefore the average phonon trapping enhancement factor is τ_{Reff}/τ_R=10.

5.5 Discussion

5.5.1 Sources of Variation in the Observed Recombination Time

The range of observed recombination times can be accounted for by several factors. Uncertainty in the temperature measurement can account for up to a factor of

40% variation in the observed recombination time. The temperature was measured with .05K accuracy using a temperature diode. Alignment gave errors of up to a factor of 50% between measurements. This was reduced by recording the derivative with at least two alignments. Finally, the effect of phonon trapping must be considered. According to these measurements the phonon trapping factor was ~10 on average. The variability of the measured recombination time is accounted for in part by the phonon trapping factor. Phonon escape and equilibration is sensitive to the nature of the tantalum surface. Roughness and oxides can alter the phonon escape rate into the superfluid He as well as changing the pair breaking and phonon equilibration times within the superconductor.

5.5.2 Effect of Large Signal Local Oscillator

In some of the derivative measurements the LO voltage had large amplitudes approaching 0.4mV or half the gap value of Δ=0.7meV. When the LO is large enough, higher order terms in the Taylor expansion of δI (Eq. 5.6) must be included. The result is that the integral of the derivative signal is no longer proportional to the photoresponse. However, most of the correction terms which alter the integral of the derivative signal are still linear in the small change in gap induced by the light. Therefore the finite bias signal will still be proportional to the induced change in gap $\delta\Delta$, and can still be used in a roll-off measurement. The highest order term in the derivative signal which does not depend on $\delta\Delta$ and still gives nonzero finite bias signal is a term that depends goes as $(d^2I/dV^2)(d^3\delta I/d\delta T dV^2)\delta T v_{LO}^3$. But since δT is of the same order of magnitude as $\delta\Delta$, this quantity can be neglected.

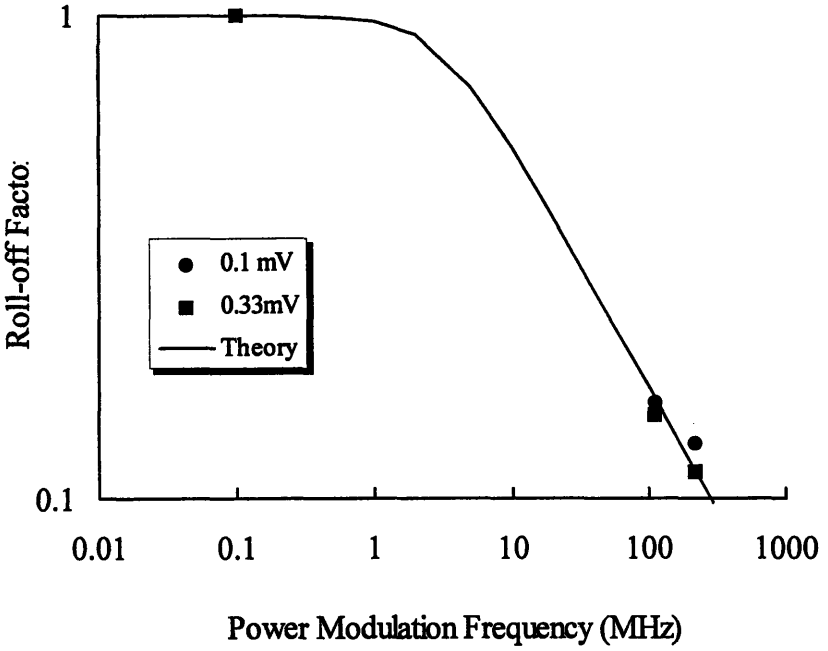

Fig. 5.6 Effect of Large Local Oscillator. The plot shows two sets of data taken on the same contact, but with different LO levels. The difference in inferred recombination times is 30%. This shows that local oscillators up to 0.3mV and even 0.4mV can be

To verify this, the derivative signals of Fig. 5.3d were recorded with two local oscillator levels, 0.1mV and 0.3mV. The roll-off observed with the local oscillator set to 0.3mV is plotted in Fig 5.6 along with the roll-off measured using a local oscillator of 0.1mV. The results are the same to within 30%, an error which can be accounted for by other sources of variation. Therefore the use of local oscillator levels up to 0.3mV and even slightly beyond this level may be tolerated.

5.5.3 Quantum Limit

This measurement technique has one fundamental limit which however is rarely of concern. When the LO frequency is close to the gap frequency Δ/h, quantum effects must be taken into account. The classical mixer response used to measure the LO voltage and used in the derivative measurements to relate them to the underlying photoresponse signal must be replaced by quantum mechanically correct expressions. The classical

nonlinearity is observed only when the currents flowing through the contact are averaged over times long compared to h/Δ. When the frequency is of order Δ/h, this is impossible, and the resulting response must include the absorption and emission of quanta of the LO photon field. The result is that the "Fermi sea" in the metal and superconductor are replaced by a linear superposition of "Fermi seas". The current is then a sum of the current from each of the excited Fermi seas of electrons. The coefficients in the sum depend on the probability of excitation to that level.

In the quantum regime, the two classical mixing responses, the LO rectification and the derivative signal, then become discrete sums, and the signals are difficult but not impossible to interpret. However, the quantum regime rarely need be considered in measuring quasi-particle recombination time. This is because the quasi-particles are well defined excitations in the superconductor and therefore have lifetimes that are long compared to their energy which is always bigger than Δ, making $\tau_R << \Delta$. Even near T_c the recombination time will be of order $\Delta/10$, (See Ref. 2) so that derivative measurements should be valid for the full temperature range of superconductivity.

Summary

This chapter has demonstrated a novel, real-time technique of measuring the quasi-particle recombination time utilizing the photoresponse of an SNPC between a sharpened tungsten whisker and bulk superconducting tantalum. The SNPC photoresponse was shown to measure the change in quasi-particle density induced by the light. The recombination time is measured in the frequency domain by recording the roll-

off of the SNPC photoresponse as the power modulation frequency of the light is increased. Limited system bandwidth is overcome by performing the measurement in a derivative mode: A local oscillator differing from the laser power modulation frequency by a frequency within the system bandwidth is coupled to the contact, and synchronous detection is performed at the difference frequency between the local oscillator and the power modulation frequency. The average measured value of the recombination time for tantalum is τ_{Reff}=50nsec. This implies a sample dependent phonon trapping factor whose average value is 10.

---

[1] J. R. Schrieffer, and D. M. Ginsburg, Phys. Rev. Lett. **8** 207 (1962).
[2] S. B. Kaplan, C. C. Chi, D. N. Langenberg, J. J. Chang, S. Jafarey, and D. J. Scalapino, Phys. Rev. B, **14**, 4854, (1976).
[3] B. I. Miller, and A. H. Dayem, Phys. Rev. Lett. **18**, 1000, (1967).
[4] J. L. Levine, and S. Y. Hsieh, Phys. Rev. Lett. **20** 994 (1968).
[5] K. E. Gray, A. R. Long, and C. J. Adkins, Phil. Mag. **20** 273 (1969).
[6] L. N. Smith, and J. M. Mochel, Phys. Rev. Lett. **35** 1597 (1975).
[7] A. Schmid, Phys. Rev. **186** 420 (1969).
[8] R. Peters, and H. Meisner, Phys. Rev. Lett. **30** 965 (1973).
[9] N. Bluzer, J. Appl. Phys. **71** (3), (1992).
[10] M. Johnson, Phys. Rev. Lett. **67** 374 (1991).
[11] W. H. Parker, and W. D. Williams Phys. Rev. Lett **29** 924 (1972).
[12] F. Jaworski, W. H. Parker, and S. B. Kaplan, Phys. Rev. B **14** 4209 (1976).
[13] G. A. Sai-Halasz, C. C. Chi, A Denenstein, and D. N. Langenberg, Phys. Rev. Lett. **33** 215 (1974).
[14] T. Gong, L. X. Zheng, W. Xiong, W. Kula, Y. Kostoulas, R. Sobolewski, and P. M. Fauchet, Phys. Rev. B **47** 14495 (1993); S. G. Han, Z. V. Vardeny, O. G. Symko, and G. Koren, IEEE Trans. Mag., **27**, 1548 (1991).
[15] M. Hangyo, S. Tomozawa, Y. Murakami, M Tonouchi, M. Tani, Z. Wang, and K. Sakai, IEEE Trans. Mag. **7** (2) 2909 (1997).
[16] M. L. Yu, and J. E. Mercereau, Phys. Rev. B, **12** 4909 (1975).
[17] W. H. Parker, Phys. Rev. B **12**, 3667 (1972).
[18] A. Rothwarf, and B. N. Taylor, Phys. Rev. Lett, **19**, 27 (1967).
[19] N. E. Glass, and D. Rogovin, Phys, Rev, B, **45**, 7346 (1992).

Chapter 6

Conclusion and Future Possibilities

This thesis has explored the properties of superconductor-normal metal point contacts (SNPCs) in new regimes. The ability to control the impedance of the contacts gave new insight into some of the anomalous behavior observed in their conductance and shed new light on the mechanisms of destruction of superconductivity at an NS interface. The thesis also presented the first extensive measurements of the response of these cryogenic SNPCs to laser irradiation in the near IR at 860nm. These measurements were described quantitatively using a model based on BTK conductance theory. This resulted in several novel measurements on both the conductance properties of the NS contact and of the nonequilibrium properties of irradiated metals and superconductors. This chapter will briefly describe refinements to these measurements and consider new research possibilities that flow from this work.

The recombination time measurement can be improved by using a semiconductor laser instead of the Ti:Sapphire laser used in these measurements. Commercial semiconductor lasers can be easily modulated internally at frequencies up to 10GHz, extending the range of the roll-off measurement. Moreover, several frequencies could be used, adding more points to the roll-off. A more subtle advantage of the semiconductor

laser is that, because there are no losses in modulating the light (as there were in the second sideband of the AOM used in the 220MHz modulation setup), the spot size can be greatly increased, while maintaining laser intensities at the level needed for the measurements. A larger spot size can improve the stability of the measurements. As pointed out in the thesis, the exact frequency of operation of the laser is unimportant since the laser light act only to break Cooper pairs in the superconductor. Therefore, there would be no need for line narrowing and frequency stabilization in the laser. Such a semiconductor laser could be purchased for a fraction of the cost of a high power Ti:Sapphire laser.

Because the point contacts respond at high frequencies, the recombination time measurement technique can be adapted for use on high temperature superconductors whose recombination times are much shorter than classical superconductors. Power modulation would be provided by mixing two lasers beams on the contact as done in this thesis. If these came from two separate lasers, the modulation frequency could then be easily tuned. Such laser mixing measurements have been performed on room T normal-normal point contacts with two CO_2 lasers[1], and could be adapted to a shorter wavelength regime.

Finally, the point contact can be studied in a more controlled manner by forming the contact in an STM. Such studies have been performed[2,3,4], but the full utility of the cryogenic STM in studying the properties of point contacts has yet to be realized. One advantage of using an STM is that the region of the contact could be studied before and after formation of the contact, providing information on the nature and size of the contact

region. The barrier could also be easily controlled in such a contact. Finally, the optical response of such contacts at visible frequencies, although examined at room temperature in normal-normal point contacts, is unstudied at cryogenic temperatures and promises the possibility of high speed nonlinear effects as well as being a tool for studying the optically induced nonequilibrium state.

---

[1] M. Volcker, W. Krieger, and H. Walter, J. Vac. Sci. Technol B **12(3)**, 2129 (1994).
[2] H. Srikanth and A. K. Raychaudhuri, Phys. Rev. B **46**, 14713 (1992).
[3] N. Agrait, J. G. Rodrigo, and S Vieira, Phys. Rev. B **46**, 5814 (1992).
[4] J. K. Gimzewski and R Moller, Phys. Rev. B **36**, 1284 (1987).

Appendix A

Force Dependence of Barrier Strength

This appendix will discuss an apparent inconsistency in the observed Ta-W SNPC dynamic resistance. The fits of chapter 3 showed that the barrier strength increased as the contact resistance decreased. This result seems at first to be inconsistent, since the contact resistance should increase with greater barrier strength. However, the change in Z is typically less than 50% between the highest and lowest resistance contacts, and therefore it cannot account for the change of 10-100 in the contact resistance. The large change must therefore be due to the increase in contact area, and so the change in barrier strength need not be related to the change in contact resistance.

Fig A.1. W-Ni Force vs Contact R

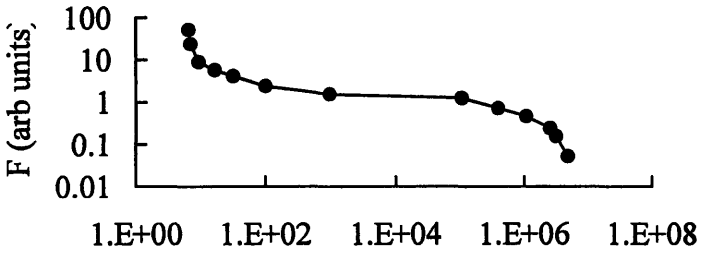

Fig. A.1 W-Ni Force vs Contact Resistance. The plot shows the measured resistance of a point contact between a sharpened W whisker and bulk Ni vs the force of the W tip on the Ni sample.

It still remains to understand, though, how the barrier strength can increase when the force on the contact is increased. The conflict can be resolved by examining the dependence of the contact resistance on the force applied

to the contact.

The dependence of contact resistance on force was measured by Liu[1] on point contacts between W whiskers and bulk Ni. Force on the contact was measured by mounting the Ni sample on a balance and recording the force and contact resistance as the W whisker was pushed into the sample. The resulting plot is shown in Fig A.1, which is reproduced from Liu's thesis. The contact resistance remains approximately constant for low force and then drops rapidly to ~10Ω where it is again slowly varying with force. The region of rapid change corresponds to a plastic deformation of the tip as force is increased (See Liu 79). Behavior similar to this is observed in the Ta-W contacts of this thesis

Fig A.2. W-Ni Pressure vs Contact R

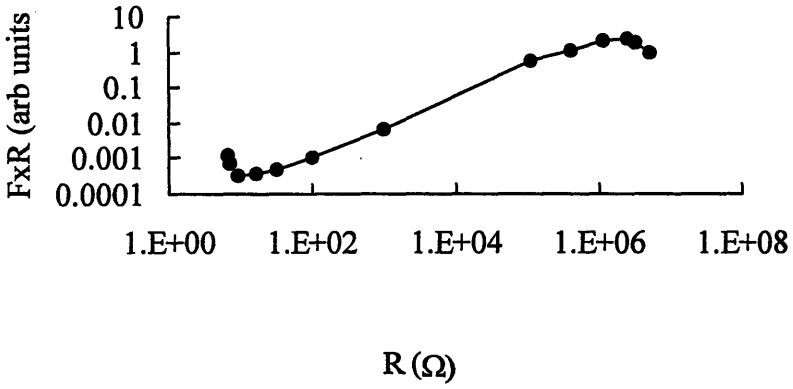

Figure A.2. W-Ni Pressure vs Contact Resistance. The y-values are the force values of Fig A.1 multiplied by the contact resistance for that point. The x values are the same. Because R in inversely proportional to area, (force)x(R) is proportional to pressure on the contact

The important determinant of the barrier strength is not force but pressure on the contact. A measure of the pressure on the contact can be extracted from the force by noting that since this is a ballistic contact, the contact resistance is proportional to the inverse of the contact area (See chapter 2). Therefore the quantity (Force)x(Resistance) is a measure of the pressure on the contact. This quantity is

plotted in Fig A.2. Clearly the pressure goes down rather than up as the contact resistance is decreased. This is consistent with the picture put forward by Liu that the contact undergoes a plastic deformation, which relieves stress and decreases the pressure. Therefore although the area increases as the force increases, the pressure on the added area is less, and one expects that the barrier will actually increase.

---

[1] K. C. Liu, MIT PhD Thesis, P. 51 (1979).

Appendix B

Zero Bias Resistance Minimum

As discussed in Chapter 3, the dynamic resistance of Ta-W superconductor normal-metal point contacts often deviates from the simple bias dependence which results from the assumption of a normal-super interface with an oxide barrier which is assumed in the BTK model. These deviations can be categorized as either finite bias or zero bias

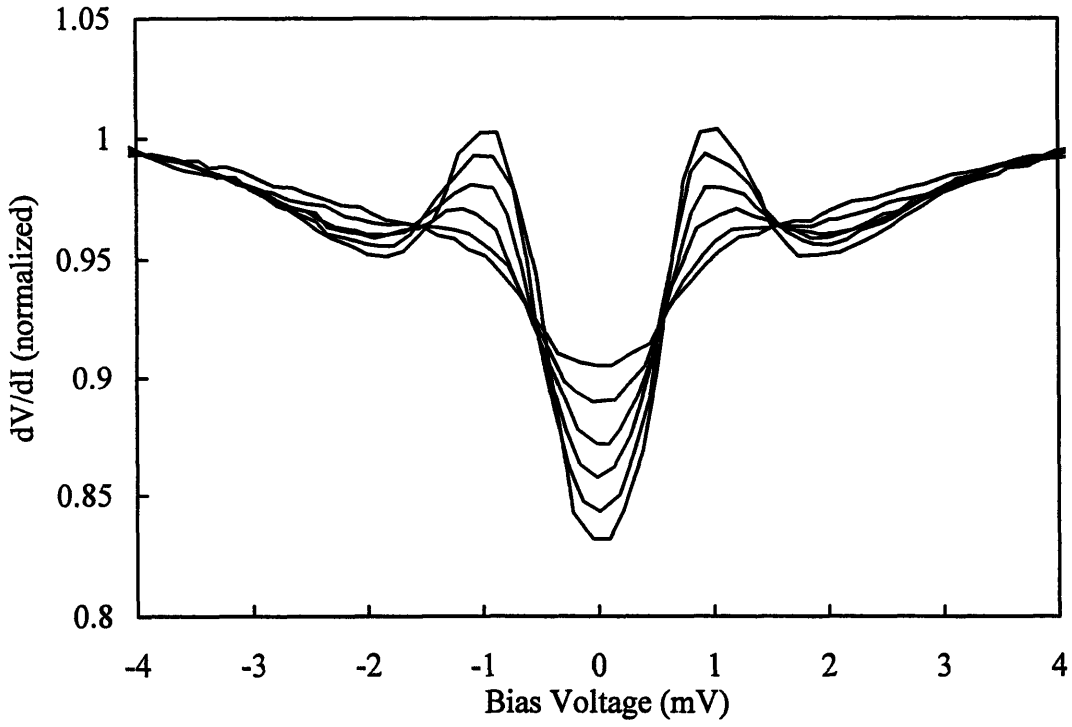

Figure B.1 W-Ta Dynamic Resistance.

anomalous behavior. The Ta-W point contacts of this thesis exhibited both types of deviation from simple BTK behavior, and Chapter 3 discussed a model of the finite bias resistance peaks observed on these contacts. This appendix presents data showing non-BTK behavior at zero bias. This was not studied in detail for this thesis, however, the temperature dependence was recorded and is displayed in this appendix.

Fig. B.1 shows the zero bias dynamic resistance of a Ta-W point contact recorded for several temperatures as the liquid He in which the contact was immersed was allowed to warm from 1.8 to 4.3K. The curves are all normalized to 1 at a bias voltage of 5mV. This dynamic resistance has a minimum at zero bias, unlike the maximum predicted by BTK theory. This dynamic resistance was observed in several contacts. The minimum at zero bias could be large, so that the minimum at V=Δ was barely visible, or so small that the dynamic resistance was essentially BTK in character except for a small dip at zero bias.

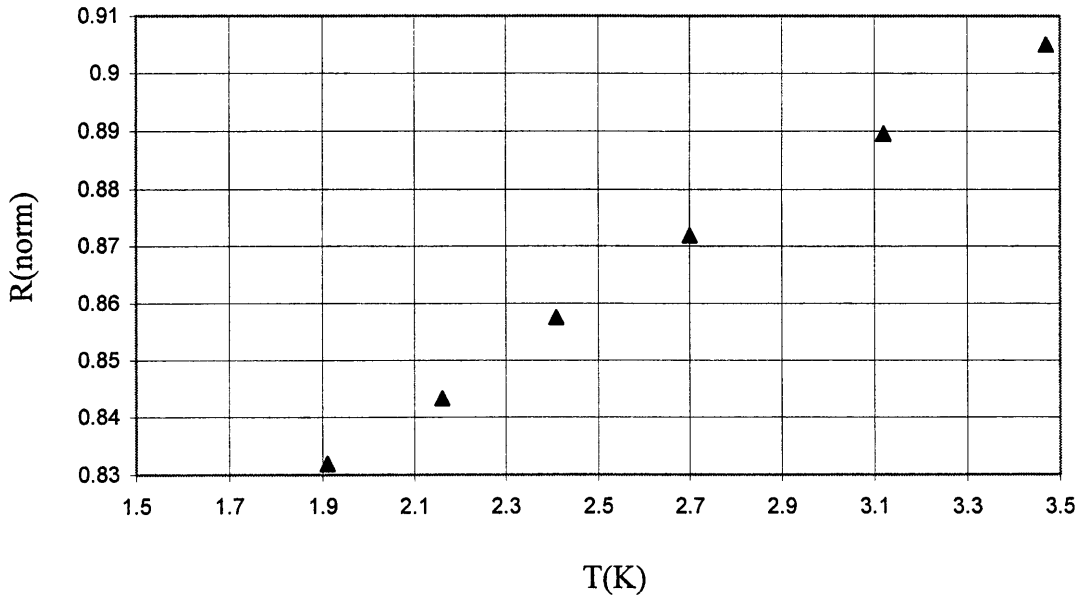

Figure B.2. Zero Bias Resistance vs Temperature

Fig. B.2 shows the value of the dynamic resistance at zero bias for each normalized curve plotted as a function of temperature. The dependence is approximately linear.

This feature has been observed before in normal-super contacts[1,2] and has been analyzed theoretically[3]. The true explanation is still a matter of debate. The explanation most likely to be true for these contacts is based on the proximity effect. It is assumed that the barrier region is not a simple NS interface, but that a region of depressed superconductivity exists in the barrier region. This region has a decreased value of the gap. The resulting dynamic resistance will then show minima at both gap values. Therefore the peak in resistance usually observed zero bias becomes a minimum. The temperature dependence of the zero bias dynamic resistance in this model has been computed[4] and is linear for various values of the proximity parameters, consistent with the linear dependence observed on this contact.

---

[1] P. Xiong, G. Xiao, and R. B. Laibowitz, Phys. Rev. Lett. 71, 1907 (1993).
[2] A. Hahn, and K. Humpfner, Phys. Rev. B 51, 3660, (1995).
[3] F. Tafuri, A. Di Chiara, F. Fontana, F. Lombardi, and G. Peluso, Phys. Rev. B **53**, 11770 (1996); A. Di Chiara, F. Fontana, G. Peluso, and F Tafuri, Phys. Rev. B **48**, 6695 (1993); C. W. J. Beenakker, Phys. Rev. B **46**, 12841 (1992).
[4] F. Tafuri, A. Di Chiara, F. Fontana, F. Lombardi, and G. Peluso, Phys. Rev. B **53**, 11770 (1996).